Hybrid Galerkin Boundary Element – Wavenumber Integration Method for Acoustic Propagation in Laterally Inhomogeneous Media

by

Woojae Seong

B.S. Naval Architecture, Seoul National University (1982)
M.S. Naval Architecture, Seoul National University (1984)

Submitted to the Department of Ocean Engineering in Partial Fulfillment of the Requirements for the Degree of

Doctor of Philosophy

at the

Massachusetts Institute of Technology
February 1991

Signature of Author _____
Department of Ocean Engineering
Dec. 17, 1990

Certified by _____
Professor Henrik Schmidt
Thesis Supervisor

Accepted by _____
Professor A. Douglas Carmichael
Chairman, Departmental Graduate Committee

Hybrid Galerkin Boundary Element – Wavenumber Integration Method for Acoustic Propagation in Laterally Inhomogeneous Media

Woojae Seong

Submitted in partial fulfillment of the requirements
for the degree of Doctor of Philosophy
Dec. 17, 1990

Abstract

A hybrid analytical–numerical method combining the Galerkin boundary integral and wavenumber integration technique is presented for two-dimensional acoustic propagation in a laterally inhomogeneous, vertically stratified medium.

The range dependent ocean is first divided into range independent sectors and the field within each sector is expressed by a boundary integral over the vertical sector boundaries in terms of a set of unknown boundary displacements. The proper choice of a set of distribution functions (in this case, Legendre polynomials) for these boundary displacements leads to an efficient evaluation of the kernel of the boundary integral by means of wavenumber integration/global matrix approach, as implemented in the SAFARI code. This leads to a matrix relation between the displacement and stress amplitudes along the vertical boundaries, similar to the stiffness matrix of finite element method. Once solved for the displacement amplitudes at the sector boundaries using a Galerkin approach, the boundary integral formulation directly yields the total field within each sector including both the forward propagating and back reverberated fields.

Illustrative numerical examp' s of canonical problems are given to explore the feasibility and efficiency of the pr posed hybrid method for solving step-wise varying range dependent ocean acoustic propagation problems. It is demonstrated that the present method yields reliable results and forms another class of solution methods for range dependent acoustic propagation problems.

Thesis supervisor : Prof. Henrik Schmidt
Associate Professor of Ocean Engineering

Acknowledgements

My most sincere gratitude is extended to my advisor, Professor Henrik Schmidt, without whom this thesis would not have been possible. His knowledgable and insightful guidance have steered me throughout the long period of my research. Not only is he a great scientist and a respectable teacher but a warm-hearted human being who constantly provided encouragements in every aspects.

I want to thank Dr. George Frisk and Professor Paul Sclavounos for their advice and comments on this thesis and for serving on my thesis committee. I also want to thank Professors Ira Dyer, Arthur Baggeroer and Michael Buckingham for introducing me to the fascinating world of underwater acoustics and Professor H.S. Choi for initiating me into the academic field of ocean engineering.

Thanks are also due to Dr. Peter Gerstoft for many discussions and to my officemates – Chifang Chen, Jea Kim, Hyun Lee, Kevin LePage, Nick Makris, Hee Song, DJ Tang, and especially Ken Rolt for correcting the English. I thank Marilyn Staruch and Denise Cormier for their administrative assistance.

It is a privilege to come from a family with so much love. To my parents I owe a special debt of love and devotion. They have been supportive of my endeavors throughout my life. I thank my brother who has always been so understanding.

Last, but certainly not least, I want to thank my wife Hyunjung and my son Sijoon for putting up with the long hours away from home. Without their tremendous love and support, none of this would have been possible.

Contents

List of Figures

List of Tables

Glossary

superscripts : $^{\bullet}$ **– source solution**
$^{\tilde{}}$ **– homogeneous source solution**
$^{\hat{}}$ **– displacement source solution**
$^{\bar{}}$ **– homogeneous displacement source solution**

$A_n^{\pm}(s)$: amplitude of up- and down-going homogeneous compressional solution in layer n due to real source

$A_{n,lk}^{\pm}(s)$: amplitude of up- and down-going homogeneous compressional solution in layer n due to displacement source of order k in layer l

$B_n^{\pm}(s)$: amplitude of up- and down-going homogeneous shear solution in layer n due to real source

$B_{n,lk}^{\pm}(s)$: amplitude of up- and down-going homogeneous shear solution in layer n due to displacement source of order k in layer l

C : medium sound speed

$C_{n,lk}^{\pm}(s)$: amplitude of up- and down-going homogeneous compressional solution in layer n due to shear source of order k in layer l

$D_{n,lk}^{\pm}(s)$: amplitude of up- and down-going homogeneous compressional solution in layer n due to shear source of order k in layer l

$G(x,z)$: total solution or Green's function

h : medium compressional wavenumber

$j_m(\cdot)$: spherical Bessel function of order m

k : medium shear wavenumber

l : layer depth

M : total order of basis function expansion

N : total number of layers

p : pressure

$P_m(\cdot)$: Legendre polynomial of order m

r : horizontal range in cylindrical coordinates

s : horizontal wavenumber

$S_{nm}(0)$: shear source strength of order m in layer n

u : horizontal displacement

$\hat{U}_{nm}(0)$: displacement source strength of order m in layer n

w : vertical displacement

w_i : Gauss-Tchebycheff quadrature weight

W_j : Gauss-Legendre quadrature weight

x_j : Gauss-Legendre quadrature point

x_s : source range

X : valid maximum range when using FFT for wavenumber integral

X_j : horizontal length of jth sector super-element

y_i : Gauss-Tchebycheff quadrature point

z_r : receiver depth

z_s : source depth

$i\alpha$: compressional vertical wavenumber($i\sqrt{s^2 - k^2}$) in horizontal wavenumber integral representation

$i\beta$: shear vertical wavenumber($i\sqrt{s^2 - k^2}$) in horizontal wavenumber integral representation

$i\gamma$: compressional horizontal wavenumber($i\sqrt{\eta^2 - k^2}$) in vertical wavenumber integral representation

$i\delta$: shear horizontal wavenumber($i\sqrt{\eta^2 - k^2}$) in vertical wavenumber integral representation

δ_{nm} : Kroenecker delta

$\delta(\cdot)$: generalized Dirac delta function

Δ : representation of small increment

ϵ : imaginary axis offset of complex contour integration

ς_m : parameter defined as $(-1)^{m-1}$

η : vertical wavenumber

κ : condition number of a matrix

λ : medium wavelength

λ, μ : Lamè constants

ρ : density of the medium

σ_{xx} : normal stress in x-direction at vertical interface

σ_{zz} : normal stress in z-direction at horizontal interface

σ_{xz} : shear stress in x-direction at horizontal interface

ϕ : compressional wave displacement potential

φ : shear wave displacement potential

ω : circular frequency of monochromatic source

Chapter 1

Introduction

The propagation of sound waves in the ocean is often considered to be range independent, where the sound propagation speed and density of the medium do not vary along the horizontal propagation path. Because the lateral inhomogeneity is usually weaker than the vertical inhomogeneity in the ocean,this generally is a very good approximation in many cases and greatly simplifies the theory [7] [59]. However, there are instances where range dependence is encountered in such forms as changes in the medium itself or the changes in the boundary such as bathymetric changes. In such cases, the approximation of a range independent ocean is no longer valid. Some examples include:

1. acoustic wave propagation across frontal zones in the ocean, such as Gulf currents, marginal ice zone, *etc.*;

2. long range propagation over thousands of kilometers, especially in the meridional direction;

3. sound propagation in a coastal wedge, or in deep water along a bottom seamount, where bottom depth variation is significant; and

4. other inhomogeneities arising in the ocean environment including anomalies of geological features, such as large amounts of trapped bubbles near the surface,

a sub-bottom salt dome, ice edge, *etc.*

Any of the above situations have significant effects on the propagating and reverberated sound fields and should be modeled to adequately incorporate such range dependent phenomena as facet reverberation, mode coupling, compressional-shear wave conversion, *etc.*, and ensure that the model correctly replicates the actual physics of sound propagation. Presently, four numerical solution techniques are well established to treat range dependent phenomena:

- adiabatic or coupled mode methods
- ray methods
- parabolic equation methods
- finite difference/finite element methods.

The Green's function methods employing direct wavenumber integration(WI) has emerged as one of the most accurate and versatile techniques in wave propagation problems with the advent of digital computing and development of highly efficient computer codes such as SAFARI [43]. The wavenumber integration method is often referred to as a fast-field program(FFP) technique [15] in the underwater acoustics community and as the discrete wavenumber method [4] [5] in seismology. These terms, FFP and discrete wavenumber, are used to represent the way of evaluating the inverse transformation following the solution of the depth separated ordinary differential equation, which is obtained from the spatial transform of the original partial differential equation governing range independent wave propagation in the frequency domain. There are several ways to evaluate the integral of which the fast Fourier transform(FFT) is preferred in underwater acoustics. But since other ways of directly integrating the inverse transform are also being employed, these solution techniques may be generally categorized as wavenumber integration methods. WI methods have not been applied to range dependent problems in underwater acoustic area until very recently. Thus, using a concept similar to the

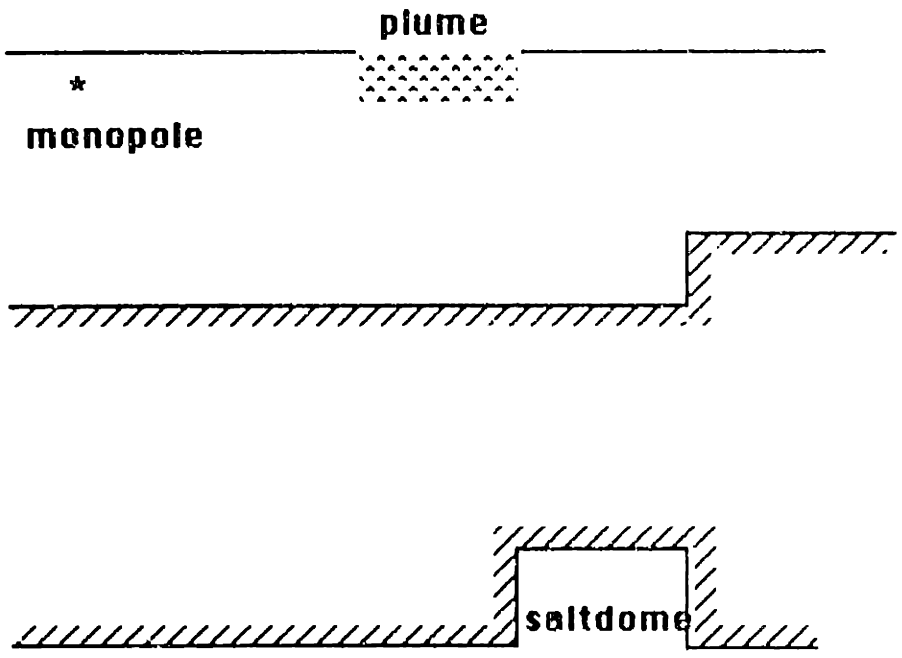

Figure 1.1: Schematic drawing of typical discretely varying range dependent ocean environment solvable by the proposed hybrid scheme.

parabolic equation method, Gilbert *et al.* [23] generalized the Green's function wavenumber integration method for exactly solving the one-way wave equation in an environment that varies discretely in range.

The boundary integral equation method is an alternative formulation of inhomogeneous media wave propagation problems. As will be detailed in Chapter 2, the boundary integral equation(BIE) method has been extensively applied to scattering problems involving inhomogeneities of limited size in otherwise homogeneous media. Due to discretization limits or limits imposed by the computer, these methods are not applicable to globally range dependent problems concerning range dependence over a long distance.

It is in this context that a new hybrid solution technique combining the wavenumber integration method and boundary integral equation is sought for wave propagation in an ocean environment that varies discretely in range as shown schematically

in Fig. 1.1. This new technique is capable of modeling both short and long range propagation and reverberation for multi-layers, discretely varying media, multiple sources and rectangular scatterers. Furthermore it is possible to extend this method to treat elastic media, enabling physical interpretation of the coupling between the elastic and the acoustic waves in a range dependent ocean environment which is essential in understanding such problems as noise propagation in an ice-keel laden arctic environment, and also the shallow-water/bottom interaction phenomena in a range dependent ocean environment.

1.1 Background

There exist a variety of techniques to model and solve range dependent acoustic propagation, each with some limitations in terms of applicability. Presently, four methods of solution techniques are well established to treat range dependent phenomena. For general description of the following methods, refer to Jensen *et al.* [29] and the special issue of the *Journal of the Acoustical Society of America*, describing benchmark solutions for two range dependent problems involving: (1) a sloping bottom problem and (2), in a parallel waveguide with continuous sound speed variations [10][18][28][53][56][57][60]. The four methods are summarized below.

- Adiabatic and Coupled mode theories: based on the local modal expansion method for homogeneously approximated segments which are matched at the boundaries using the continuity conditions, adiabatic and coupled mode methods are applicable to weakly and strongly range dependent problems, respectively. Coupled mode theory [16] accounts for the exchange of the energy between the modes but are not amenable to efficient numerical treatment. Simplifying the numerical complexity of coupled mode, the adiabatic theory ignores the cross coupling between modes [41] as an approximation to model weakly range dependent problems. Ignoring the back-scattered waves, one-way propagating coupled mode is used for numerical simplicity. Based on

the normal mode formulation, extensions to deal with the elastic media have been made in seismology [31]. Their application is limited to SH-wave(shear horizontal wave) propagation in a simple model due to the complexity in numerically implementing the theory to a general environmental model.

- Parabolic equation(PE) method: this method reduces the elliptic, Helmholtz equation to a parabolic equation by means of a small angle (paraxial) approximation. A further approximation of neglecting the back-scattered component leads to a one-way initial value problem in range which can be solved by a marching solution technique. The conventional small angle PE valid for grazing angles within 10-20° off the horizontal is solved by a split-step Fourier technique [55] whereas various wide angle PE's valid for greater angles are usually solved by a finite difference scheme [39]. Neglecting the back-scattered component gives rise to energy conservation problems and because of the approximations made in PE method, it is only applicable to weakly range dependent problems. The question of propagation in elastic media is a current research topic, but in any case the PE is limited to weak range dependence.

- Ray theory: this method is based on the conservation of energy principle and geometrical optics, and can deal with an arbitrary environment but is essentially a high frequency approximation requiring the wavelength to be much smaller than the relative gradient of the sound velocity with singularities such as caustics, shadow zones and head waves (which need special treatment [9]). In dealing with the elastic media, the splitting of a ray into the compressional and shear waves for every bounce at the interface of two different media complicates the problem to a great extent.

- Finite difference(FD) and finite element methods(FEM): these methods have recently become very popular with the availability of large computing power. FD and FEM can in principle solve range dependent elastic problems, but in reality, due to the discretization problem, they are restricted to local prop-

agation within a few wavelengths or water depths in range. The interval of discretized grid must be less than one-tenth of the wavelength to avoid what is known as the 'grid-dispersion' [2]. Since the discretization is limited to a finite region, the radiation condition can only be satisfied approximately by replacing the outer boundary with an absorbing boundary.

These four methods cannot effectively model and give full solution to the discretely varying range dependent seismo-acoustic propagation for both short and long ranges. In order to treat these ocean environment scenarios, a new solution technique combining the spectral wavenumber integration method for range independent seismic propagation and the boundary integral method is presented.

1.2 Approach

The approach in this thesis, first divides the model environment into a convenient geometrical form. Mathematics are then introduced to both solve the wavefield in each geometrical sector and to provide sector-to-sector continuity. As shown in Fig. 1.2, we divide the range dependent ocean into segments of range independent *sectors* separated by vertical boundaries (or vertical cuts), where each sector is allowed to be horizontally stratified. Then we express the solution within each sector in terms of a set of arbitrary basis functions and finally solve for the amplitudes of these basis functions by satisfying the boundary conditions at the boundaries between the sectors. This basic idea of discretization into homogeneous sectors and matching at the boundaries is similar to the coupled mode approach but the details are significantly different. In the coupled mode approach, the solution within each homogeneously approximated sector is constructed using standard normal modes, allowing numerical implementation for coupling between sectors in the fluid part of the waveguide only. Here, a wavenumber integration method combined with a boundary integral approach is applied, allowing for any sequence of fluid and solid

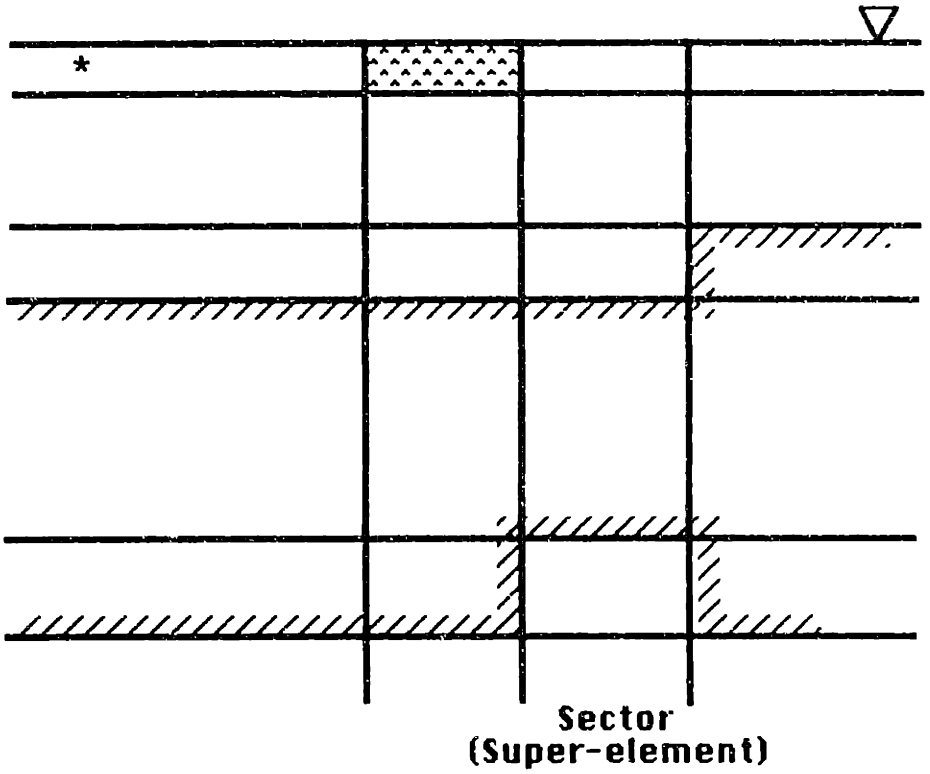

Figure 1.2: Schematic drawing of typical discretely varying range dependent ocean environment which is modeled as range independent sectors.

layers within each sector.

Within each sector, the field can be expressed as a boundary integral with the kernel being the depth dependent Green's function. By properly choosing a set of distribution functions for the field along the vertical cuts, the wavenumber integral-global matrix solution technique [43] can be applied to determine the *influence matrix* for the sector, *i.e.* the relation between the displacement and stress distributions on the vertical cuts. Due to the global nature of the method it allows for simultaneous treatment of multiple sources and receivers, and the influence matrix can therefore be computed in a single step for each multi-layered sector.

Once these kernels are determined, the amplitude of the vertical distribution functions are found by matching the appropriate boundary conditions between the sectors, which is conveniently performed in a Galerkin approach [19]. After solving the boundary element equations, the acoustic field within each sector is determined

directly by a wavenumber integral, including both forward and backward propagating wavefields.

This hybrid method is intended for observing both short and long range sound propagation in multiple isovelocity layered, sharp medium contrasted range dependent ocean environments. In this respect, there are several advantages of this approach compared to existing methods described in the previous section.

- Compared to PE, it is a full wave solution including both forward and backward propagating waves. These waves can be treated separately enabling analysis of reverberation from individual features in the environment.

- In contrast to normal mode approaches, problems with halfspaces can be treated, *i.e.* problems with branch line integral contributions. Normal mode has to include virtual (complex wavenumber) modes [58] to represent the continuous spectrum whereas this method directly deals with a wavenumber integral.

- The cumbersome radiation conditions for FD and FEM in the frequency domain are conveniently handled and automatically included in the wavefield representation. In addition, this method is applicable to both short and long range propagation problems.

- The wavenumber integration within each sector enables elimination of the range discretization within each sector from the degrees of freedom. The length of each sector can therefore be chosen arbitrarily large without affecting the number of degrees of freedom in the BIE solution. Furthermore, the Galerkin boundary integral formulation reduces the degrees of freedom to the amplitudes of the distribution functions in the vertical cuts. The proposed technique is therefore more suited to problems in ocean acoustics, where the range variation of the environment is much slower than the depth variation. Additionally, as will be demonstrated, this method is robust in the degrees of freedom employed.

- As in the case of traditional wavenumber integration methods, the field within each sector is directly represented as a wavenumber integral, the kernel of which is important for physical interpretation purposes such as mode coupling and coupling into seismic waves in the bottom and an ice cover.
- The method is applicable to elastic range dependent environments.
- Finally, a marching solution including single back-scattering can be obtained if multiple back-scattering is ignored, significantly reducing the computational requirements.

1.3 Thesis Organization

Following the introduction, this thesis is composed of five chapters and appendices.

In Chapter 2, the preliminary knowledge required for the formal derivation of the hybrid Galerkin boundary integral–wavenumber integration method is discussed. We begin by describing the boundary integral method which is appropriate for a vertically stratified acoustic medium. This is formulated in the frequency domain in terms of Helmholtz indirect boundary integral equation. Subsequently, a brief outline is presented of the numerical wavenumber integration method algorithm, SAFARI (acronym for Seismo Acoustic Fast-field Algorithm for Range Independent environments), for horizontally layered, range homogeneous problems employing the so-called direct global matrix method [43] for determining the depth dependent Green's function.

Formal derivation of the proposed method for acoustic media is given in Chapter 3. The solution is comprised of four separable components: the real point source solution, solution of line distributed fictitious sources of unknown strength used to represent the vertical boundary contributions, and two homogeneous solutions which must accompany these source solutions to satisfy the horizontal boundary conditions in the layered media. Each component is simultaneously expressed as

a basis function expansion and as a horizontal wavenumber integration. The basis function expansion is used for the matching of the boundary conditions at the vertical interfaces while the horizontal wavenumber integration is needed to find the homogeneous solutions for the satisfaction of the horizontal boundary conditions for the vertical stratification of the media. Following the field expressions derivation, the Galerkin boundary integral equation technique for the discretely varying range dependent problem is explained along with the final field evaluation method. Derivation of the field equations for elastic media is presented in Appendix A.

Chapters 4 and 5 are devoted to examining the feasibility and efficiency of the proposed hybrid method for solving stepwise varying range dependent ocean acoustic propagation problems. Description of various numerical aspects of the proposed hybrid method are given to clarify which types of problems it is most appropriately applied. Illustrative numerical examples of canonical problems, which indirectly proves the validity of this method, are presented, followed by other examples of ocean acoustics reverberation problems.

Finally, concluding remarks of this study are presented along with suggestions for further research direction in the realm of combined boundary integral–wavenumber integration method.

Chapter 2

Review of Boundary Integral Equation and Wavenumber Integration Method

Although the boundary integral equation formulation for acoustic waves was introduced more than a century ago by Helmholtz and Kirchoff, the use of this method to solve problems of wave propagation in multi-layered media has been limited due to the difficulty of determining the kernels. Recent development of Green's function methods using wavenumber integration techniques enables the evaluation of the kernel of the boundary integral equation formulation for multi-layered media in an efficient manner. In this chapter, preliminary discussions needed for the formal derivation of combining the two methods will be given. We begin by describing the boundary integral method which is appropriate for vertically stratified acoustic media and subsequently briefly outline the wavenumber integration method using the direct global matrix method for horizontally layered range homogeneous problems.

2.1 Boundary Integral Equation(BIE) Formulation

Given a governing equation and boundary conditions for a physical problem, the shape of the boundary is of significance in the classical approach of separation of variables where only a limited class of geometries are available. Other methods which relieve this restriction can be categorized as differential or integral type depending on whether the numerical procedure precedes or follows the integration of the governing equations. Compared to a differential method such as FDM and FEM which requires discretization of the whole domain, BIE is based on an integral formulation requiring only a surface discretization. Thus in ocean related acoustic propagation where the domain is of "infinite" extent, BIE is more suited for solving long range propagation problems. Numerous examples of the boundary integral equation method applied to acoustic scattering problem can be found in the literature (for reference listing, see Shaw [52]). Colton and Kress [11] have detailed the theory of the acoustic integral equation and Schuster *et al.* [50] give a comprehensive treatment of various direct BIE schemes along with analytic and numerical considerations in scattering theory.

Applications of BIE are primarily found in wave scattering problems in unbounded media where the free-space Green's function can be used. Unfortunately in ocean acoustic problems, the number of known Green's function for specific geometry and boundary condition is quite small and corresponds essentially to those problems which could have been solved by separation of variables. Thus, with a free-space Green's function formulation, the surface integration term in the time harmonic Helmholtz integral equation has to be performed not only for the scatterers but also for the upper and lower interfaces of the ocean environment in which case the numerical solution via discretization of the surface turns out to be computationally very expensive. Use of the Green's function which satisfies the boundary conditions for these infinite interfaces has to be made, in which case only

the scatterers boundary needs to be discretized. The Green's function for ocean environments can be represented by either ray representation, modal expansion or spectral wavenumber integration. Ray representation is a high frequency approximation with too many rays required for large source-receiver separation. On the other hand, modal expansion requires introduction of a false bottom and inclusion of many complex modes for short source-receiver separation even when the frequency is relatively low. Dawson *et al.* [13] have used the modal expansion to provide the Green's function for solving scattering from compact deformation of an acoustic oceanic waveguide's surfaces. Lu [38] combined the ray and mode expansion for the Green's function to solve wave scattering by scatterers in layered acoustic media.

Spectral wavenumber integration yields a full wave solution at the expense of computational difficulty and time. With the advent of fast field algorithms and digital computing power, it is being favored over other methods of finding the Green's function. In seismology, much research has been conducted using hybrid BIE and discrete wavenumber approach to solve scattering problems for layered elastic media [6] [3] [20] [30]. Schuster *et al.* [49] [51] have combined boundary integral method with Haskell-Thomson method to solve for scatterers in plane-layered media using spectral expansion of the Green's function. In parallel with the work presented in this thesis, Gerstoft and Schmidt [21] combined the direct global matrix-wavenumber integration method and boundary integral method to solve scattering and reverberation problems for facets in plane-layered seismo-acoustic media.

All of the above cited works have applied BIE method to solve for inhomogeneity of limited size in an otherwise homogeneous medium. Range dependence occurring in a step-wise manner and continuing for long spatial duration, like abrupt sea bottom elevation in the continental shelf or arctic surface ice in marginal zones with cutting edges or possible medium characteristics change where currents meet, are not amenable to treatment by these methods. In this context, the present new method has the power to solve these acoustic scattering and reverberation

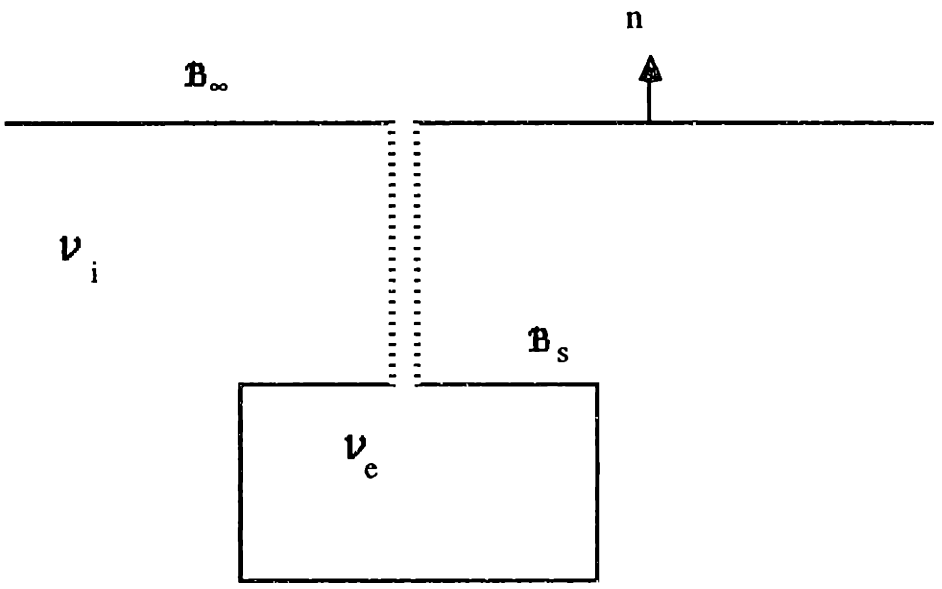

Figure 2.1: Schematic diagram of scatterer in infinite half-space. The interior($\mathcal{V}_i$) and the exterior domain($\mathcal{V}_e$) are separated by the boundaries $\mathcal{B}_s$ and $\mathcal{B}_\infty$.

problems as long as the variance of the ocean and possibly scatterers can be divided into rectangular homogeneous acoustic media. To gain some insight to the present method, review of the Helmholtz integral equation in plane geometry will be given with emphasis on the *indirect* method of monopole-only distribution.

2.1.1 Helmholtz Integral Equation

For the scalar functions φ_1 and φ_2 which are twice continuously differentiable in a region $\mathcal{V}$ bounded by the closed surface $\mathcal{B}$, Green's theorem can be written as

$$\int\int_{\mathcal{V}} (\varphi_1 \nabla^2 \varphi_2 - \varphi_2 \nabla^2 \varphi_1) dA = \oint_{\mathcal{B}} \vec{n} \cdot (\varphi_1 \nabla \varphi_2 - \varphi_2 \nabla \varphi_1) dl \qquad (2.1)$$

with $\vec{n}$ being the outward normal vector. This is essentially the Gauss (divergence) theorem which is the building block of the boundary integral equation method.

Consider an inhomogeneity in an otherwise homogeneous infinite half-space as

shown in Fig. 2.1. The displacement potentials in the interior and the exterior domain are called ϕ and ϕ^* respectively. For simplicity we concentrate on the interior domain problem. In each of the domains, the potentials satisfy the Helmholtz reduced wave equation with time harmonic dependence $e^{i\omega t}$ implied.

$$\nabla^2\phi + h^2\phi = Q(\vec{x}) \tag{2.2}$$

where Q represents the volume source term and h is the acoustic medium wavenumber equal to ω/C where C is the medium sound speed. We define the Green's function G as the function satisfying the same governing equation except for replacement of the right hand side by the inhomogeneous Dirac-delta function with yet arbitrary boundary conditions.

$$\nabla^2 G(\vec{x};\vec{x}_o) + h^2 G = \delta(\vec{x} - \vec{x}_o)\,. \tag{2.3}$$

$\vec{x}$ is the field point and $\vec{x}_o$ the source point. Identifying ϕ as φ_1 and G as φ_2, Eq. 2.1 combined with Eqs. 2.2 and 2.3 becomes

$$\int\int_{\mathcal{V}_i} \phi\delta(\vec{x} - \vec{x}_o)dA(\vec{x}) = \int\int_{\mathcal{V}_i} GQ(\vec{x})dA + \oint_{\mathcal{B}} \left(\phi\frac{\partial G}{\partial n} - G\frac{\partial\phi}{\partial n}\right) dl(\vec{x})\,. \tag{2.4}$$

The integral involving the source term Q will be treated separately and will be denoted as ψ_s in the following and we will treat only the homogeneous solution. The value of the volume integral of the delta function is either the kernel itself or zero depending on whether the observation point $\vec{x}_o$ is located inside or outside of the volume of interest. For the observation point on the boundary, we follow the conventional rule of taking half the value of its kernel since the indentation of the singularity becomes a semi-circular arc. Then we arrive at the Helmholtz integral equation for ϕ as

$$\oint_{\mathcal{B}} \left(\phi\frac{\partial G}{\partial n} - G\frac{\partial\phi}{\partial n}\right) dl = \begin{cases} \phi(\vec{x}_o) & \vec{x}_o \in \mathcal{V}_i \\ \phi/2 & \vec{x}_o \in \mathcal{B} \\ 0 & \vec{x}_o \in \mathcal{V}_e \end{cases}\,. \tag{2.5}$$

For the two-dimensional case, this is often referred to as Weber integral equation [52]. The corresponding equation in the time domain, referred to as Kirchoff integral equation, can be obtained in a similar manner for the full wave equation. Here it is more convenient to work in the frequency domain with harmonic time dependence since we will be combining this integral equation with the wavenumber integration-global matrix method.

2.1.2 Discussion

The original governing partial differential equation and boundary conditions have been transformed to a single integral equation with boundary conditions absorbed in the surface integral. Once this equation is solved for values on the boundary, the field at every point inside the volume of interest is given by the integration over the boundary.

The boundary condition along with radiation condition for the Green's function can be chosen arbitrarily. Simply, it can be chosen as the free-space Green's function satisfying Sommerfeld radiation condition which in plane geometry is a Hankel function $H_0^{(2)}(k|\vec{x} - \vec{x}_o|)$. Using the free-space Green's function then requires integration over the infinite boundary $\mathcal{B}_s + \mathcal{B}_\infty$ as shown in Fig. 2.1. Truncation of the boundary along with absorbing boundary conditions have to be introduced for numerical treatment when closed form solutions cannot be found. This is especially critical for ocean environments where the free surface and bottom boundaries extend to "infinity". If we choose the Green's function G to satisfy the same boundary condition as ϕ for certain regions of the boundary, the integration over $\mathcal{B}$ for that portion of the boundary is identically zero.

Assuming that the exterior domain is filled with same medium as the interior one, the Helmholtz integral equation for the '*saltus*' problem, corresponding to replacing the physical surface by a geometrically identical boundary of monopoles

and dipoles, in terms of the exterior solution ϕ^* becomes

$$\oint_B \left(\phi^* \frac{\partial G}{\partial n'} - G \frac{\partial \phi^*}{\partial n'} \right) dl(\vec{x}) = 0 \tag{2.6}$$

for an observation point $\vec{x}_o$ in $\mathcal{V}_i$. Adding Eq. 2.5 and Eq. 2.6 using the relation $\vec{n} = -\vec{n}'$ gives

$$\phi(\vec{x}_o) = \oint_B \left[(\phi - \phi^*) \frac{\partial G}{\partial n} - G \left(\frac{\partial \phi}{\partial n} - \frac{\partial \phi^*}{\partial n} \right) \right] dl(\vec{x}) \tag{2.7}$$

for field point located within $\mathcal{V}_i$. If we choose the potential to be continuous across the boundary B but allow the normal derivative of it to be discontinuous, we arrive at the simplified integral equation

$$\phi = \oint_B G \nu \, dl \tag{2.8}$$

where $\nu = \left(\frac{\partial \phi}{\partial n} - \frac{\partial \phi^*}{\partial n} \right)$ is the *indirect* unknown source strength. Physically, the Green's function G can be viewed as the solution from the distribution of sources on the boundary B pulsating symmetrically in the normal direction of the boundary. Thus for a straight boundary, this will cause the field to be symmetric with respect to the boundary. It can be shown that Eq. 2.8 is also valid on the boundary B by adding Eq. 2.5 and Eq. 2.6 and realizing that ϕ equals ϕ^* on the boundary.

Following the above two arguments, we are led to an *indirect* integral equation which has been greatly simplified at the expense of finding the appropriate Green's function. This can be justified since, in a layered ocean environment, we can efficiently find the Green's function which satisfies the boundary conditions at the horizontal interfaces, as well as satisfying the symmetry of the potential at the vertical boundaries, using the global matrix method described in the following section.

2.2 Wavenumber Integration(WI) Method

With the introduction of the efficient numerical code SAFARI [43], the wavenumber integration method has become very popular over the last few years for solving various range independent ocean related acoustic problems. Using the direct global matrix method, Schmidt and Jensen [46] give full wave solution for plane-layered seismo-acoustic medium in terms of spectral integration. Schmidt et al [45] [48] have extended the formulation and numerical implementation to arbitrary three-dimensional range independent problems. Using the same formalism, Kim [33] implemented various seismic sources into SAFARI.

For the multi-layered range independent problem, the solution is comprised of the field produced by the source in the absence of layers and an unknown field which satisfies the homogeneous wave equation in each layer. The unknown field is determined by requiring the boundary conditions at each of the interfaces to be satisfied along with appropriate radiation conditions. In a full wave solution these fields are expressed as a wavenumber integral, the kernels of which enables direct physical interpretation. Another advantage of wavenumber integration method is its capability to treat various scenarios of ocean acoustic problems, i.e. multiple sources, arbitrary fluid-solid layering [43], transverse isotropy and some degree of interface roughness [36].

In this section a brief outline is presented of the wavenumber integration method which forms one of the basic tools for the present solution technique, along with some discussions concerning the incorporation of this scheme into the present hybrid method.

2.2.1 Derivation of Field Equations

Consider an ocean environment which can be modeled as range independent and horizontally stratified. Here we will limit the presentation to a plane layered acoustic medium remembering that the extension to other geometries and elastic media follows directly without further complications. Harmonic time dependence $e^{i\omega t}$ is assumed, but transient solutions can be obtained by Fourier synthesis. In each of the layers, the acoustic medium is assumed to be homogeneous, characterized by its compressional sound speed C and density ρ. In each layer, there exists a scalar (displacement) potential ϕ which satisfies either the inhomogeneous or homogeneous, reduced Helmholtz equation in an xz-cartesian coordinate system depending on the presence or absence of sources. The reduced Helmholtz equation is given by Eq. 2.9.

$$\nabla^2\phi_n + h_n^2\phi_n = \begin{cases} \delta(x - x_s)\,\delta(z - z_s) \\ 0 \end{cases} . \tag{2.9}$$

Referring to Fig. 2.2, the subscripts refer to the layer number and h_n is the compressional medium wavenumber, $h_n = \omega/C_n$. The inhomogeneous term represents a compressional line source perpendicular to the x-z plane located at $x = x_s$ and $z = z_s$ and its contribution $\dot{\phi}$ will be superimposed whenever a source is present in that layer. The boundary conditions to be satisfied are continuity of pressure and normal displacement at all ranges for upper and lower boundary of the layer, together with the radiation condition of no incoming waves from infinity. For a half-space layer one of the interface boundary condition changes to a radiation condition requiring that no waves originate at infinity.

Applying the forward Fourier transform in range x to Eq. 2.9, we obtain the depth-separated wave equation as

$$\frac{\partial^2}{\partial z^2}\phi_n(s,z) - (s^2 - h_n^2)\phi = \begin{cases} \delta(z - z_s)e^{isx_s} \\ 0 \end{cases} \tag{2.10}$$

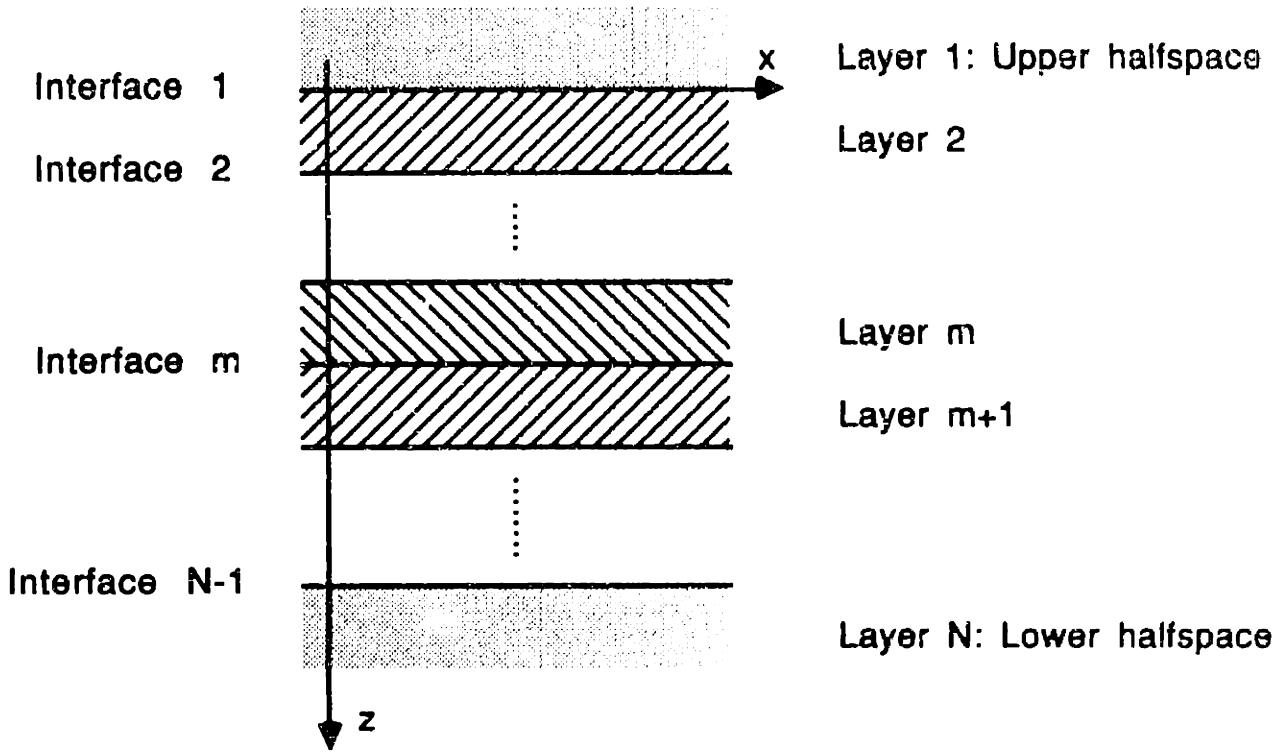

Figure 2.2: Horizontally stratified medium where each layer is homogeneous, characterized by its medium wavenumber h_n and density ρ_n.

where s is the horizontal wavenumber and $i\alpha(s) = i\sqrt{s^2 - h_n^2}$ is the vertical wavenumber. After solving the depth-separated equation and applying the inverse Fourier transform, a particular solution of the inhomogeneous equation Eq. 2.9 is given by

$$\dot{\phi}\,(x,z) = -\int_{-\infty}^{\infty} \frac{e^{-|z-z_s|\alpha_n}}{\alpha_n} e^{-is(x-x_s)}\, ds\,. \tag{2.11}$$

The solution of the homogeneous version of Eq. 2.10 followed by the inverse transform, is given by the following integral representation for the solution to the homogeneous equation.

$$\phi_n(x,z) = \int_{-\infty}^{\infty} \left[A_n^-(s)e^{-z\alpha_n(s)} + A_n^+(s)e^{(z-l)\alpha_n}\right] e^{-is(x-x_s)}\, ds \tag{2.12}$$

where $A_n^{\pm}(s)$ are unknown functions of the horizontal wavenumber s to be found by imposing boundary conditions and l is the depth of the layer.

Note how the depth eigenfunctions, $e^{-z\alpha_n}$ and $e^{(z-l)\alpha_n}$, are written in terms of a local coordinate system with origin at the top of the layer. This ensures that unconditional stability is achieved when the global system of equations is solved for the unknowns. Each element of the global system is comprised of functions of wavenumber and depth eigenfunctions. For purely imaginary arguments of the exponential functions, the magnitude of the exponentials is unity. For evanescent waves with real arguments of the exponential functions, the magnitude of the exponentials do not exceed unity for any value of z within the layer, and the solution becomes unconditionally stable for any value of the wavenumber. Note also the source range x_s appearing in the exponential. This accounts for the offset of the source from the origin of the local coordinate system, making the unknown spectrum function symmetric with respect to horizontal wavenumber s.

By definition and *via* Hooke's law, displacements and pressure in the field are given by

$$\begin{aligned} u_n(x,z) &= \frac{\partial \phi}{\partial x} \\ w_n(x,z) &= \frac{\partial \phi}{\partial z} \\ p_n(x,z) &= -\rho\omega^2\phi\,. \end{aligned} \tag{2.13}$$

For multi-layered media, the unknowns $A_n^{\pm}(s)$ can only be found numerically by imposing the boundary conditions at the interfaces. This is achieved by matching the kernels of the integral representations for each horizontal wavenumber s. This gives the full wave solution which is termed the depth-dependent Green's function because the kernel is only a function of depth. In the next section the direct global matrix method is described for finding the unknowns of the depth dependent Green's function.

2.2.2 Numerical Solution Technique

For multi-layered media, the exact response of the layer stack is computed using Haskell matrices [25], or Kennett iteration [32], or the direct global matrix method(DGM) [43]. The DGM approach has the capability of efficiently treating multiple sources in a single step which is essential in the present hybrid method as will be evident in the next chapter.

In the direct global matrix method, the unknown arbitrary functions of s are found numerically at a discrete number of horizontal wavenumbers from the system of equations that express the boundary conditions to be satisfied. If the kernels for the relevant field variables to be matched for layer n(subscripts) at interface m(superscripts) are denoted in column vector as $\{v\}_n^m$ with the source terms written with an asterisk on top, then the local system of equations at interface m is

$$\{v\}^m = \{v\}_m^m + \{\mathring{v}\}_m^m = \{v\}_{m+1}^m + \{\mathring{v}\}_{m+1}^m \,. \tag{2.14}$$

Rearrangement of Eq. 2.14 for the unknown arbitrary vector $\{a\}_m$, i.e. $A_m^{\pm}(s)$'s , with coefficient matrix $[c]_n^m$ which consists of functions of the wavenumber and the depth exponentials gives

$$[c]_m^m\{a\}_m - [c]_{m+1}^m\{a\}_{m+1} = \{\mathring{v}\}_{m+1}^m - \{\mathring{v}\}_m^m \,. \tag{2.15}$$

Combining the local system of equations for $N-1$ number of total interfaces into the global system using the *pointers* similar to topology matrices found in finite-element

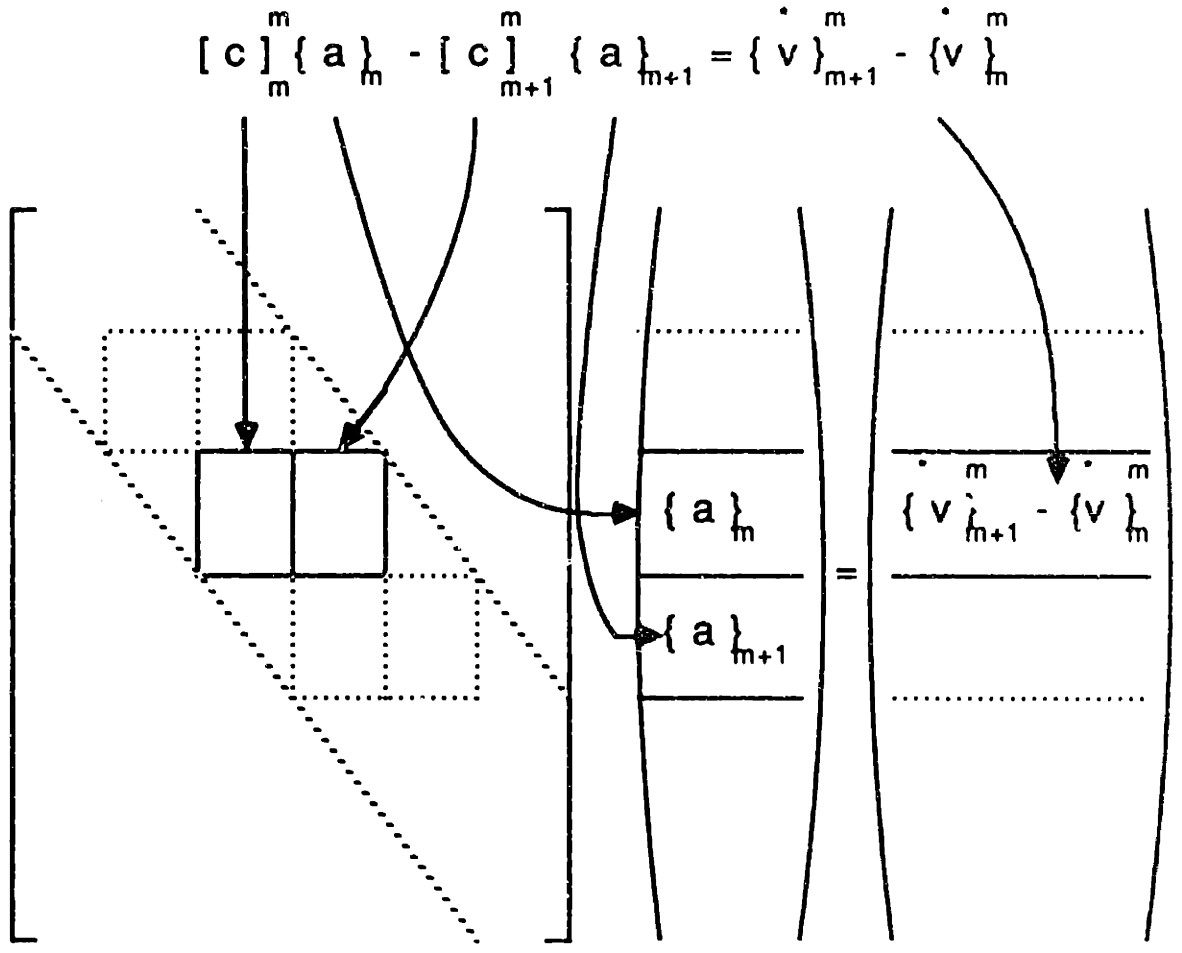

Figure 2.3: Mapping between the local and the global systems of equations. The local systems of equation is written for the mth interface.

method, a global system of equation is obtained as follows (Fig. 2.3).

$$[C]\{A\} = \{\dot{V}\}\,. \tag{2.16}$$

Although this equation has to be solved for every horizontal wavenumber, the mapping of the local systems to a global matrix is unique for a given environment as seen in Fig. 2.3. So once the pointers for the mapping are determined, the calculations needed at each horizontal wavenumber are reduced to the creation of the local coefficient matrices $[c]$ and solving Eq. 2.16. This is done by Gaussian

elimination with partial pivoting and unconditionally stable solution is obtained with this method. For detailed explanation of numerical stability, refer to Schmidt and Jensen [46]. Another advantage in using this scheme is its capabilities of treating multiple right hand sides, i.e. multiple sources. This property is crucial for the development of the present hybrid method.

Once the global system of equation has been solved at a discrete wavenumber, the kernels for the field variables can be readily evaluated at any depth by superimposing Eq. 2.11 and Eq. 2.12. The depth eigenfunctions e^{-sa_n} and $e^{(s-l)a_n}$ are the only additional terms to be calculated.

For numerical treatment, the wavenumber integrals extending to infinity have to be truncated at some point where its contribution is negligible. This is usually truncated at 10 to 20 % higher than the maximum medium wavenumber [43] to include all possible modes present. Sudden truncation of the integrand when it is not fully zero could cause what is known as the Gibb's phenomenon even though the remaining part of the kernel does not contribute to the field due to cancellation from the oscillatory term e^{-isz}. This can be avoided by tapering the envelope of the kernel over several oscillations from the truncation point.

Within the truncated horizontal wavenumber interval, the global system of equations are solved at equidistantly separated M sampling points

$$s_m = s_{\min} + m\Delta s, \qquad m = 0, 1, \ldots, (M-1)\,. \tag{2.17}$$

For plane geometry, these sampling points must include both the positive and the negative part of the spectrum. Since the unknown function was set up to be symmetric with respect to s (by taking into account the offset of the source from the origin of the local coordinate system by the shift in the exponentials in Eq. 2.11 and Eq. 2.12), only the positive spectrum part needs to be determined, dividing the numerical effort in half. Integration of the kernel can be performed conveniently using the FFT by selecting the number of sampling points M to be an integer power

of 2, simultaneously yielding all values of the field at M equidistant ranges

$$x_n = x_{\min} + n\Delta x, \qquad n = 0, 1, \ldots, (M-1) \tag{2.18}$$

where range increment is given by the sampling theorem as

$$\Delta x = \frac{2\pi}{\Delta s M} \tag{2.19}$$

and the valid maximum range is simply $X = \Delta x M$. Then the following discrete approximation of the integral is obtained.

$$\begin{aligned} G(x_n, z) &= \int_{-\infty}^{\infty} g(s, z) e^{-isx} ds \\ &\simeq \Delta s e^{-is_{\min} x_n} \sum_{m=0}^{M-1} \left[g(s_m, z) e^{-is_{\min} m \Delta s} \right] e^{-i2\pi mn/M} \end{aligned} \tag{2.20}$$

where the summation is performed by means of an FFT. Thus signals outside the maximum range X are aliased (or "wrapped around"). Aliasing can be reduced by selecting the parameters such that X becomes large enough to ignore the wrapped around signals. Another way to overcome aliasing problem is to use complex contour integration, reducing the wrapped around signals. This is explained in detail by Schmidt [43] for cylindrical geometry. Following the same argument, explanation of complex contour integration for plane geometry with both the positive and the negative part of the spectrum will be given in chapter 3.

In the next chapter, details of the indirect boundary integral equation method of distributing vertical line displacement sources combined with the wavenumber integration approach for solving a laterally inhomogeneous vertically stratified problem will be presented.

Chapter 3

Formulation of Hybrid Galerkin Boundary Integral and Wavenumber Integration Approach

The previous chapter has provided the basic starting tools, *i.e.* indirect boundary integral equation method(BIE) and the wavenumber integral/direct global matrix method(DGM), for the development of the hybrid range-dependent layered media solution technique. In this chapter, the formal derivation of the hybrid Galerkin boundary integral and wavenumber integration method is given.

First we divide the range dependent ocean into range independent *sectors* where each sector is allowed to be horizontally stratified. By employing the concept of the saltus problem, the solution within each sector is expressed as a boundary integral, described in the previous chapter as a distribution of sources on the vertical boundaries of the sector by using the Green's function, noting that Green's function already satisfies the boundary conditions for horizontal interfaces. Each sector then becomes a range independent problem for which the kernels are conveniently found using the global matrix approach. Once these kernels are determined, the

amplitude of the vertical distribution functions are found by matching the appropriate boundary conditions between the sectors, conveniently performed in a Galerkin approach.

3.1 Statement of the Problem

We are concerned with the range dependent problem in a stratified acoustic medium, where the range dependence occurs in a stepwise manner such that the environment can be geometrically separated into rectangular elements as depicted in Fig. 3.1. Each rectangular element is assumed to be isotropic and homogeneous and characterized by its sound speed and density.

Here we intentionally focus the derivation on acoustic media, but we note that it is not difficult to extend the idea to elastic media by including the shear wave potential together with the additional boundary conditions. Expressions for the elastic media are derived in Appendix A. Compared to other existing range dependent solution methods such as the parabolic equation(PE) or the coupled mode, no difficulties are encountered when extension to elastic medium is considered. Since the present method is based on a global matrix method, the treatment of elastic medium can be considered simply by adopting the shear wave terms in the same manner.

The derivations now developed are for a two-dimensiona. geometry with a line source extending infinitely in the direction perpendicular to the plane. Cylindrical geometry where medium changes in the radial direction , *i.e.* superposition of concentric layered rings, with a point source located at the origin of the cylindrical geometry may be considered when the cylindrical spreading effect is accounted for in the final stage of evaluating the field. The sources are assumed to be harmonic with angular frequency ω and the time dependence $e^{i\omega t}$ is implied in the following development.

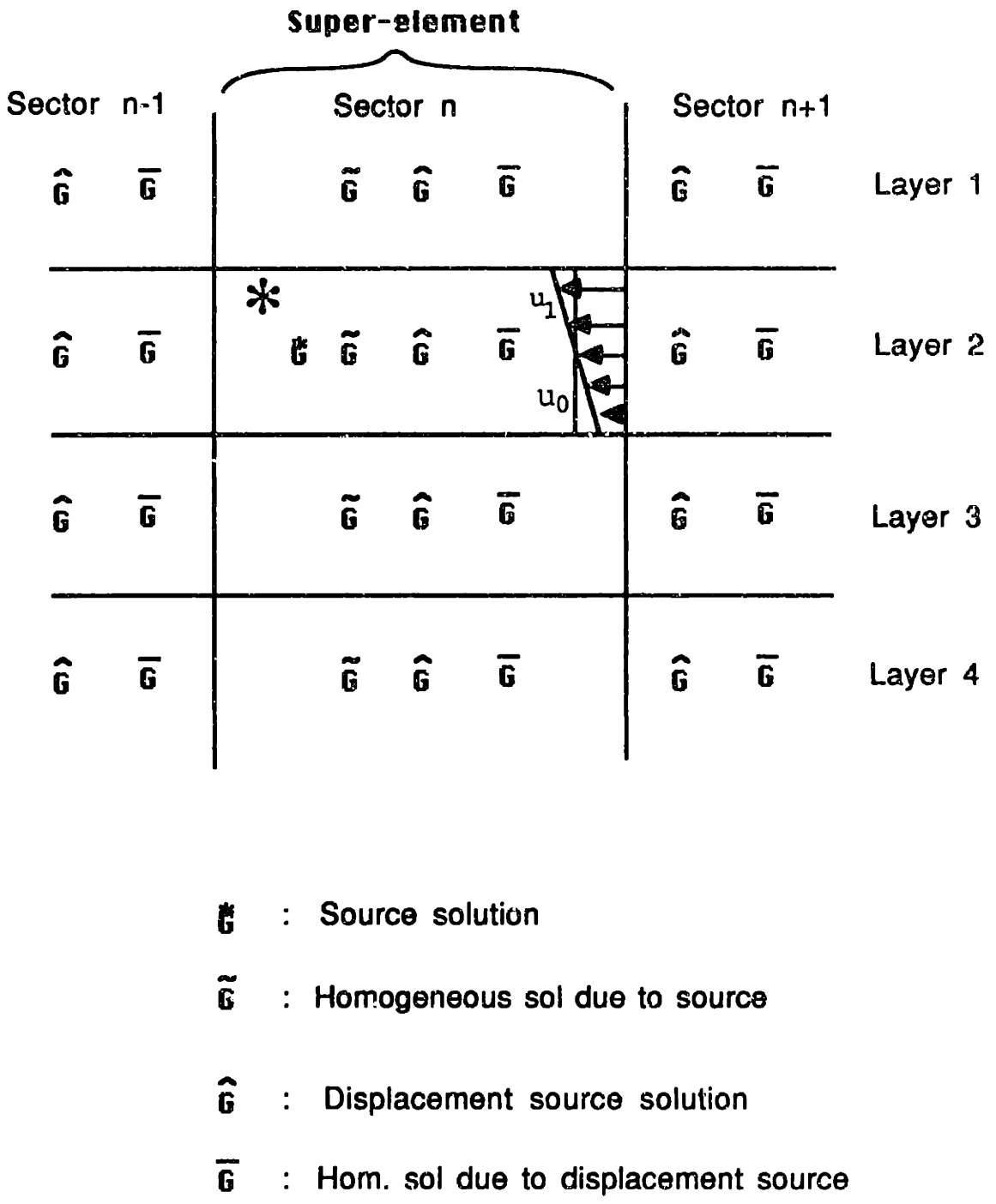

Figure 3.1: Nomenclature for hybrid BIE+WI method. After discretization into homogeneous rectangular elements, range and depth direction partitions are called sectors and layers, respectively with decomposed total solution as shown.

3.2 Overview of Approach

Before we proceed, an analogy to the 'super-element' used in finite element methods(FEM) will aid in understanding the approach more clearly. Referring to Fig. 3.1, the range discretized or 'sub-structured' sectors can be regarded as a 'super-element' where the horizontal interfaces, *i.e.* 'nodes', within the super-element are treated by the wavenumber integration method. The 'nodal displacements' of the super-element are the unknown source strengths where the influence of these sources, or equivalently the 'stiffness' matrix, are determined by the Galerkin boundary integral method.

We first divide the range dependent ocean into segments of range independent *sectors* separated by the vertical boundaries at each discontinuity, where each sector is allowed to be horizontally stratified. Within each sector, the field can be expressed as an integral over the enclosing boundary, *per* Eq. 2.8. In the boundary integral equation, the kernel G is chosen to be the depth dependent Green's function for a multi-layered media. This already satisfies the horizontal interface boundary conditions, reducing the integration to the vertical portion only. Additionally, by distributing continuous line sources of various shapes extending over the whole depth of each stratified layer, we can adopt Galerkin's method for the solution of the boundary integral equation. Thus the kernel G consists of the field produced by the distributed source in the absence of layers ($\hat{G}$ in Fig. 3.1) and an unknown field which satisfies the homogeneous wave equation in each layer ($\tilde{G}$). These sources are artificial constructions which allow the boundary conditions throughout the model to be satisfied from sector to sector. Thus, it is important to distinguish between the sources used strictly for boundary condition purpose(the artificial sources) and the true sound sources(real sources).

In the case where a real source is present in a particular sector, we add its contributions ($\dot{G}$ and $\tilde{G}$). By properly choosing a set of distribution functions (basis functions) for the field along the vertical cuts, the wavenumber integral-global

matrix solution technique [43] can be applied to determine the kernel G for a unit line distributed source strength. Due to the global nature of the method it allows for simultaneous treatment of multiple sources and receivers, and the influence matrix can therefore be computed in a single step for each multi-layered sector.

Once these kernels are determined, the amplitude of the vertical distribution functions are found by matching the appropriate boundary conditions between the sectors, conveniently performed in a Galerkin approach. Since the field variables are expanded using orthogonal basis functions, we can simply match each expansion coefficients of the basis function. This leads to a local system of equations for each vertical interface. After collecting all the local system of equations into a global system of equations in a manner similar to that of the range independent global matrix method [46], we solve the system of equations using Gaussian elimination technique. This will simultaneously reveal all the vertical distribution function amplitudes. After solving the boundary element equations, the acoustic field within each sector is determined directly by a wavenumber integral, including both the forward and the backward propagating wavefields.

In the following sections, the derivation will be given of the Green's function, as tailored for the boundary integral, combined with the global matrix method (and subsequently the solution of the boundary integral equation by Galerkin's method).

3.3 Green's Function for Layered Medium

Derivation of the Green's function used in the indirect boundary integral method is given for a layered acoustic medium. As discussed in the previous chapter, the field within each partitioned sector can be found from the boundary integral Eq. 2.8 as

$$\phi = \oint_B \mathcal{G}\, \nu\, dl + \phi_s\,, \tag{3.1}$$

where ϕ_s is the real compressional source term if it exists in that particular sector(this will be dealt with in the following section), B consist of two horizontal

interfaces at the top and bottom plus two vertical interfaces, thus entirely bounding the discretized range-depth rectangular sector; and ν is the indirect unknown to be found from conditions of continuity across boundaries. Since we have eliminated the normal derivative of the Green's function in Eq. 2.5, ν is a source which oscillates symmetrically about the vertical axis, giving rise to the Green's function $\mathcal{G}$. This indirect source strength ν, which can be viewed as a discontinuity of the normal displacement at the vertical boundaries, has no physical meaning attached to them as described in Chapter 2. Although this is the case, they are termed *displacement sources* due to the fact that their displacements are discontinuous and are of an explosive source type.

Because the ocean invariably has to be modeled as layered media within each sector, it is impossible to find an analytic expression for the Green's function for the entire layered sector. Instead we resort to numerical methods to find the Green's function as a wavenumber integral. Traditionally this is accomplished by distributing point sources. Here we use continuous line sources of various shapes extending over the whole depth of 'each' horizontally stratified layer. This reduces the total number of sources to be distributed which is advantageous when the Green's function has to be found for multi-layered problems. Here, tensor summation notations are discarded, and each summation is written out explicitly for clarity. Denoting the total number of layers as N and the depth of the ith layer as l_i, with the source contribution ϕ_s suppressed for the time being, Eq 3.1 can be written as

$$\phi_j(x,z) = \sum_{i=1}^{N} \int_{l_i} \mathcal{G}_{ji}(x,z)\, \nu_i \, dl_i \tag{3.2}$$

where $\mathcal{G}_{ji}$ represents the depth-dependent Green's function at layer j due to displacement source of unit strength at layer i. The closed contour integral of Eq. 3.1 has been reduced to integration along the vertical boundaries only, as mentioned in Chapter 2, since the Green's function is chosen to satisfy the same boundary condition, *i.e.* the radiation condition, along the horizontal part of the contour integration. The summation in Eq. 3.2 implies both sides of the vertical boundaries

for a finite sector whereas for a half-infinite sectors they reduce to a single boundary since the integration at infinity vanishes if $\mathcal{G}$ satisfies the radiation condition. It will be shown in the following context that each line integral over the vertical cut can be performed analytically, reducing Eq. 3.2 to

$$\phi_j(x,z) = \sum_{i=1}^{N} G_{ji}(x,z)\,\nu_i \tag{3.3}$$

where integration of $\mathcal{G}$ over the depth direction for each layer has been replaced by G. Thus the Green's function G_{ji} can be viewed as the influence of a distributed line source at the vertical boundary of layer i onto a field point in layer j.

Analogous to the concept of the direct global matrix method for horizontally layered medium, this Green's function can be divided into two components as

$$G_{ij} = \hat{G}_i\delta_{ij} + \bar{G}_{ij} \tag{3.4}$$

where $\hat{G}$ is the solution for a homogeneous infinite medium and applies only to the layer at which the displacement source is located, represented by the Kroenecker delta

$$\delta_{ij} = \begin{cases} 0 & \text{for } i \neq j \\ 1 & \text{for } i = j \end{cases} \tag{3.5}$$

and $\bar{G}$ is the homogeneous counterpart for horizontally layered medium to satisfy the boundary conditions at each horizontal interfaces. In addition to these two components, contributions arising from the real source must be added in sectors where they are present. They are denoted as $\dot{G}$ for source in an infinite medium, and as $\tilde{G}$ for the homogeneous solution in a stratified medium.

Recapping the decomposition of the total solution, we write

$$G(x,z) = \underbrace{\hat{G} + \bar{G}}_{I} + \underbrace{\dot{G} + \tilde{G}}_{II} \tag{3.6}$$

where the first two terms are the combination of the displacement source distributions and the homogeneous solutions; the second terms are for real compressional source and its homogeneous solution. For clarity they are called

$G(x,z)$: total solution or Green's function

$\hat{G}$: (vertical boundary) displacement (source) solution

$\tilde{G}$: (vertical boundary) displacement (source) homogeneous solution

$\dot{G}$: source solution

$\tilde{G}$: (source) homogeneous solution.

which is also shown in Fig. 3.1. In the following sections, analytic expressions for each of the components are dealt with separately.

3.3.1 Displacement Source Green's Function

As mentioned previously, the displacement source Green's function is the solution to Helmholtz equation for a vertically distributed line source in an infinite medium. Two forms of representations are needed for this solution.

1. When the boundary conditions are matched for vertical interfaces, we equate Eq. 3.2 for the left and right sector resulting in a Fredholm integral equation of the first kind for the unknown source strength ν. Numerical solution to this integral equation is performed either by a distribution of point sources which results in a collocation method or by utilizing various sources of finite length in terms of summation of basis functions which lead to the Galerkin method. Since we can perform the integration analytically in the depth direction, it is more efficient to adopt the latter method. Thus we need a representation of the field in terms of a basis function expansion.

2. To arrive at the displacement homogeneous solution for multi-layered media, it is expedient to resort to the DGM approach which takes care of multiple sources in a single computation step. This requires the displacement source solution, which act as sources in this approach, to be represented in terms of a horizontal wavenumber integration.

The above argument is also true for the other solutions $\bar{G}, \dot{G}$, and $\tilde{G}$. An added note is that half-spaces must be treated separately from finite layers since a common basis function cannot be used. Thus far in the math literature, they do not possess a basis function expansion suitable for modification into horizontal wavenumber integral representation. This results because of a convergence problem when the conversion between the vertical and the horizontal wavenumber integral is made (Appendix B). This poses no difficulty for the upper half-space which can be modeled as vacuum for the ocean environment. For the lower half-space, we simply introduce additional layers until there is no significant back-reflected energy. In contrast to the coupled mode theory, where a false bottom is introduced to discretize continuous modes in order to achieve coupling between sectors, causing false energy to propagate back [16], in the method shown here we do not generate any type of false propagation although we might lose some of the energy if the half-space is not sampled to sufficient depth.

Pertinent field variables for matching the boundary conditions are written out explicitly using the same superscript notations for each component as given by Eq. 3.6. The boundary conditions involve the normal displacement u and pressure p for vertical interfaces, and w and p for horizontal interfaces.

Basis Function Expansion

Consider the nth layer of an N layered homogeneous sector depicted in Fig. 3.2. Using the local coordinates it is convenient to use an expansion of the following form based on physical and mathematical considerations [34] [35] [47].

$$\begin{Bmatrix} \hat{u}_n(x,z) \\ \hat{p}_n(x,z) \end{Bmatrix} = \frac{2\pi}{l} \sum_{m=1}^{\infty} \begin{Bmatrix} \hat{U}_{nm}(x) \\ \hat{S}_{nm}(x) \end{Bmatrix} P_{m-1}\left(\frac{z - \frac{l}{2}}{\frac{l}{2}}\right) \tag{3.7}$$

where m is the order of expansion and P_m is the Legendre function and l is the thickness of the layer.

Displacement sources distributed along the vertical boundary of the nth layer

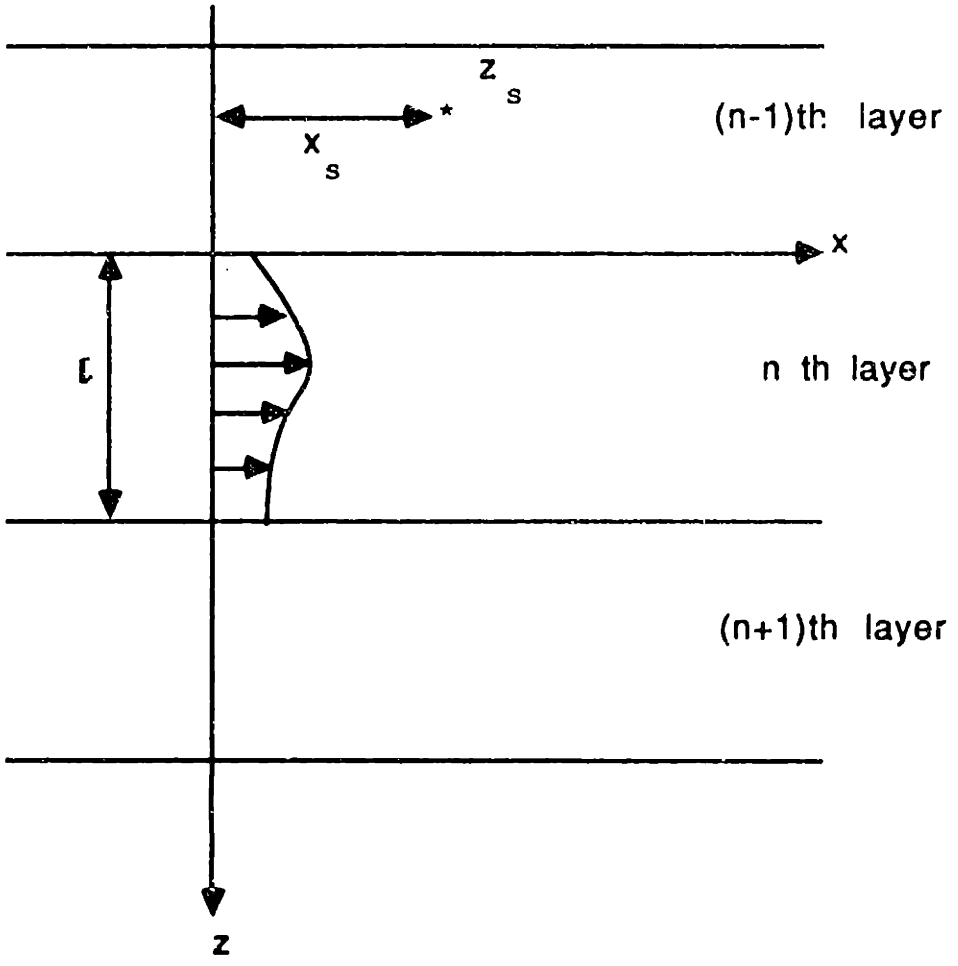

Figure 3.2: Local coordinate system for rectangular elements. l is the layer depth and (x_s, z_s) is the coordinate of the source.

are simply represented as boundary conditions in terms of the unknown source strength $\hat{U}_{nm}(0)$

$$\hat{u}_n(0,z) = \begin{cases} 0 & z<0\,,\ z>l \\ \frac{2\pi}{l}\sum_m \hat{U}_{nm}(0) P_{m-1}\left(\frac{z-\frac{l}{2}}{\frac{l}{2}}\right) & 0\le z\le l \end{cases} . \tag{3.8}$$

and appropriate radiation condition.

Finding the Green's function for this displacement source is equivalent to expressing the expansion functions $\hat{U}(x)$ and $\hat{S}(x)$ in terms of source strength. In this thesis, the inverse and forward Fourier transform pairs are defined as

$$\begin{aligned} f(x) &= \int_{-\infty}^{\infty} g(k)\, e^{-ikx}\, dk \\ g(k) &= \frac{1}{2\pi}\int_{-\infty}^{\infty} f(x)\, e^{ikx}\, dx\,. \end{aligned} \tag{3.9}$$

The displacement potential which satisfies the Helmholtz equation and the radiation condition can be written in terms of the vertical wavenumber spectral representation as

$$\hat{\phi}(x,z) = \int_{-\infty}^{\infty} A(\eta)\, e^{-x\gamma} e^{-i\eta(z-\frac{l}{2})}\, d\eta \tag{3.10}$$

with η being the vertical wavenumber and $i\gamma$ is the horizontal wavenumber given by $i\sqrt{\eta^2-h^2}$ where h is the medium wavenumber. The spectral density $A(\eta)$ is determined by the conditions at the source [26]. We first differentiate Eq. 3.10 with respect to x to produce the horizontal displacement $\hat{u}$ and take the forward Fourier transform with respect to z to give

$$A(\eta)\, e^{-x\gamma} e^{i\eta\frac{l}{2}} = \frac{1}{2\pi}\int_{-\infty}^{\infty} \hat{u}(x,z) e^{i\eta z}\, dz\,. \tag{3.11}$$

Substituting the boundary condition at $x = 0$, Eq. 3.8, and making use of the identity [24]

$$\int_0^l P_{m-1}\left(\frac{z-\frac{l}{2}}{\frac{l}{2}}\right) e^{i\eta z} dz = l e^{i\eta\frac{l}{2}} i^{m-1} j_{m-1}\left(\frac{l\eta}{2}\right) \tag{3.12}$$

gives

$$A(\eta) = -\frac{1}{\gamma}\sum_m i^{m-1}\hat{U}_{nm}(0) j_{m-1}\left(\frac{l\eta}{2}\right)\,. \tag{3.13}$$

Here we can see that the integration over z in the transform has been performed analytically and is accounted for by the spherical Bessel function j_{m-1}. Back substitution into Eq. 3.10 yields

$$\hat{\phi}(x,z) = \sum_m \hat{U}_{nm}(0)\, i^{m-1} \int_{-\infty}^{\infty} e^{-z\gamma} e^{-i\eta(z-\frac{l}{2})}\, j_{m-1}\left(\frac{l\eta}{2}\right) d\eta\,. \tag{3.14}$$

This is the desired Green's function for the displacement source solution in the form of Eq. 3.3 where the depth integration has vanished.

Finally, we rewrite the field variables for the horizontal displacement and the pressure in terms of the basis functions:

$$\begin{aligned} \hat{u}_n(x,z) &= \frac{2\pi}{l} \sum_{m=1}^{\infty} \hat{U}_{nm}(x) P_{m-1}\left(\frac{z-\frac{l}{2}}{\frac{l}{2}}\right) \\ \hat{p}_n(x,z) &= \frac{2\pi}{l} \sum_{m=1}^{\infty} \hat{S}_{nm}(x) P_{m-1}\left(\frac{z-\frac{l}{2}}{\frac{l}{2}}\right)\,. \end{aligned} \tag{3.15}$$

The expansion coefficients, which are a function of range only, are found by equating the displacement and the pressure derived from Eq. 3.14, and Eq. 3.15 and using the orthogonality relation for the Legendre functions [1]

$$\int_0^l P_{m-1}\left(\frac{z-\frac{l}{2}}{\frac{l}{2}}\right) P_{n-1}\left(\frac{z-\frac{l}{2}}{\frac{l}{2}}\right) dz = \frac{l}{2m-1}\delta_{mn} \tag{3.16}$$

where δ_{mn} is the Kroenecker delta. This yields

$$\begin{aligned} \hat{U}_{nm}(x) &= \sum_{k=1}^{\infty} C_{nm,k}(x) \hat{U}_{nk}(0) \\ \hat{S}_{nm}(x) &= \sum_{k=1}^{\infty} B_{nm,k}(x) \hat{U}_{nk}(0) \end{aligned} \tag{3.17}$$

where the influence functions of the kth order source on the mth order expansion for the displacement and the pressure are given by

$$\begin{aligned} C_{nm,k} &= \frac{l}{2\pi}(2m-1)(-1)^{m-1} i^{m+k-2} \int_{-\infty}^{\infty} e^{-z\gamma} j_{m-1}\left(\frac{l\eta}{2}\right) j_{k-1}\left(\frac{l\eta}{2}\right) d\eta \\ B_{nm,k} &= \frac{l}{2\pi}\lambda_n h_n^2 (2m-1)(-1)^{m-1} i^{m+k-2} \int_{-\infty}^{\infty} \frac{e^{-z\gamma}}{\gamma} j_{m-1}\left(\frac{l\eta}{2}\right) j_{k-1}\left(\frac{l\eta}{2}\right) d\eta \end{aligned} \tag{3.18}$$

and λ is a Lamè constant. Since the displacement source solution applies only at the layer at which it is located, no summation for multiple layers appears. When $x = 0$, the influence of kth order source for mth order displacement should be

$$C_{nm,k}(0) = \begin{cases} 0 & m \neq k \\ 1 & m = k \end{cases} \tag{3.19}$$

since we have used symmetric displacement sources. This is seen to be true when the following identity [24] is substituted into Eq. 3.18.

$$\int_{-\infty}^{\infty} j_{m-1}\left(\frac{l\eta}{2}\right) j_{k-1}\left(\frac{l\eta}{2}\right) d\eta = \frac{2\pi}{l(2m-1)}\delta_{mk} \,. \tag{3.20}$$

The kth order displacement source influences the mth order pressure at $x = 0$ only when $m + k$ is even. Had we used dipoles instead in the boundary integral formulation, *i.e.* the stress source, the situation would be reversed and this is analogous to the displacement or stiffness method in finite element analysis. When $x \neq 0$ displacement sources of every order influences every order of the field expansion as long as $m + k$ is even.

These influence functions and all others that follow, which construct the influence matrix for the unknown source strength $\hat{U}_{nm}(0)$, should be evaluated with precision since the success of the hybrid BIE+WI method depends highly on the accuracy of the source strength. The integration in Eq. 3.18 is performed using Gauss-Tchebycheff quadrature scheme (Appendix D) with square-root weight functions included explicitly to account for $\gamma = \sqrt{\eta^2 - h^2}$.

Horizontal Wavenumber Integral Representation

The homogeneous displacement solution accompanying the displacement source solutions for the multi-layered medium is found by the DGM approach which requires the integral representation to be expressed in terms of the horizontal wavenumber.

Using contour integration, the vertical wavenumber integral Eq. 3.10 can be deformed into a horizontal wavenumber integral (Appendix B) as

$$\hat{\phi}(x,z) = i \int_{-\infty}^{\infty} A\left(-\text{sign}(z - \frac{l}{2})i\alpha\right) e^{-|s-\frac{1}{2}|\alpha} \frac{s}{\alpha} e^{-isx} \, ds \tag{3.21}$$

where we have used s for horizontal wavenumber and vertical wavenumber $i\alpha = i\sqrt{s^2 - h^2}$. The above representation is valid only for $z \leq 0$ and $z \geq l$ (Appendix B), but still allows the application of the global matrix method for satisfying the horizontal interface boundary conditions since it is at the interfaces at $z = 0, z = l$ of each layer that the fields are being matched. When the field is sought inside the layer($0 \leq z \leq l$), we resort to numerical quadrature of equivalent discrete source distribution (Appendix C).

From Eq. 3.13

$$A\left(-\text{sign}(z - \frac{l}{2})i\alpha\right) = -\frac{1}{is}\sum_m \hat{U}_{nm}(0)i^{m-1}j_{m-1}\left(-\text{sign}(z - \frac{l}{2})\frac{il\alpha_n}{2}\right) \qquad (3.22)$$

and upon substitution into Eq. 3.21, the following set of equations are obtained for the vertical displacement $\hat{w}$ and pressure $\hat{p}$, which are the field parameters involved in the boundary conditions at the horizontal interfaces:

$$\begin{aligned}
\hat{w}_n(x,z) &= \text{sign}(z - \frac{l}{2})\sum_{m=1}^{\infty}\hat{U}_{nm}(0)i^{m-1} \\
&\quad \int_{-\infty}^{\infty} j_{m-1}\left(-\text{sign}(z - \frac{l}{2})\frac{il\alpha_n}{2}\right)e^{-|s-\frac{l}{2}|\alpha_n}e^{-ixs}ds \\
\hat{p}_n(x,z) &= \lambda_n h_n^2\sum_{m=1}^{\infty}\hat{U}_{nm}(0)i^{m-1} \\
&\quad \int_{-\infty}^{\infty} j_{m-1}\left(-\text{sign}(z - \frac{l}{2})\frac{il\alpha_n}{2}\right)\frac{e^{-|s-\frac{l}{2}|\alpha_n}}{\alpha_n}e^{-ixs}ds\,. \qquad (3.23)
\end{aligned}$$

The above two equations are similar to the real compressional point source potential (Eq. 2.11) when the source depth z_s is replaced by the midpoint of the line source $z = \frac{l}{2}$, and with the source wavenumber spectrum modulated by the spherical Bessel function j_{m-1} for the various line sources of shape P_{m-1}.

3.3.2 Displacement Homogeneous Solution

The previous displacement Green's function is not complete until we add the homogeneous contributions arising from satisfaction of horizontal interface boundary conditions for the multiple layered sector. These contributions arise for each order of

the line source distribution at every layer. This means that the global matrix equations have to be solved a number of times equal to the total number of expansion orders multiplied by the total number of layers, times the number of discontinuities in range. When we resort to the global matrix method, the mapping pointers need to be set up only once for different layering, and multiple right hand side is relatively easy to handle with small additional computing time. Thus, all displacement sources within a sector can be treated simultaneously.

Horizontal Wavenumber Integral Representation

Following the global matrix approach, the horizontal wavenumber integral for the homogeneous solution in layer n consists of sum over all contributions from displacement sources of order k located in layer l:

$$\begin{aligned} w_n(x,z) &= \sum_{l=1}^{N}\sum_{k=1}^{\infty}\hat{U}_{lk}(0) \\ &\quad \int_{-\infty}^{\infty}\left[-\alpha_n A^-_{n,lk}(s)e^{-s\alpha_n} + \alpha_n A^+_{n,lk}(s)e^{(s-l)\alpha_n}\right]e^{-izs}ds \\ p_n(x,z) &= -\lambda_n h_n^2\sum_{l=1}^{N}\sum_{k=1}^{\infty}\hat{U}_{lk}(0) \\ &\quad \int_{-\infty}^{\infty}\left[A^-_{n,lk}(s)e^{-s\alpha_n} + A^+_{n,lk}(s)e^{(s-l)\alpha_n}\right]e^{-izs}ds \end{aligned} \tag{3.24}$$

where N is the total number of vertical stratification. These solutions satisfy homogeneous Helmholtz equation and the radiation condition is easily satisfied when the up or down going wave is neglected in the half-spaces. Again, the unknowns $A^{\pm}_{n,lk}$ are the horizontal wavenumber amplitudes of the up and down going component of the displacement homogeneous solution at layer n due to a displacement source of unit strength $\hat{U}_{lk}(0) = 1$ of order k located in layer l. They are found at a discrete number of horizontal wavenumbers from the system of equations that expresses the boundary conditions for horizontal interfaces with displacement source terms Eq. 3.23 on the right hand side. The wavenumber sampling needs to be done only for the positive spectrum since the unknowns are symmetric in s. Again, each combination of indices l and k represents a single SAFARI run. Due to the nature

of SAFARI which can treat multiple right hand side efficiently, these unknowns can be found with single global matrix set up.

Basis Function Expansion

For the purpose of matching boundary conditions at the vertical cuts, expansion of the homogeneous solutions in terms of the basis functions is needed. Using a similar expansion as Eq. 3.15, we express the displacement and pressure as

$$\begin{aligned} u_n(x,z) &= \sum_{m=1}^{\infty} \bar{U}_{nm}(x) P_{m-1}\left(\frac{z-\frac{l}{2}}{\frac{l}{2}}\right) \\ p_n(x,z) &= \sum_{m=1}^{\infty} \bar{S}_{nm}(x) P_{m-1}\left(\frac{z-\frac{l}{2}}{\frac{l}{2}}\right) \end{aligned} \tag{3.25}$$

and subsequently the range expansion coefficients are extracted by equating the above equations to Eq. 3.24 and using the orthogonal property of the Legendre functions to produce

$$\begin{aligned} \bar{U}_{nm}(x) &= -(2m-1)i^m \sum_{l=1}^{N}\sum_{k=1}^{\infty} \hat{U}_{lk}(0) \\ &\quad \int_{-\infty}^{\infty} \left[s A^-_{n,lk}(s) + (-1)^{m-1} s A^+_{n,lk}(s)\right] e^{-\frac{il\alpha_n}{2}} j_{m-1}\left(\frac{il\alpha_n}{2}\right) e^{-isx} ds \\ \bar{S}_{nm}(x) &= -\lambda_n h_n^2 (2m-1) i^{m-1} \sum_{l=1}^{N}\sum_{k=1}^{\infty} \hat{U}_{lk}(0) \\ &\quad \int_{-\infty}^{\infty} \left[A^-_{n,lk}(s) + (-1)^{m-1} A^+_{n,lk}(s)\right] e^{-\frac{il\alpha_n}{2}} j_{m-1}\left(\frac{il\alpha_n}{2}\right) e^{-isx} ds \,. \end{aligned} \tag{3.26}$$

Similar to the case with the displacement solution, there should be no contribution to the horizontal displacement at the cut, *i.e.* $\bar{U}_{nm}(0) = 0$, since the integrand is odd with respect to s for $x = 0$. Numerical integration of the above influence functions are best performed by means of a trapezoidal rule [22].

3.3.3 Source Solution

Whenever a real point source (for the two–dimensional case a line source extending infinitely in the y direction) exists in a certain sector of the discretized environment,

its contribution has to be added separately along with the homogeneous solution. Representation of these components are similar to the displacement solutions so a detailed derivation will not be given. These sources act as the inhomogeneous term when displacement source strengths are sought from the matching of the boundary conditions at the vertical boundaries.

Horizontal Wavenumber Integral Representation

A compressional source in acoustic medium has the integral representation [17]

$$\begin{aligned} \overset{*}{w}_n(x,z) &= -\text{sign}(z-z_s)\int_{-\infty}^{\infty} e^{-|z-z_s|\alpha_n} e^{-i(z-z_s)s} ds \\ \overset{*}{p}_n(x,z) &= -\lambda_n h_n^2 \int_{-\infty}^{\infty} \frac{e^{-|z-z_s|\alpha_n}}{\alpha_n} e^{-i(z-z_s)s} ds \end{aligned} \tag{3.27}$$

where z_s is the source depth from the upper interface (lower for upper half-space) and x_s is the horizontal range from the discontinuity.

Basis Function Expansion

When the source is not located on the interface, *i.e.* $z_s \neq 0$, we cannot express the source solution in terms of a Legendre polynomial expansion. The reason for this is the absolute value $|z-z_s|$ in the argument to the exponential function which makes the kernel and all its derivatives discontinuous inside the layer, and so a regular expansion using a complete set of orthonormal functions is impossible. One way to avoid this problem is to introduce an artificial interface at the depth of the source to impose $z_s = 0$, making the kernel and its derivatives continuous inside each layer.

Following the same argument used in the displacement source solution, the basis function expansion can be found as;

$$\begin{aligned} \overset{*}{u}_n(x,z) &= \sum_{m=1}^{\infty} \overset{*}{U}_{nm}(x) P_{m-1}\left(\frac{z-\frac{l}{2}}{\frac{l}{2}}\right) \\ \overset{*}{p}_n(x,z) &= \sum_{m=1}^{\infty} \overset{*}{S}_{nm}(x) P_{m-1}\left(\frac{z-\frac{l}{2}}{\frac{l}{2}}\right) \end{aligned} \tag{3.28}$$

with the range expansion coefficients given by

$$\begin{aligned}
\overset{*}{U}_{nm}(x) &= -(2m-1)i^m \\
&\quad \int_{-\infty}^{\infty} \frac{s}{\alpha_n} e^{-\frac{l\alpha_n}{2}} j_{m-1}\left(\frac{il\alpha_n}{2}\right) e^{-is(x-x_s)} ds \\
\overset{*}{S}_{nm}(x) &= -\lambda_n h_n^2 (2m-1) i^{m-1} \\
&\quad \int_{-\infty}^{\infty} \frac{1}{\alpha_n} e^{-\frac{l\alpha_n}{2}} j_{m-1}\left(\frac{il\alpha_n}{2}\right) e^{-is(x-x_s)} ds \,. \qquad (3.29)
\end{aligned}$$

As is the case with the displacement sources, these influence functions should also be evaluated with precision since they determine the accuracy of the solution of the unknown displacement source strengths. The horizontal wavenumber integration in Eq. 3.29 is therefore performed using a Gaussian quadrature scheme (Appendix D).

3.3.4 Source Homogeneous Solution

We next consider the homogeneous solutions corresponding to a real source in a stratified media.

Horizontal Wavenumber Integral Representation

Following the previous discussions, the homogeneous solution is expressed as an integral of up and down going waves with unknown spectrum $A_n^{\pm}(s)$, with s being the horizontal wavenumber

$$\begin{aligned}
\tilde{w}_n(x,z) &= \int_{-\infty}^{\infty} \left[-\alpha_n A_n^-(s) e^{-s\alpha_n} + \alpha_n A_n^+(s) e^{(s-l)\alpha_n}\right] e^{-i(x-x_s)s} ds \\
\tilde{p}_n(x,z) &= -\lambda_n h_n^2 \int_{-\infty}^{\infty} \left[A_n^-(s) e^{-s\alpha_n} + A_n^+(s) e^{(s-l)\alpha_n}\right] e^{-i(x-x_s)s} ds \,. \qquad (3.30)
\end{aligned}$$

Since the source does not have to be located at the origin of the local coordinate system, as shown in Fig. 3.2, we have expressed its dependence explicitly as $e^{-i(x-x_s)}$. This makes the unknowns symmetric with respect to the horizontal wavenumber s, enabling the reduction of discretization of the wavenumber integral to the positive part of the spectrum only.

Basis Function Expansion

For the purpose of matching the vertical boundary conditions, similar basis function expansion to those of Eq. 3.15 can be written as

$$\begin{aligned} \tilde{u}_n(x,z) &= \sum_{m=1}^{\infty} \tilde{U}_{nm}(x) P_{m-1}\left(\frac{z-\frac{l}{2}}{\frac{l}{2}}\right) \\ \tilde{p}_n(x,z) &= \sum_{m=1}^{\infty} \tilde{S}_{nm}(x) P_{m-1}\left(\frac{z-\frac{l}{2}}{\frac{l}{2}}\right) \end{aligned} \tag{3.31}$$

with the range expansion coefficients given by

$$\begin{aligned} \tilde{U}_{nm}(x) &= -(2m-1)i^m \\ &\quad \int_{-\infty}^{\infty} \left[sA_n^-(s) + (-1)^{m-1} sA_n^+(s)\right] e^{-\frac{l\alpha_n}{2}} j_{m-1}\left(\frac{il\alpha_n}{2}\right) e^{-is(x-x_s)} ds \\ \tilde{S}_{nm}(x) &= -\lambda_n h_n^2 (2m-1) i^{m-1} \\ &\quad \int_{-\infty}^{\infty} \left[A_n^-(s) + (-1)^{m-1} A_n^+(s)\right] e^{-\frac{l\alpha_n}{2}} j_{m-1}\left(\frac{il\alpha_n}{2}\right) e^{-is(x-x_s)} ds \,. \end{aligned} \tag{3.32}$$

Numerical evaluation of the above influence functions is again performed by a trapezoidal rule integration scheme.

3.4 Solution of Discrete Range Dependent Problem

Now we are ready to solve the discrete range dependent acoustic wave propagation problem. First the global matrix for the unknown source strengths is established and solved for the unknowns; then the fields are calculated at each desired receiver depth for all ranges within each sector as in the global matrix approach to the range independent case, except that in each sector, contributions from the left and the right vertical section must be added.

3.4.1 Solution of Displacement Source Strength

Originally we started out with the boundary integral equation Eq. 3.2, which is a Fredholm integral equation of the 1st kind with the unknown indirect displacement source strength appearing inside the integral. Applying the various line source distributions over the vertical boundary of each layer and carrying out the boundary integral for these layers analytically, this integral has been transformed to summation over all orders of the basis function. Truncating this basis function expansion to M orders, each vertical discontinuity in range produces M unknown source strengths for N layers at both sides of the interface. Thus $M \times N \times 2$ conditions must be supplied for each vertical cut which is provided by requiring continuity of both the normal displacement and the pressure for the M orders of the expansion in each of the N layers. This is exactly the Galerkin method which requires that the difference between two integrals appearing on both sides of the vertical interface be orthogonal to M linearly independent weighting functions over the interval in each layer. This method can also be interpreted as weighting two integral for both sides of the interface and requiring that the integral of the weighted members be equal. By selecting the weighting function and approximating the basis function to be identical orthogonal functions, this reduces to simply matching each expansion coefficients of the basis functions.

Since all physical variables to be matched were expanded in terms of orthogonal basis function with integration over the vertical boundary of each layer performed analytically, imposing the boundary condition at a vertical interface will generate a local system of algebraic equations for the unknown expansion coefficients or source strengths $\hat{U}_{nm}(0)$. These local systems of equations for every vertical interface are then combined into a global system of equations analogous to the homogeneous layered case. Denoting the physical parameters, normal displacement u and pressure p, at interface(node) j for the lth sector(super-element) as $\{u\}_l^j$, which is a row vector of dimension $M \times N \times 2$, the local system of equations to be satisfied at the

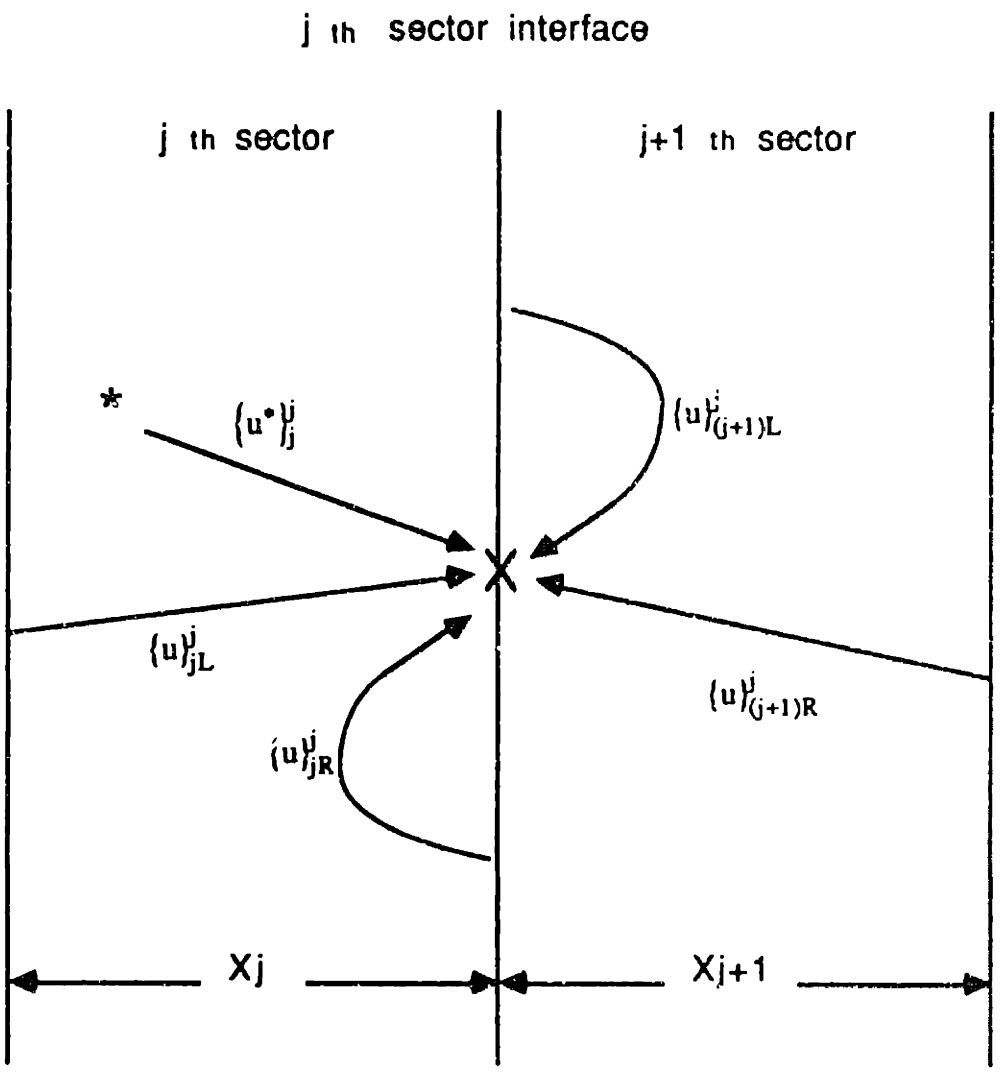

Figure 3.3: Heuristic diagram of the components for matching the boundary condition at the *j*th vertical interface.

vertical interface j is

$$\begin{aligned}\{u\}^j &= \{u\}^j_{jL} + \{u\}^j_{jR} + \{\dot{u}\}^j_j \\ &= \{u\}^j_{(j+1)L} + \{u\}^j_{(j+1)R} + \{\dot{u}\}^j_{j+1} \,. \end{aligned} \tag{3.33}$$

Each term of Eq. 3.33 is shown schematically in Fig. 3.3, where for simplicity the horizontal stratification is not shown. Arrows represent influences from all layers to that layer being matched where only a single arrow has been drawn. $\{u\}$ is displacement source related, and $\{\dot{u}\}$ is the real source related terms with subscripts L and R meaning contribution from the left and the right part of the sector element being considered. For half-infinite sectors, contributions from infinity vanish because of the radiation condition inherent in the wavenumber integral. Again, each of these terms consist of particular and homogeneous solutions. For clarity, we will write out the elements of the full column vector for the real source solution assuming that the source is located at layer i:

$$\begin{aligned}\{\dot{\tilde{u}}\}^j_j &= \{\dot{\tilde{u}}\}^j_j + \{\tilde{u}\}^j_j \\ &= \left\{\tilde{U}_{11}(X_j), \cdots, \tilde{U}_{i1} + \dot{U}_{i1}, \tilde{U}_{i2} + \dot{U}_{i2}, \cdots, \tilde{U}_{NM}, \tilde{S}_{11}, \cdots, \tilde{S}_{i1} + \dot{S}_{i1}, \cdots, \tilde{S}_{NM}\right\}^T \end{aligned} \tag{3.34}$$

where the expansion coefficients $\tilde{U}(x), \tilde{S}$ and $\dot{U}, \dot{S}$ are given by Eqs. 3.29 and 3.32. Range x in the expansion function should be the sector length X_j for jth sector and 0 for $(j+1)$th sector since origin of the x-coordinate for the source solution was chosen to be on the far-left vertical cut of the sector being considered. For the displacement solution it is written as a sum of the displacement source and displacement homogeneous solution as

$$\begin{aligned}\{u\}^j_{jL} &= \{\hat{u}\}^j_{jL} + \{\bar{u}\}^j_{jL} \\ &= [A(X_j)]_j\{a\}_{jL} + [B(X_j)]_j\{a\}_{jL} \end{aligned} \tag{3.35}$$

where $\{a\}_{jL}$ is the unknown displacement source strength at the left interface of

sector j

$$\{a\}_{jL} = \left\{ \begin{array}{c} \hat{U}_{11}(0) \\ \hat{U}_{12}(0) \\ \vdots \\ \hat{U}_{NM}(0) \end{array} \right\}_{jL} \tag{3.36}$$

and the influence function matrices of the jth sector $[A(x)]_j$ and $[B(x)]_j$, which have dimension of $N \times M \times 2$ by $N \times M$, are given by Eqs. 3.17 and 3.26 respectively. Since the displacement source influences are restricted to its own layer, $[A(x)]_j$ is seen to be a block diagonal matrix, per Eq. 3.17, while the influence matrix of the homogeneous solution becomes a fully populated matrix since the homogeneous solution propagates through all layers. Again, the range appearing in the expansion coefficients is 0 when it is self influencing and X_j when influencing the other vertical interface.

Rearranging Eq. 3.33, contributions from the unknown displacement source, Eq. 3.35, are isolated on the left hand side as

$$\begin{aligned} &[A(X_j)]_j\{a\}_{jL} + [B(X_j)]_j\{a\}_{jL} + [A(0)]_j\{a\}_{jR} + [B(0)]_j\{a\}_{jR} - \\ &[A(0)]_{j+1}\{a\}_{(j+1)L} - [B(0)]_{j+1}\{a\}_{(j+1)L} - [A(X)]_{j+1}\{a\}_{(j+1)R} - [B(X)]_{j+1}\{a\}_{(j+1)R} \\ &\qquad = \{\dot{u}\}^j_{j+1} - \{\dot{u}\}^j_j \ . \end{aligned} \tag{3.37}$$

Combining both influence matrices into $[C(x)]$, this equation reduces to

$$\begin{aligned} [C(X_j)]_j\{a\}_{jL} + [C(0)]_j\{a\}_{jR} \ - \ &[C(0)]_{j+1}\{a\}_{(j+1)L} - [C(X_{j+1})]_{1+1}\{a\}_{(j+1)R} \\ = \ &\{\dot{u}\}^j_{j+1} - \{\dot{u}\}^j_j \ . \end{aligned} \tag{3.38}$$

Referring to Fig. 3.4, these local systems of equations for all vertical interfaces are combined into a global system of equations for the discretely varying range dependent problem. Again, the global system is solved by Gaussian elimination.

Compared to range independent solution technique for layered media, this global system needs to be constructed only once. Solution of the global system reveals all the displacement source strengths at all vertical cuts simultaneously. If the ocean

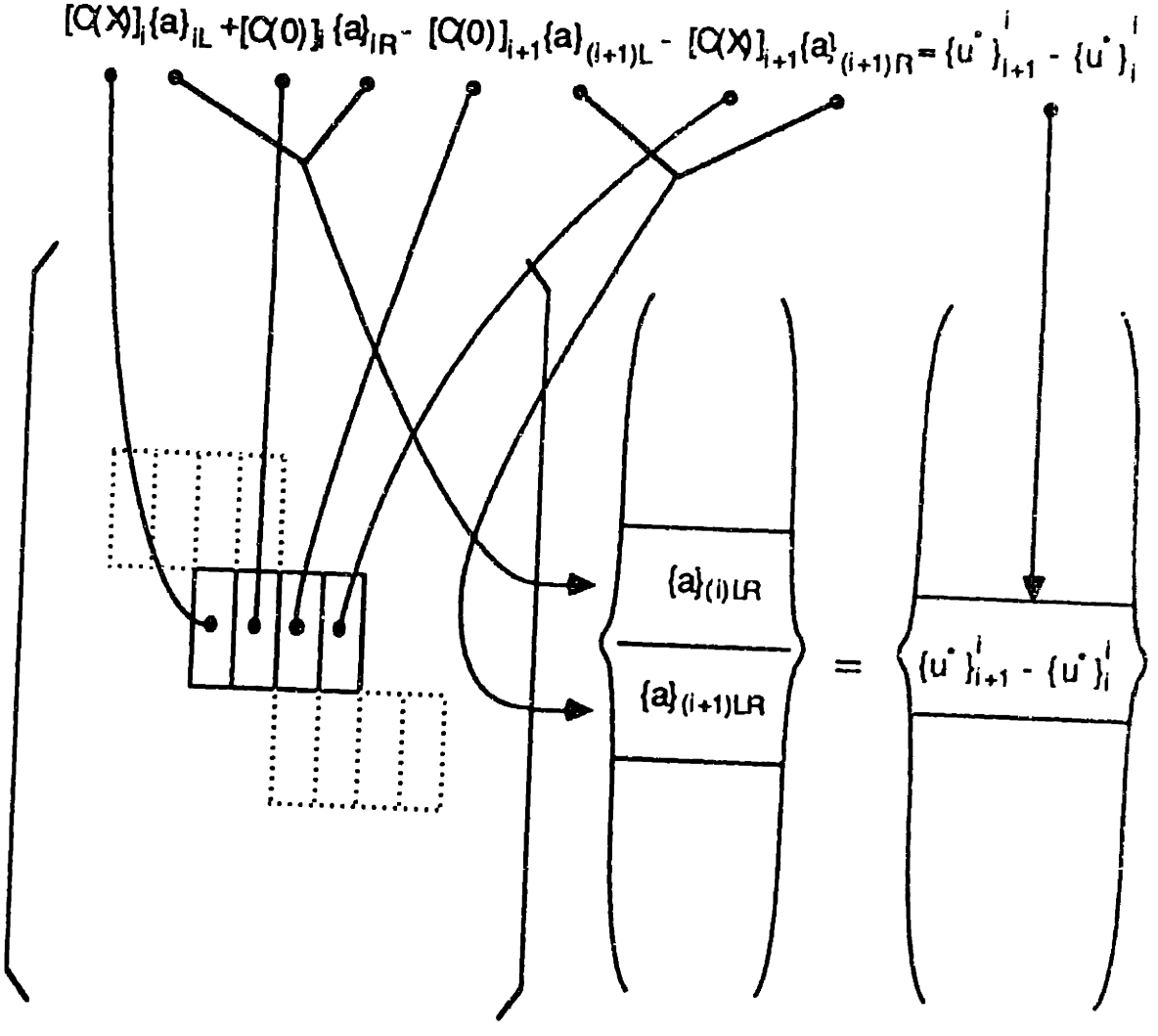

Figure 3.4: Mapping of local to global systems of equations for the vertical interface. The local systems of equation is written for the boundary conditions at the ith vertical interface.

changes such that numerous discretization in range is required, a marching solution can be obtained by ignoring multiple backscattering, significantly reducing the computational requirements, and allowing analysis of reverberation from individual features in the environment.

3.4.2 Field Evaluation

Once the global matrix has been set up and the unknown indirect source strengths at the vertical interfaces are found, we can compute the field at any desired receiver depth and ranges. Comparison of the two forms of the solutions (for example, Eq. 3.24 and Eq.3.25,3.26) shows that the basis function expansion solution contains one more summation over all orders of expansion than the horizontal wavenumber solution. Thus it is much more efficient to use the horizontal wavenumber integral representation. Furthermore, this solution form allows the use of the FFT for the integration, yielding the field at multiple ranges simultaneously. If instead the field was desired at multiple depths for a relatively few fixed ranges, for example for vertical receiver arrays, it seems likely that use of the basis function expansion is more desirable since the depth function is given analytically. By comparing the previous equations for both solution forms, the basis function solution still contains one more summation with the kernels of the integration numerically more expensive to compute. Therefore the basis function expansion is used only to satisfy the vertical interface continuity condition.

Returning to the horizontal wavenumber integral for the field at multiple ranges for designated receiver depths, it is given by the summation of contributions from forward propagation and reverberation from the discontinuity with an additional real source component if it exists in that sector, conveniently written as

$$G(x,z) = G_L + G_R + G_S \tag{3.39}$$

where contributions coming from right(subscript R) and the source(subscript S) are coordinate transformed to a local coordinate with $x = 0$ at the left interface,

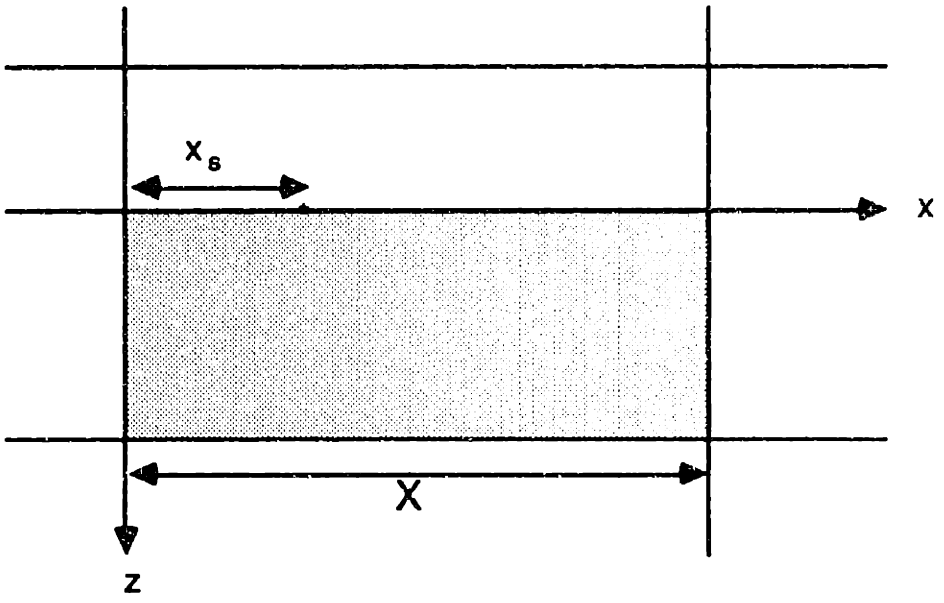

Figure 3.5: Local coordinate system for wavenumber integration. x_s is the source location and X is the length of the sector element.

as shown in Fig. 3.5. This coordinate transform is convenient when the fields are calculated for multiple ranges using an FFT technique, where the range sampling is uniquely determined by the horizontal wavenumber sampling as shown in Chapter 2. If the origin of the local coordinate systems were chosen differently, we would have to adjust the starting point of the range sampling to be identical for each sector.

There is an aliasing problem when performing the FFT, which is fully discussed for the cylindrical geometry in [43]. To avoid this problem we can always deform the integration contour in the complex wavenumber domain. For plane geometry where the integral bounds are from $-\infty$ to ∞, the contour has to be deformed as shown in Fig. 3.6. The integration is truncated at $\pm s_{\max}$ and consist of 3 separate contours. The contribution from the vertical contour C_2 is negligible when the offset ϵ is small. Following SAFARI [43], it is chosen to be

$$\epsilon = \frac{3}{2\pi(L-1)\log e} s_{\max} \tag{3.40}$$

where L is the number of sampling points for horizontal wavenumber. This gives

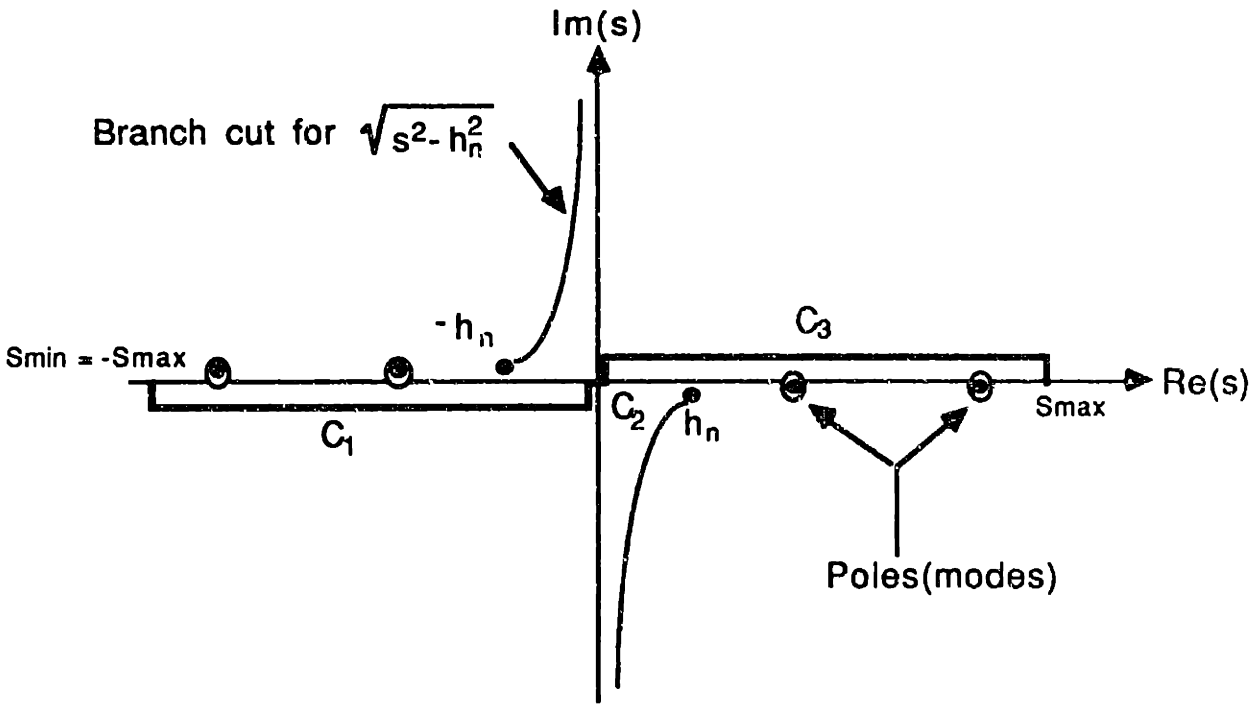

Figure 3.6: Complex integration path for poles lying close to the real axis.

an attenuation of the alias wrap-around by at least 60 dB which is proven to be sufficient for most practical purposes.

Expressing the wavenumber integral in terms of depth-dependent Green's function $g(s,z)$ as

$$G(x,z) = \int_{-\infty}^{\infty} g(s,z)e^{-isx}ds\,, \tag{3.41}$$

the discrete approximation of the above integral for the G_L component, with complex contour and same notation as Chapter 2 introduced, is given by

$$\begin{aligned} G_L(x_j,z) \;=\; & \Delta s e^{-is_{min}x_j}e^{-\epsilon x_j}\left[\sum_{l=0}^{L/2-1} g_L(s_l - i\epsilon; z)e^{-ix_{min}l\Delta s}\right]e^{-i\frac{2\pi}{L}lj} + \\ & \Delta s e^{-is_{min}x_j}e^{\epsilon x_j}\left[\sum_{l=L/2}^{L-1} g_L(s_l + i\epsilon; z)e^{-ix_{min}l\Delta s}\right]e^{-i\frac{2\pi}{L}lj}\,. \end{aligned} \tag{3.42}$$

The negative and positive spectra have been separated due to offset in different directions. Both summations are performed by means of an FFT. Contributions from the right sector interface become

$$G_R(x_j,z) \;=\; \Delta s e^{-is_{min}(X-x_j)}e^{-\epsilon(X-x_j)}\left[\sum_{l=0}^{L/2-1} g_R(s_l - i\epsilon; z)e^{-i(X-x_{min})l\Delta s}\right]e^{i\frac{2\pi}{L}lj} +$$

$$\Delta s e^{-is_{min}(X-x_j)} e^{\epsilon(X-x_j)} \left[\sum_{l=L/2}^{L-1} g_R(s_l + i\epsilon; z) e^{-i(X-x_{min})l\Delta s} \right] e^{i\frac{2\pi}{L}lj} \quad (3.43)$$

Notice the change of sign in the Fourier transformation which is caused by the coordinate transform. Similarly, for the source term

$$\begin{aligned} G_S(x_j, z) \;=\; & \Delta s e^{-is_{min}(x_j-x_s)} e^{-\epsilon(x_j-x_s)} \left[\sum_{l=0}^{L/2-1} g_S(s_l - i\epsilon; z) e^{-i(x_{min}-x_s)l\Delta s} \right] e^{-i\frac{2\pi}{L}lj} + \\ & \Delta s e^{-is_{min}(x_j-x_s)} e^{\epsilon(x_j-x_s)} \left[\sum_{l=L/2}^{L-1} g_S(s_l + i\epsilon; z) e^{-i(x_{min}-x_s)l\Delta s} \right] e^{-i\frac{2\pi}{L}lj} \quad (3.44) \end{aligned}$$

Cylindrical geometry

For cylindrical geometry with source located at the center of concentric rings, the Helmholtz reduced wave equation is

$$\frac{1}{r}\frac{\partial}{\partial r}(r\frac{\partial \Phi}{\partial r}) + \frac{\partial^2 \Phi}{\partial z^2} + h^2\Phi = 0\,. \quad (3.45)$$

Separating out the cylindrical spreading effect by introducing a new function

$$\phi(r, z) = \sqrt{\frac{\pi r}{2}}\Phi(r, z) \quad (3.46)$$

Eq. 3.45 becomes

$$\frac{\partial^2 \phi}{\partial r^2} + \frac{1}{4r^2}\phi + \frac{\partial^2 \phi}{\partial z^2} + h^2\phi = 0\,. \quad (3.47)$$

When the $\phi/4r^2$ term is dropped for large r, cylindrical spreading can be treated with the present 2-dimensional derivation simply by multiplying $\sqrt{\frac{2}{\pi r_j}}$ in the final evaluation of the field.

This procedure is equivalent to performing a Hankel transform to the cylindrical 3-D Helmholtz equation, arriving at the same depth-separated ordinary differential equation. When the inverse Hankel transform is performed, the Bessel function is split up as a sum of two Hankel functions with negative propagating waves neglected and the use of the principal asymptotic expansion for large arguments of the Hankel function is made, enabling the use an of FFT for the integration. In the former 'transformation of variable' method, the inhomogeneous source condition is changed

accordingly and this is the reason for the difference of the $\frac{\pi}{4}$ phase shift and $\sqrt{s}$ in the kernels of the conventional fast-field program and the present derivations. Another minor difference between the two methods is retention of both the negative and the positive spectrum in the present method. This essentially has no effect on the final field values but is convenient for the sake of book-keeping.

Chapter 4

Convergence and Performance Analysis

This chapter and the next chapter will be devoted to examining the feasibility and efficiency of the proposed method for solving stepwise varying range dependent ocean acoustic propagation problems. First we will describe various numerical aspects of the present hybrid method. This discussion will clarify the types of problems most appropriate for this method. In the following chapter, numerical examples of canonical problems of underwater acoustics, which directly and indirectly prove the validity of this method, will be presented along with application to matched field processing for active localization of a volume inhomogeneity in an otherwise range independent ocean.

The primary measure used for the solutions in this and the following chapter, is the transmission loss, which is defined as the drop in sound pressure level in decibels(dB) from the pressure expected at 1 m from the source, defined as TL $= -20\log(|p|/|S|)$ dB. S is customarily taken as 1μPa in underwater acoustics. Results of transmission loss are presented in either of two formats: a) transmission loss versus range for a fixed receiver depth; b) the transmission loss contours plotted over depth and range. For reference purposes, the magnitude of the kernel of the depth dependent Green's function is presented in the horizontal wavenumber (m^{-1})

domain.

4.1 Numerical Considerations

There are numerous complications in numerically implementing the hybrid boundary integral and global matrix method. Some of the principal questions regarding the numerical implementation and, more importantly, its correct use in ocean acoustic simulation, can be stated by the following:

- How many degrees of freedom should be used in the polynomial expansion for the solution to converge ?
- Where should the horizontal wavenumber spectrum truncation be made and what is the proper wavenumber sampling ?
- Will the range discretization cause any stability problem in the global matrix when solving for the unknown source strength ?
- To which depth do we have to discretize the half-space for a reliable result ?

The numerical aspects concerning the hybrid method are addressed in this chapter, which will clarify these four issues.

4.2 Convergence of Basis Function Expansion

According to the Weierstrass approximation theorem [12], the algebraic polynomial expansion of a continuous function over a bounded interval converges to its true value. The convergence is faster when the continuous function is smoother and its interval is narrower. The convergence is also known to be even faster when orthogonal polynomials are used. Infinite series for the basis function representation should eventually converge to its true value since physically, the field being represented is a continuous function except for the source point.

For numerical treatment, this infinite series has to be truncated to a finite sum. Truncation should be made with caution since not only does it directly introduce errors in the field values, but also couples to other sectors and layers through the influence matrix which was constructed to solve for the displacement source strengths.

First, we investigate the convergence problem by applying the present hybrid technique to a problem with a known analytic result. An example is the acoustic propagation of a source signal of two discrete frequencies in a waveguide with perfectly reflecting boundaries (Fig. 4.1). The depth of the waveguide is 10 m. The source, having frequencies 250 and 750 Hz, is located at the midpoint of the water channel. The medium is homogeneous with 1500 m/sec constant sound speed and the density is a uniform 1 g/cm^3. We introduce an arbitrary vertical interface at 500 m to the right of the source location to determine the ability of the present approach to correctly represent the coupling between two sectors, and the water properties are the same on both sides of the vertical interface. The dependence on the separation distance between the source and the dummy vertical interface will be investigated in a later section. The sector to the left of the interface contains the source and is referred to as the first sector and the right as the second sector.

For the 250 Hz source centered in the waveguide, only the first and the third modes will be excited. The depth dependent Green's function for each sector, at a receiver depth of 5 m is shown in Fig. 4.2. The peaks are due to the poles corresponding to the normal modes. Because the poles are located very close to the real axis, it is difficult to accurately sample the integrand. The complex integration scheme previously described is adopted, and is responsible for the magnitude of the third mode integrand being larger than the first. For only one term included in the expansion, it is seen from the integrands that complete coupling between two identical sectors is not properly achieved. As we increase the total degrees of freedom used in the expansion, the ratio of the magnitude of the maximum integrand value to its true value approaches unity as shown in Fig. 4.3 for both

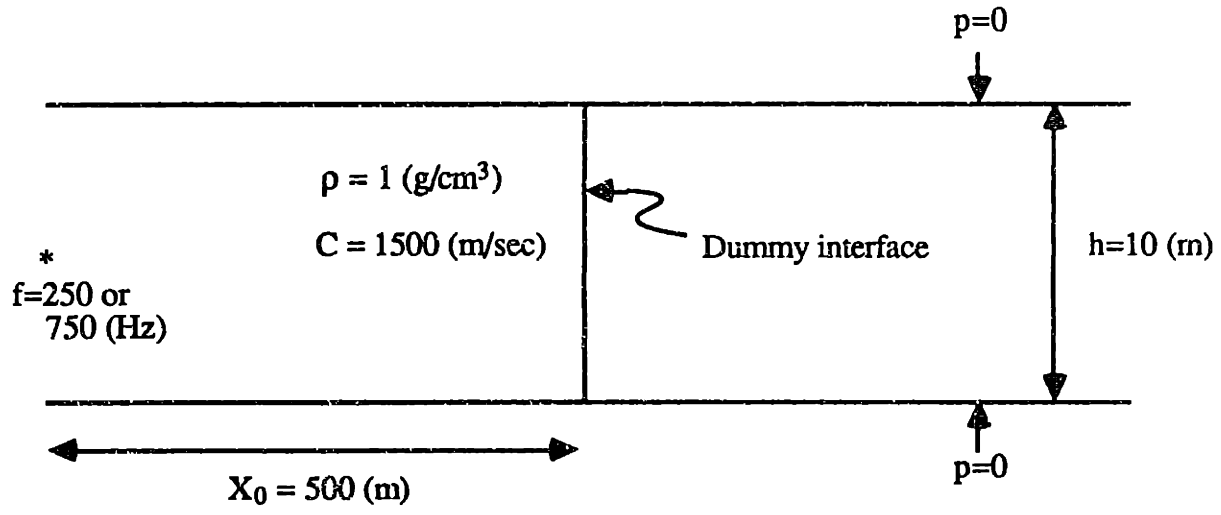

Figure 4.1: Homogeneous waveguide with perfectly reflecting boundaries and a dummy vertical interface.

modes. Since the first mode shape is smoother than the third mode, convergence is achieved with fewer degrees of freedom. Complete coupling into the right sector, and also its convergence, is achieved with 4 degrees of freedom; this is also verified by the excellent agreement between the computed transmission loss and the analytic result. In contrast, the conventional boundary element method requires at least ten or more nodes per dominant wavelength for an accuracy of better than few percent [50], which converts to 20 nodes over the vertical depth for the current example. Meanwhile, Galerkin's method produces an accurate result with only 3 or 4 degrees of freedom.

By raising the source frequency to 750 Hz, the first five symmetric modes (modes no.1,3,5,7,9) are generated by the mid depth source. Fig. 4.4 represents the ratio of the magnitude of the maximum integrand at both sectors to its true value, versus total order of the basis function expansion used, and shown separately for each mode. Since the mode shape in the depth direction for the 9th mode has 8 nulls, accurate modeling of the field variation would require $P_0, \ldots, P_8$ as can be seen from Fig. 4.4. The total degrees of freedom required for lower modes follow a similar

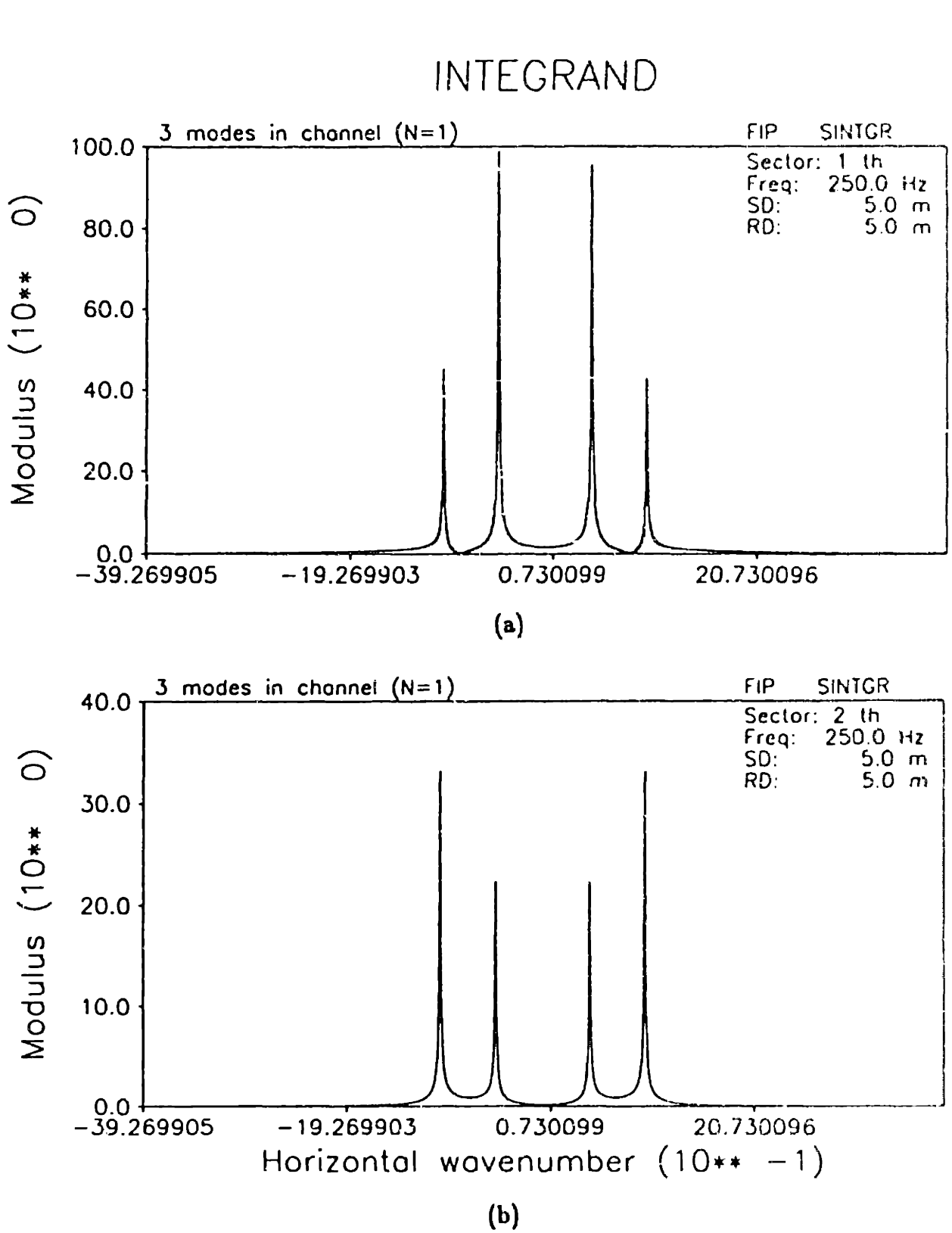

Figure 4.2: Depth dependent Green's function using only zeroth order polynomial expansion (P_0): (a) integrand in the first sector ; (b) integrand in the second sector.

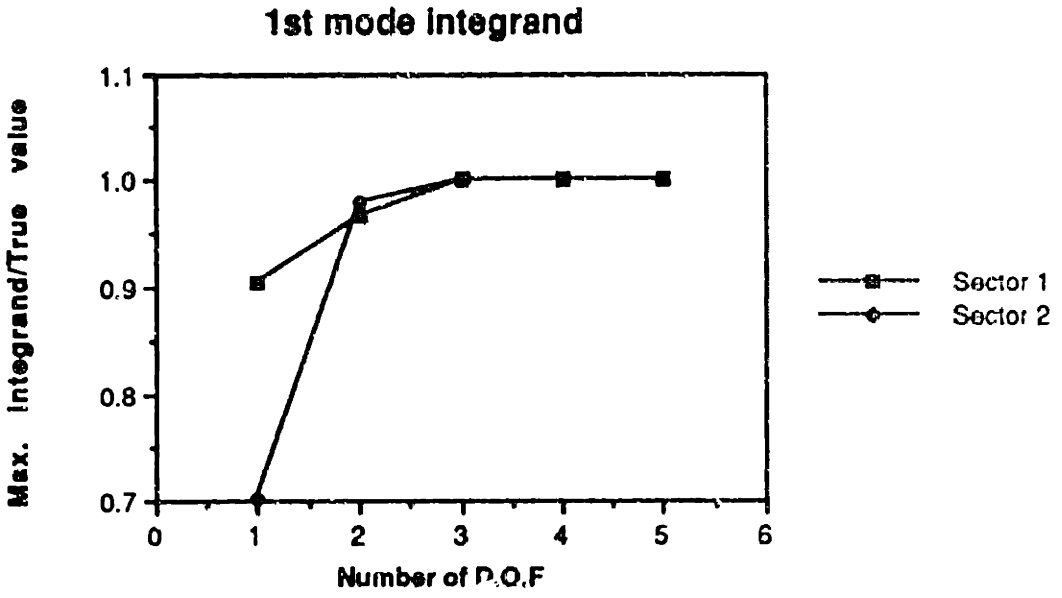

(a)

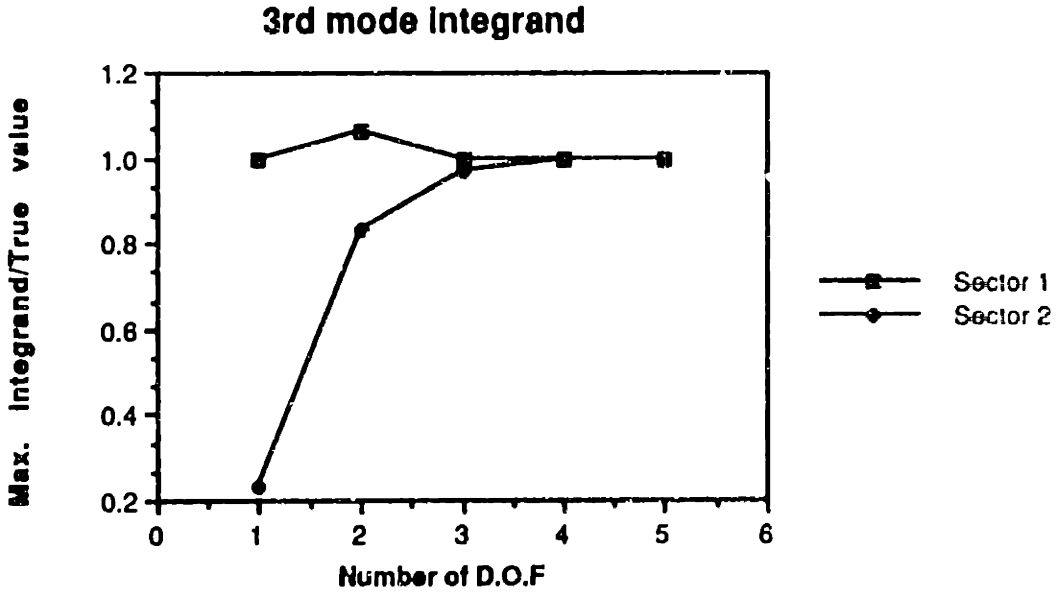

(b)

Figure 4.3: Convergence of the maximum of depth-dependent Green's function on total degrees of freedom employed for: (a) 1st mode ; (b) 3rd mode.

argument with extra expansion necessary to take into account the coupling between modes. This example is a worst-case scenario, in terms of expansions needed, since for perfect modes complex wavenumber integration has to be performed. This magnifies the higher modes present which results in requirement of more expansion terms to accurately represent the field variation.

In the second example, we examine the mode conversion in a waveguide with an abrupt change in the medium propagation speed. The acoustic waveguide has perfectly reflecting boundaries with sound speed changing from 1500 m/sec to 600 m/sec as shown in Fig. 4.5. A simple source of 100 Hz frequency is located at depth $z = 6$ m and 500 m away from the vertical discontinuity interface. Only the first mode can be generated in the first sector whereas up to 3 modes 'can' be generated in the right. The source in the left sector generates the first mode which partially couples into the right sector as the first mode only because of the orthogonality of the mode shapes which are sine functions and the remaining energy is back-reflected. Fig. 4.6 represents the ratio of the magnitude of maximum integrand at both sectors to its true value versus total order of the basis function expansion used.

When a single degree of freedom is used in the expansion (*i.e.* P_0) it corresponds to a collocation method with 2 nodes. This is the reason for poor performance with erroneous 2nd and 3rd modes generated in the right sector. Increasing the expansion to 2 degrees of freedom results in correct magnitudes for the first mode but higher modes of small magnitude are also coupled into the right sector giving errors in the total field value. This is because the mode shape of the first mode which is a sinusoid cannot be represented accurately by P_0 and P_1 alone. The transmission loss compared to analytic result will be shown for this case in the next chapter.

Convergence of the infinite series for the basis function has been tested for various problems and it is found that this scheme is very robust to the degrees of freedom used as long as they are able to represent the actual variation of the field along the vertical cut reasonably well. This can be translated as the following: If

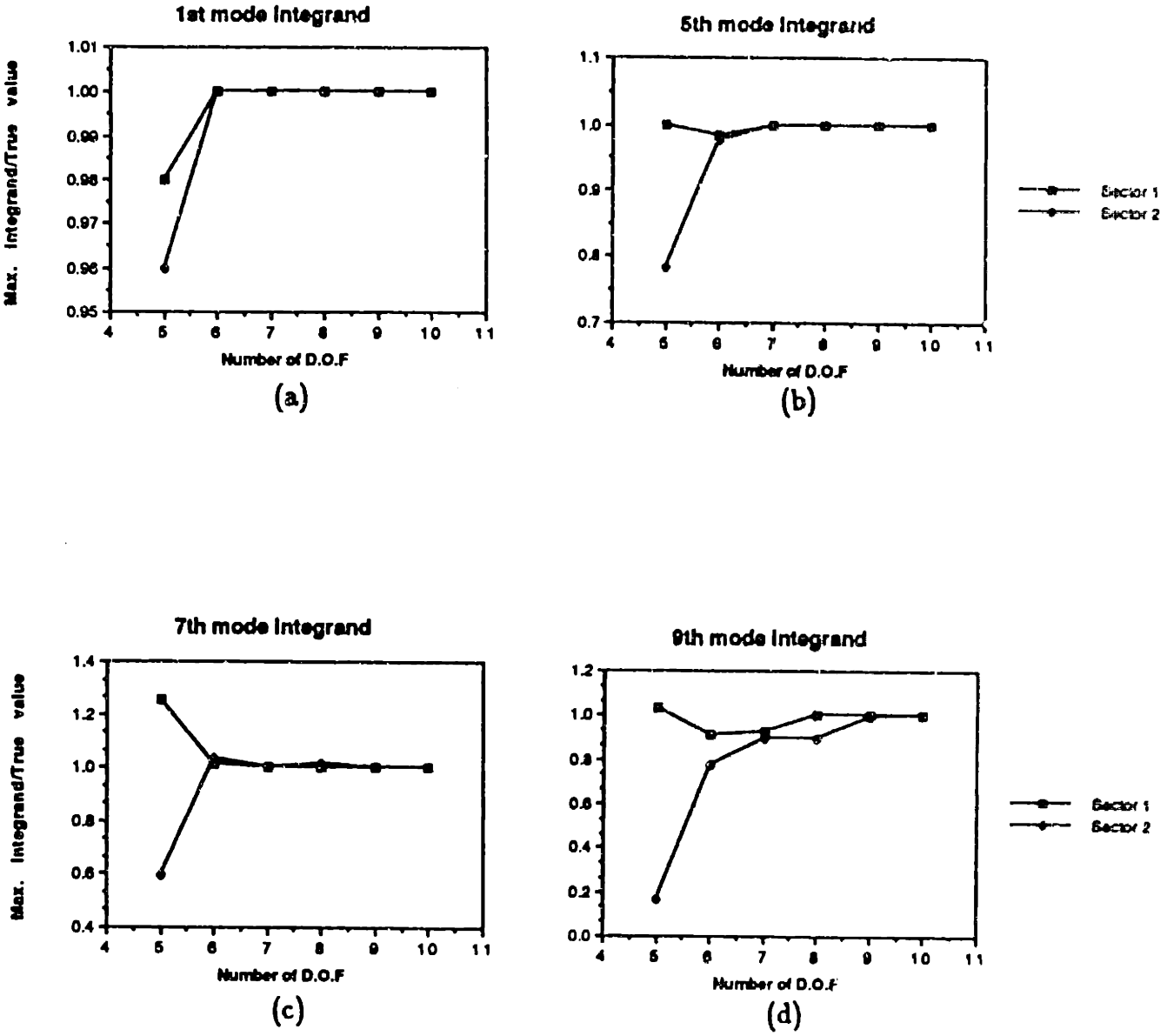

Figure 4.4: Convergence of the maximum of depth-dependent Green's function on total degrees of freedom employed for: (a) 1st mode ; (b) 5th mode ; (c) 7th mode ; (d) 9th mode.

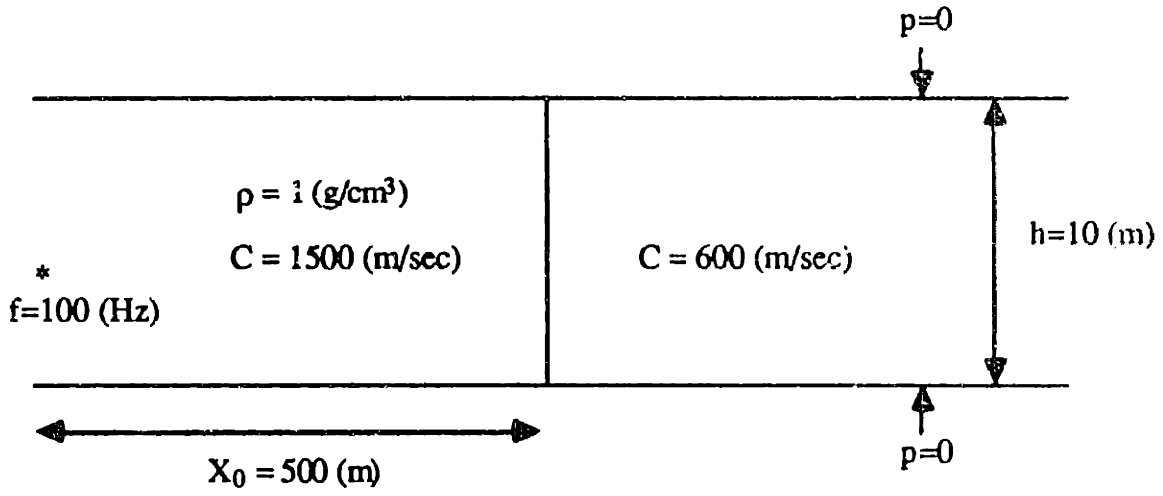

Figure 4.5: Waveguide with perfectly reflecting boundaries with abrupt propagation speed change from 1500 to 600 m/sec. Source (6 m depth) of 100 Hz is located 500 m to the left of the discontinuity.

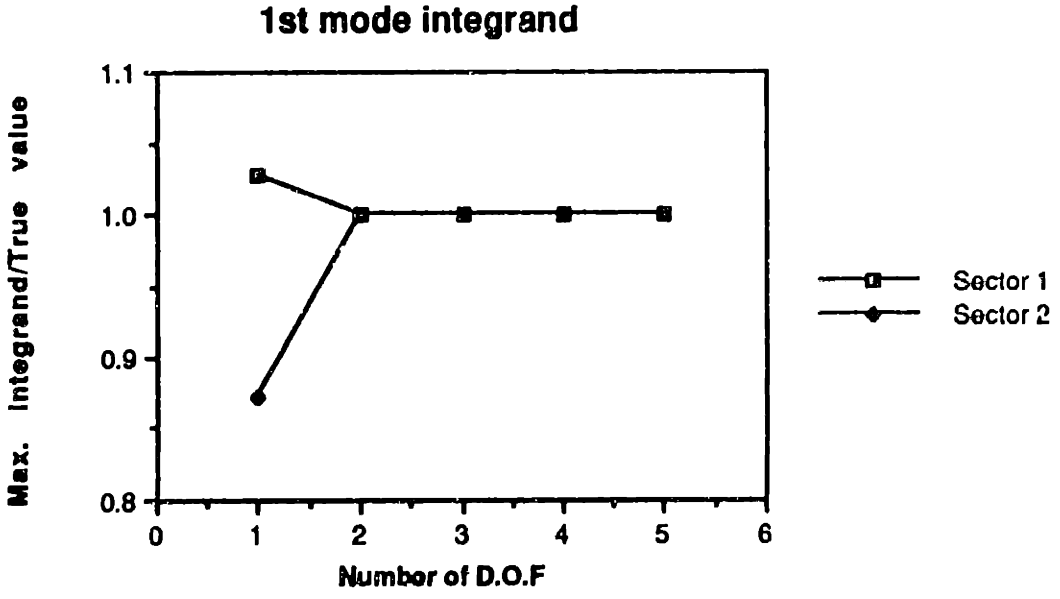

Figure 4.6: Convergence of the maximum of depth-dependent Green's function on total degrees of freedom employed.

there are n number of modes propagating, where $n > 2$, then employing n degrees of freedom in the expansion is sufficient to represent the actual field at the vertical interfaces since they have an equal number of nulls in the mode shape. For $n = 1$ or 2 modes, we need at least 3 expansion terms (P_0, P_1, P_3) to account for smooth variation of the field. This is a conservative statement since, for most cases, only the dominant lower modes will contribute to shaping the actual field variation in which case the total expansion needed is drastically reduced. In this manner, predetermination of the number of degrees of freedom to be employed can be made from a rough physical understanding of the actual problem to be solved although it is always possible to check its convergence by brute force.

4.3 Wavenumber Integration

The numerical evaluation of the Green's function for both displacement sources and real sources is important for the success of the present hybrid scheme. Improper evaluation of these solutions leads to incorrect influence matrix coefficients, yielding inaccurate displacement source strengths.

The inhomogeneous solutions of the displacement (artificial) source and the real source are given in closed form and are evaluated by a quadrature scheme described in Appendix D. The homogeneous solutions for each sector are found using the range independent wavenumber integration algorithm. Numerical evaluation of the wavenumber integrals is a critical point for wavenumber integration approaches. As already discussed in Chapter 2, truncation of the horizontal wavenumber integration interval and wavenumber sampling are two critical issues governing the success of wavenumber integration algorithms.

Truncation of the horizontal wavenumber spectrum can be performed with similar philosophy to that of the range independent SAFARI code, with an extra issue which has to be considered. Truncation should be made to include all possible waves that couples not only through layers but also through sectors. When the

wavenumber integration is the final step in the computational sequence as is the case in range independent problems, this truncation point can be taken as 10 to 20 % higher than the maximum medium wavenumber present. This introduces little or no detectable local errors in the field, especially with smcothing of the kernel for large wavenumbers where cancellation occurs due to the highly oscillating e^{-ikx} term when $x \neq 0$. In our present formulation, the influence matrix must be found for $x = 0$, in which case there are no cancellations and the truncation point must move up higher than the range independent cases. This is also critical since a small error in the influence matrix evaluation will introduce errors in the displacement source strength giving rise to global errors in the final evaluation of the field at all ranges.

The previous example of mode conversion in a waveguide with abrupt change in medium propagation speed (Fig. 4.5) is taken as an example to demonstrate the influence of the truncation point. Since the maximum wavenumber present corresponds to the minimum wave propagation speed present, 600 m/sec, then $C_{\min} = \omega/s_{\max}$ of 500 m/sec should be enough to ensure an accurate solution if we follow the guidelines of the range independent wavenumber integral approach. For example, the transmission loss for a 5 m depth receiver is shown in Fig. 4.7 along with its integrands. An erroneous third mode is generated in the second sector which results from selecting too small a truncation point for the wavenumber integration. Although the integrand value is virtually zero from the truncation point, small error in the influence matrix evaluation has resulted in the phenomena of the third mode coupling into the right sector.

As we increase the truncation point or equivalently lower the $C_{\min}$ value, the fluctuating transmission loss in the 2nd sector of Fig. 4.7 decreases and eventually stabilizes to the correct value. The fluctuating magnitude of transmission loss in dB is plotted as function of $C_{\min}$ along with the relative error expressed in percentile in Fig. 4.8. As $C_{\min}$ approaches 100, the relative error reduces to less than 1 percent. Again this is a worst case scenario where perfectly trapped modes inside the channel

(a)

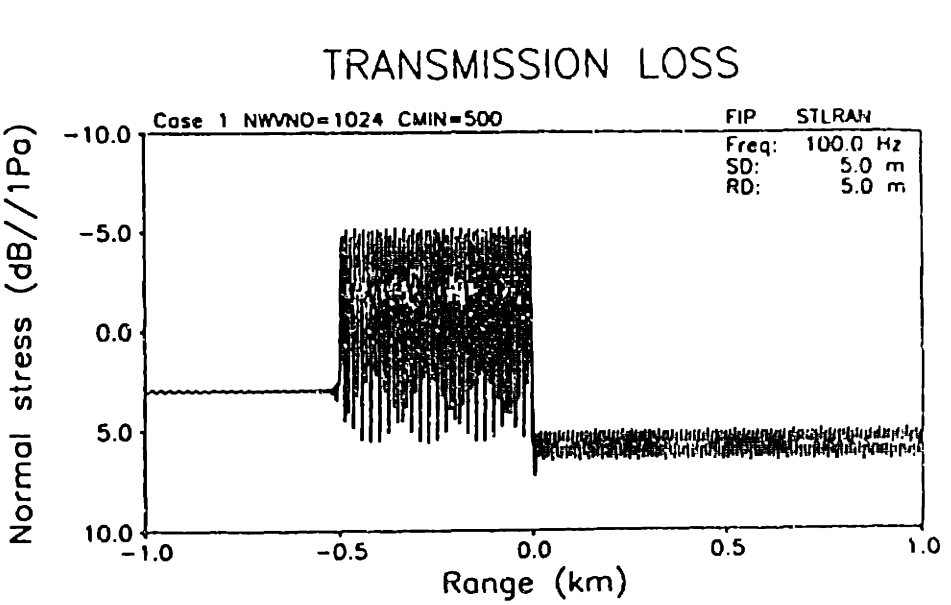

(b)

(c)

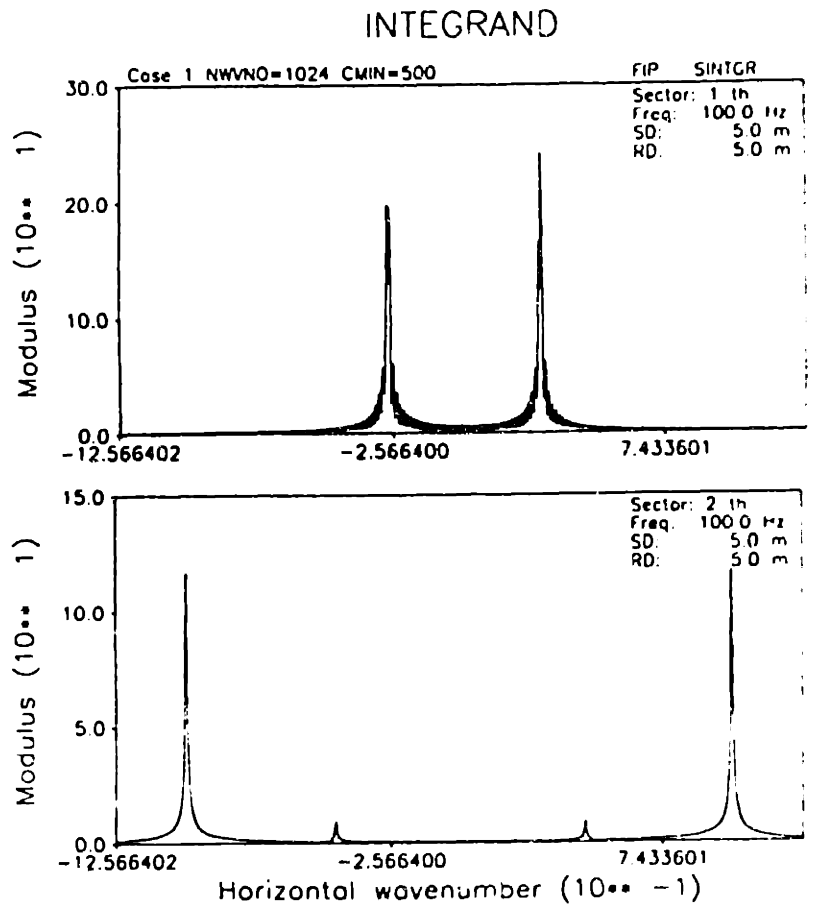

Figure 4.7: Solutions of p.opagation in a perfect waveguide with medium contrast(Fig.4.5): (a) Transmission loss curve ; Depth-dependent Green's function at ; (b) 1st sector ; (c) 2nd sector.

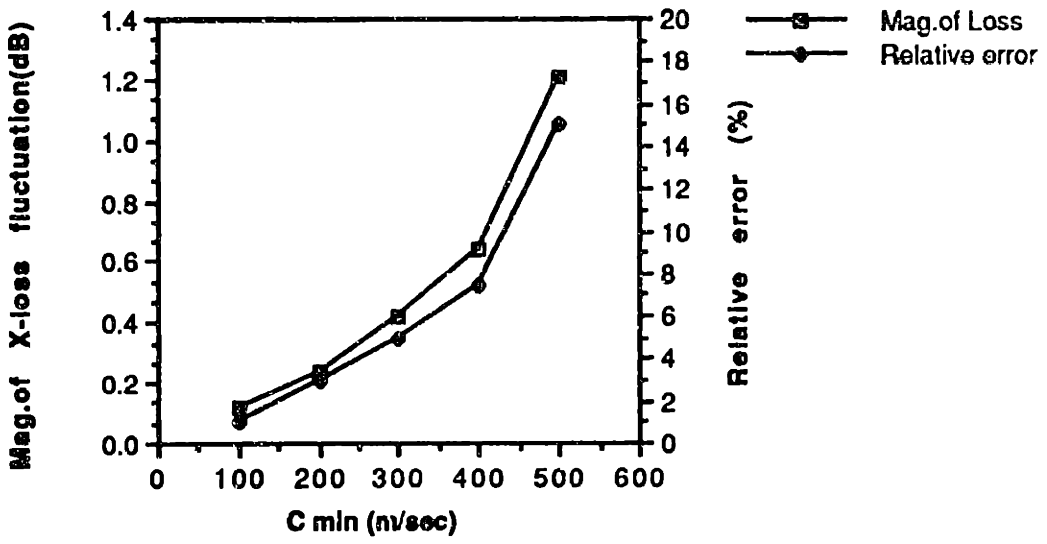

Figure 4.8: Fluctuating component of the transmission loss in the 2nd sector of Fig.4.7(a) in absolute value and its relative error.

are not amenable to numerical treatment due to near singular behavior even with complex integration scheme. For most cases explored, $C_{\min}$ selected to be half of the minimum present propagation speed was found to be sufficient.

The wavenumber sampling within a truncated horizontal wavenumber spectrum is less critical as long as the integrands between sampling points vary smoothly. It is relatively straightforward to determine an adequate sampling through the sampling theorem in combination with choosing a complex wavenumber integration scheme, as described in detail in [43]. Denoting the larger of the two between the maximum range of interest and the largest finite sector length present as X, the wavenumber sampling interval Δs should satisfy the inequality

$$\Delta s < \frac{2\pi}{aX} \tag{4.1}$$

where a is a factor which can be taken as 2 to account for the negative spectrum in the case of a plane geometry.

4.4 Numerical Stability

We investigate the numerical stability problems that might arise when solving a system of equations, *i.e.* one for layering and the other for sectors.

Solution of the global system of equations, Eq. 2.16, at each sampled wavenumber for every sector is done by Gaussian elimination with partial pivoting. As described in detail by Schmidt [46], unconditionally stable solutions are obtained simply by choosing a proper local coordinate system located at the top of each layer and writing the depth eigenfunctions as appearing in Eq. 2.12.

The stability analysis of the global matrix for the unknown displacement source strength is fairly straightforward. Referring to Fig. 3.4, the global matrix for the vertical stratification is a banded matrix with bandwidth $4 \times M \times N$, where M is the total degrees of expansion employed and N is the number of layers excluding half-spaces. The influence of displacement sources on themselves, denoted as $[C(0)]_i$, are bound to be greater than the influence on the other vertical interfaces within the sector, written as $[C(X)]_i$ where X is the sector length. Thus the global matrix becomes diagonally dominant in which case pivoting is not required. Qualitative numerical stability checking is not feasible since the elements of the matrix are determined numerically. Instead, its stability has been tested with a condition number κ using a subordinate matrix bound norm defined analogously to the maximum vector norm as

$$\begin{aligned} \kappa(C) &= \| C \|_\infty \| C^{-1} \|_\infty \\ \| C \|_\infty &= \max_{1 \le i \le n} \sum_{j=1}^{n} | c_{ij} | \quad . \end{aligned} \tag{4.2}$$

In all of the tested cases which are physically well defined, including very sharp medium contrasts in range, condition numbers were found to be in the range of $0 \sim 10^4$ which is a safe indication of numerical stability for the global matrix for vertical interfaces.

Once the stability has been checked, it remains to verify the accuracy of these solutions. By arbitrarily varying the range discretization, elements of the global

matrix are changed along with its dimension. Propagation of an acoustic signal in a homogeneous waveguide shown in Fig. 4.1 was investigated. From 2 to 5 dummy vertical interfaces were placed at various positions. Transmission loss over all ranges matched with analytic result within few percent of error for all cases.

4.5 Modeling of Half-space

As described in Appendix B, it is not possible to find a basis function expansion for half-spaces which also have horizontal wavenumber integral representations. Thus free space radiation problems are not suited for treatment by the present hybrid method. In ocean acoustic problems, where there is a free surface and a bottom to trap acoustic energy, most of the energy is confined to a combination of the finite water column and some part of the bottom half-space; this may be handled in the following way.

When there is penetration of energy into the bottom half-space, which for some cases will back radiate this energy into the layer, we introduce a dummy horizontal interface down to the point where the back radiation is negligible. The half-space existing below this dummy interface is truncated only in relation to coupling between sectors which is negligible for evanescent waves in the half-space. The radiation condition within a sector is correctly represented in contrast to the coupled mode theory where a false bottom and attenuation have to be introduced.

This depth location of the dummy interface depends on various factors, particularly on the geometry of the anomalies existing in the half-space, frequency of the source, attenuation in the medium and mode wavenumber. Since mode wavenumber is not known *a priori*, the bottom half-space can only be modeled by trial and error by checking the convergence of the kernel. In the following chapter, examples with bottom half-spaces are investigated and the depth of the dummy interface is listed in the text along with other modeling parameters. From these, and numerous other examples tested, a general rule-of-thumb is to model the bottom half-space

as finite thickness layers having a thickness equal to or not much greater than the water column depth.

Chapter 5

Numerical Examples

This chapter discusses and shows numerical examples including four canonical problems, and with applications to matched field processing. Critical modeling parameters such as wavenumber sampling, degree of orthogonal polynomials, number of equivalent point sources and half-space modeling will be discussed for each example.

5.1 Canonical Problems

By applying the hybrid numerical algorithm code, solutions of following canonical problems are given in this chapter. These include:

1. Mode conversion in a perfect waveguide of discretely varying medium parameters;
2. Mode conversion in a Pekeris waveguide with changing bottom parameters;
3. Acoustic propagation in a stepwise depth varying environment;
4. Propagation in an ocean environment with a buried salt diapir.

The first example, which has an analytic solution using coupled mode theory, is chosen to demonstrate the overall accuracy of the hybrid BIE+WI method. The second example demonstrates the feasibility of modeling abrupt medium change

problems which are not amenable to treatment by other range dependent solution techniques. The third example compares the hybrid method with the coupled mode solution and with the parabolic equation method. Finally, the fourth example demonstrates the effect of a buried salt dome in the sub-bottom on the received signals at various depths.

5.1.1 Mode Conversion in a Perfect Waveguide

Consider a waveguide with perfectly reflecting boundaries on both the top and the bottom interface as shown in Fig. 5.1. In the left region, only the first perfect mode can be generated by the source of frequency 100 Hz located at the mid-depth of the water channel whereas up to 3 modes can propagate in the right sector. We use 2^{11} wavenumber sampling points to cover the horizontal phase velocity interval from $C_{\min} = -400$ to $C_{\max} = 400$ m/sec and a total of 3 polynomials(P_0, P_1, P_2) are used. The displacement source solution, in terms of horizontal wavenumber integral valid inside the layer, is found from the discrete equivalent point source representation given in Appendix C. Ten equivalent point sources have been used. The perfect mode present in the channel reveals itself as a sharp peak in the wavenumber integration kernel which makes it necessary to adopt the complex integration scheme for smoothing the kernel, as mentioned in Chapter 3.

Fig. 5.2 shows the transmission loss *vs.* range for receiver at the source depth. The discontinuity of the medium is at range = 0 km. The transmission loss between the source and the discontinuity reveals interference of the back-scattered signal with the forward propagating first mode and only the first mode is coupled into the right water column. To the left of the source, the interference pattern does not arise since the two signal are propagating in the same direction with equal phase speed.

Table 5.1 shows the transmission loss values at the right sector, which is a constant, for receivers located at 2.5 and 5.0 m respectively. They are independently

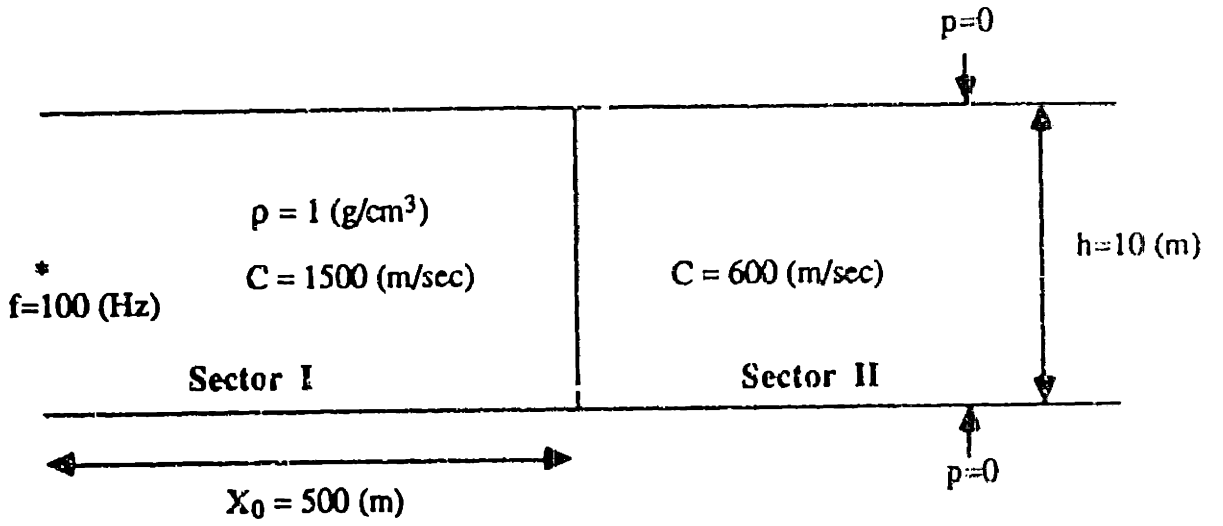

Figure 5.1: Waveguide with perfectly reflecting boundaries with abrupt propagation speed change from 1500 to 600 m/sec. Source of 100 Hz is located 500 m to the left of the discontinuity at 5 m depth.

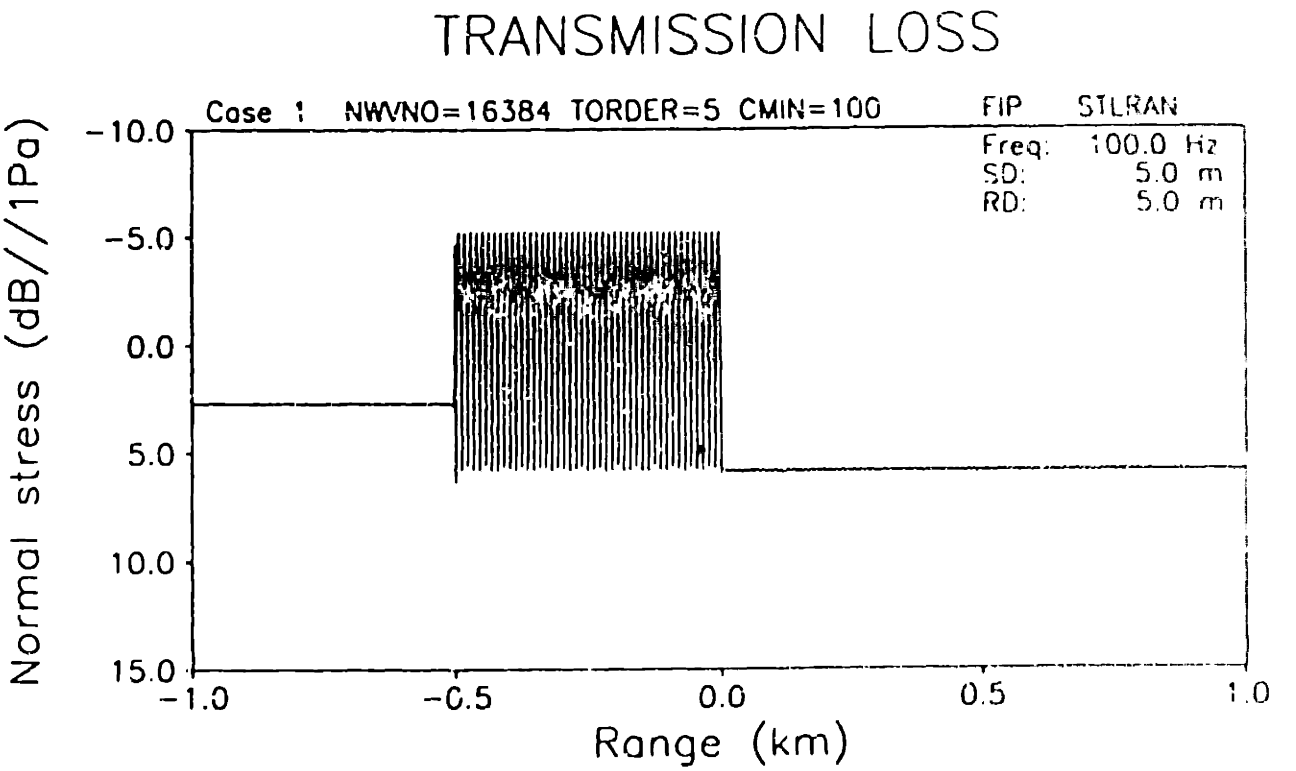

Figure 5.2: Transmission loss for perfect waveguide of Fig.5.1.

calculated from both the analytic expression and the hybrid BIE+WI scheme. The last result is from a coupled mode code [16] where difficulty in modeling lower vacuum half-space was reported. Using the hybrid method, the largest relative error of the pressure is 3 % for this example. The inherent numerical errors involved in the hybrid method are: truncation of the basis function expansion to a finite number of terms, and truncation of the horizontal wavenumber spectrum. Aside from the inherent numerical errors, complex integration in the horizontal wavenumber domain was performed and neglecting the contribution of the small vertical contour is another source of numerical error. In spite of these errors, the overall accuracy is satisfactory. In underwater acoustics modeling, an accuracy to within 1 dB of the true solution is more than sufficient.

As a further check on the validity of the solution, and hence the model, we employ reciprocity, which is a check of correctness. We exchange the locations of the source and the receiver and again calculate the pressure field. Reciprocity, however, has to be tested with care when the media are inhomogeneous. When the source and the receiver are interchanged, the calculated pressure field at the receiver has to be multiplied by the medium impedance (ρC). Table 5.2 shows the received pressures for the source and the receiver interchanged. After the impedance correction, the results are found to comply reciprocity, which again validates the hybrid method and model.

Receiver	Transmission loss at right sector (dB)		
depth (m)	Analytic	Present	Coupled mode
$z_r = 2.5$	8.72	8.7	7.25
$z_r = 5.0$	5.71	6.0	4.24

Table 5.1: Transmission loss comparison

5.1.2 Mode Conversion in a Pekeris Waveguide

The second example examined is propagation of the acoustic signal in a waveguide having a bottom contrast. A canonical choice is the Pekeris waveguide [40]. The water column is 10 m deep with a pressure release upper boundary and the bottom layer medium parameters change abruptly as shown in Fig. 5.3, denoted as region *III* and *IV* respectively. As in the previous test case, we use left and right sectors. In the left Pekeris waveguide (region *I* and *III* combined) only one trapped mode is generated by a 200 Hz source located at the mid point of the water column. To the right of the discontinuity (region *II* and *IV* combined), up to two trapped modes can propagate. Again, 2^{11} wavenumber sampling points are used to cover a horizontal phase velocity interval from $C_{\min} = -1000$ to $C_{\max} = 1000$ m/sec and a total of 5 polynomials and 10 equivalent point sources are used. The bottom half-space is modeled to a depth of 20 m which is found to be sufficient in this case.

Contoured transmission losses over depth and range are given in Fig. 5.4 where an attenuation of 0.1 dB/λ is introduced in every medium. The bottom left-right discontinuity is at range = 0 km and Fig. 5.4(a) is for a source at range = -0.5 km whereas Fig. 5.4(b) is for a source at range = 0.5 km. When the source is located at the left of the discontinuity, which excites the first mode, the Pekeris modal pattern and the continuous spectrum (which constantly leaks energy into the bottom

Received signal	Source & receiver coordinate (m)	
	$(x_s, z_s) = (-500, 5)$ $(x_r, z_r) = (500, 2.5)$	$(x_s, z_s) = (500, 2.5)$ $(x_r, z_r) = (-500, 5)$
Transmission loss	9.09 (dB)	5.01 (dB)
Impedance corrected $(p^2\rho C)$	4.87×10^4	4.75×10^4

Table 5.2: Reciprocity test

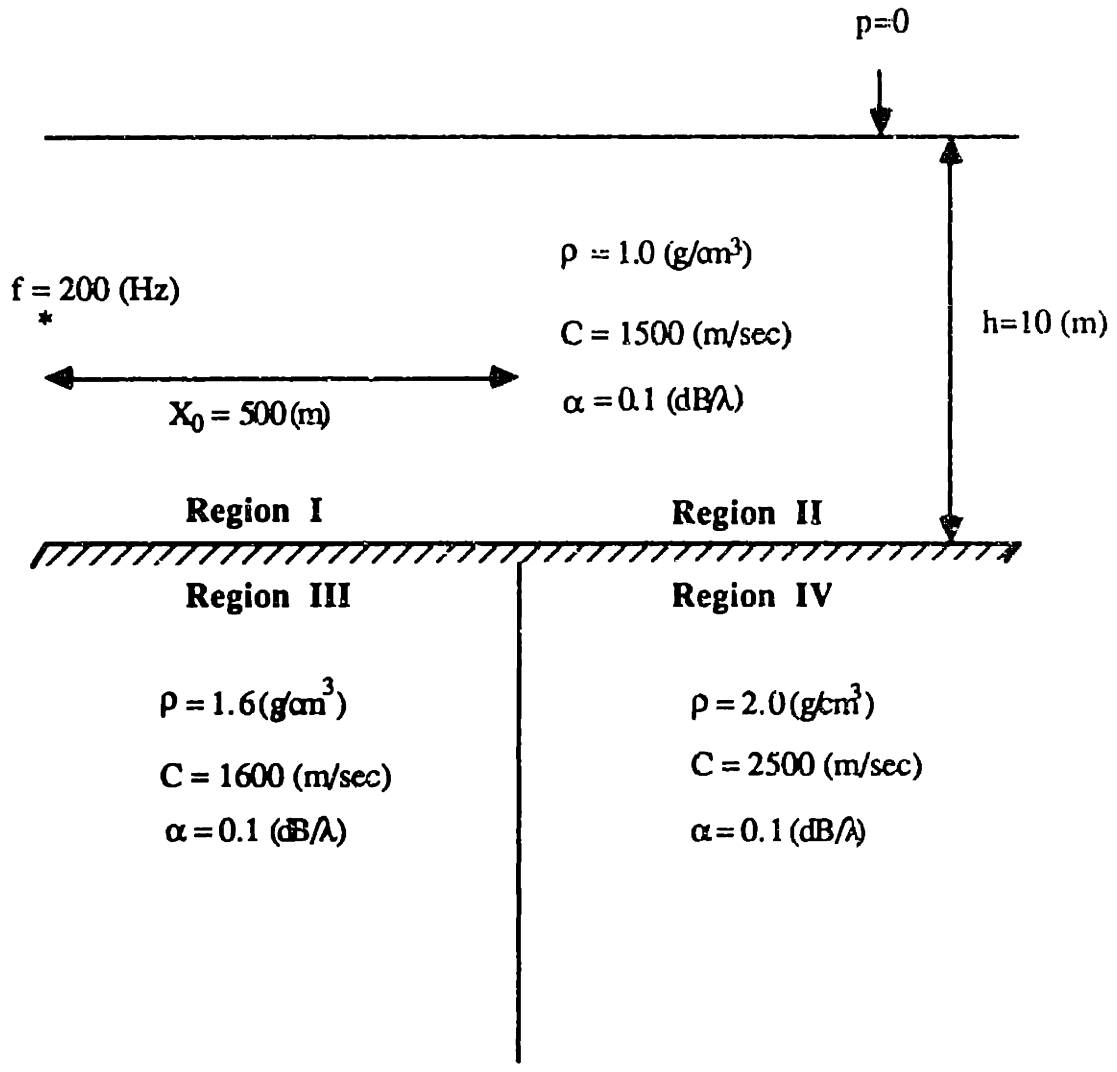

Figure 5.3: Pekeris waveguide with bottom discontinuity. Media parameters are as shown and the source (5 m depth) of 200 Hz is placed at 500 m to the left of the bottom discontinuity.

directly below the source location) can be seen for the left sector. Interference arising from the back-scattered field due to the bottom contrast can also be seen. In the right sector, energy is coupled into two trapped modes, giving rise to a modal interference pattern. The continuous spectrum is also observed, leaking energy into the bottom at the discontinuity. For the *vice versa* reciprocal case, where the source is to the right of the discontinuity and excites two Pekeris modes, the interference pattern is more pronounced due to the first and second mode and the back-scattered propagation. To the left, only the first mode is coupled into the medium.

This example demonstrates the class of problems the present method is most suited for, and which are not amenable to treatment by other existing range dependent solution techniques. This method yields reliable full-wave solutions even for half-space problems, by modeling the half-space as finite layers and introducing a dummy horizontal interface.

5.1.3 Cylindrical Seamount Problem

Consider a cylindrically symmetric ocean environment with a ring-like seamount. The seamount has a rectangular cross section as shown in Fig. 5.5. A source of frequency 25 Hz is located at the mid-depth of a 200 m water column. A 135 m high seamount is located with inner radius at 5 km and an outer radius at 10 km. The water column is homogeneous with the customary medium parameters and the bottom is a homogeneous half-space with attenuation of 0.5 dB/λ. 2^{10} wavenumber sampling points are used to cover a horizontal phase velocity interval from C_{min} = 1300 to $C_{max} = 1.0 \times 10^8$ m/sec. A total of 4 polynomials(P_0, P_1, P_2, P_3) and 10 equivalent point sources are used, along with complex integration for smoothing the kernel for trapped modes present in the channel. The bottom half-space is modeled to the depth of 300 m which is found to be sufficient in this case because of relatively large attenuation in the bottom half-space.

This numerical example was treated using a one-way wave propagation Green's

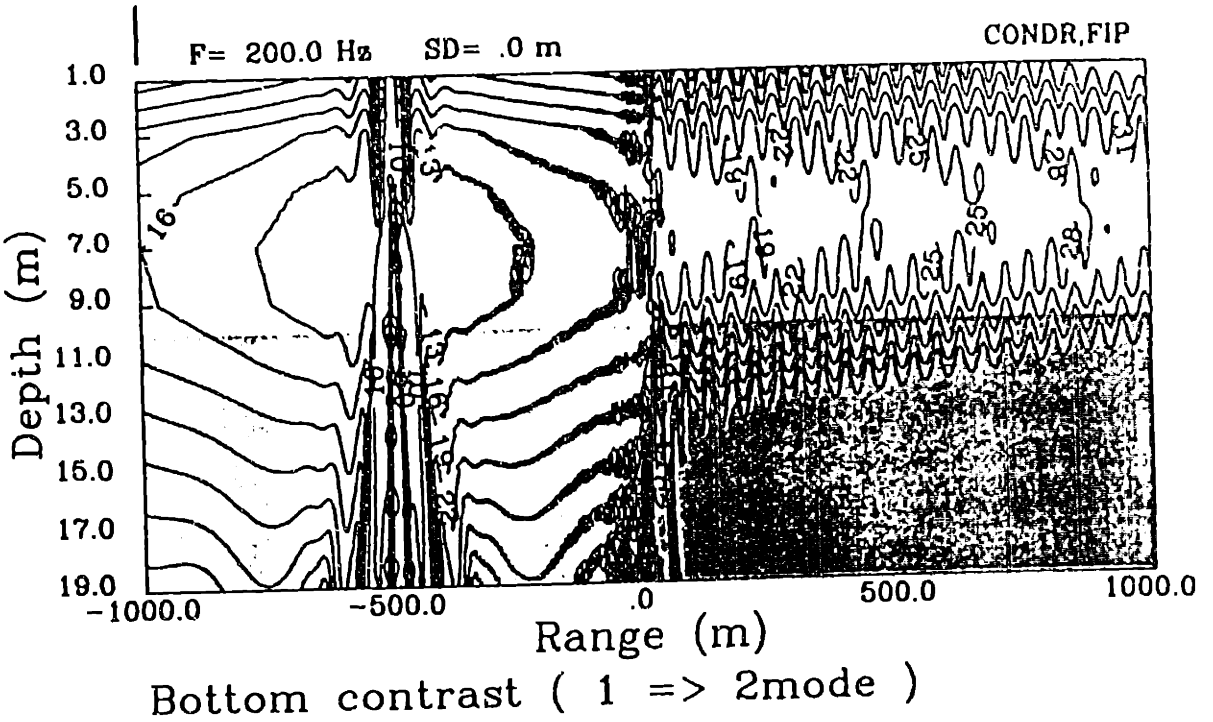

(a)

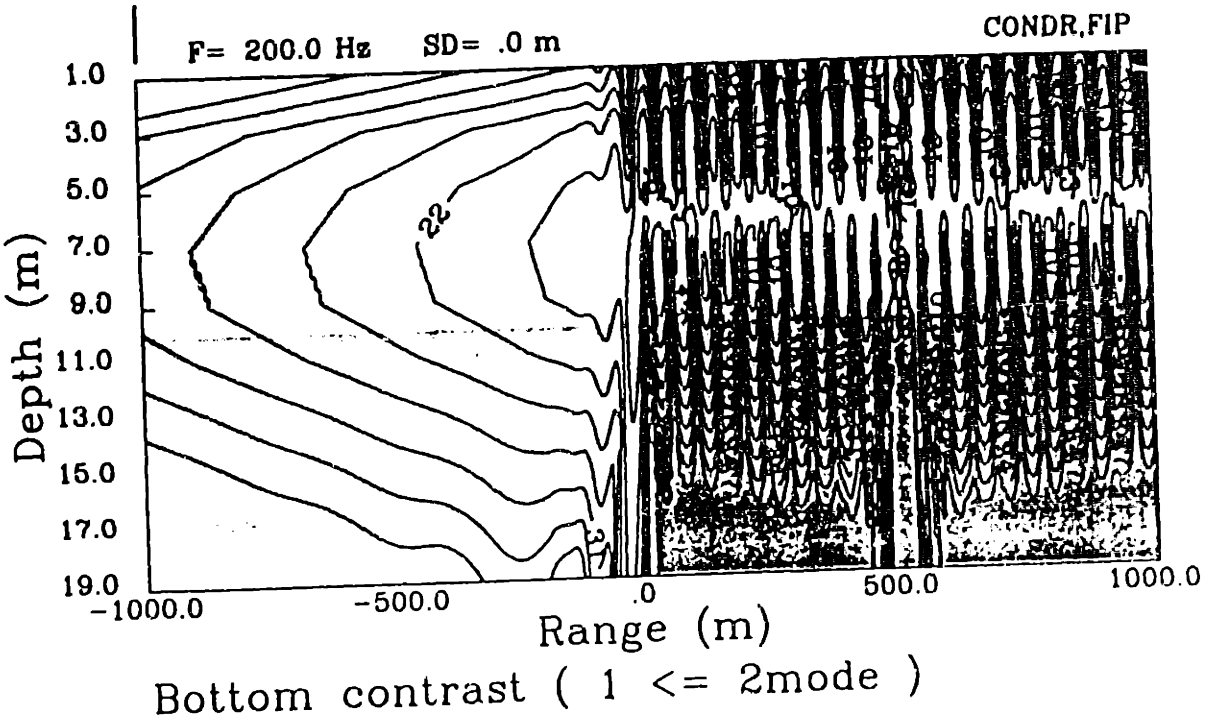

(b)

Figure 5.4: Contoured transmission loss for the Pekeris waveguide with the source located at: (a) $x_s = -0.5$ km ; (b) $x_s = 0.5$ km. Shaded area represent bottom.

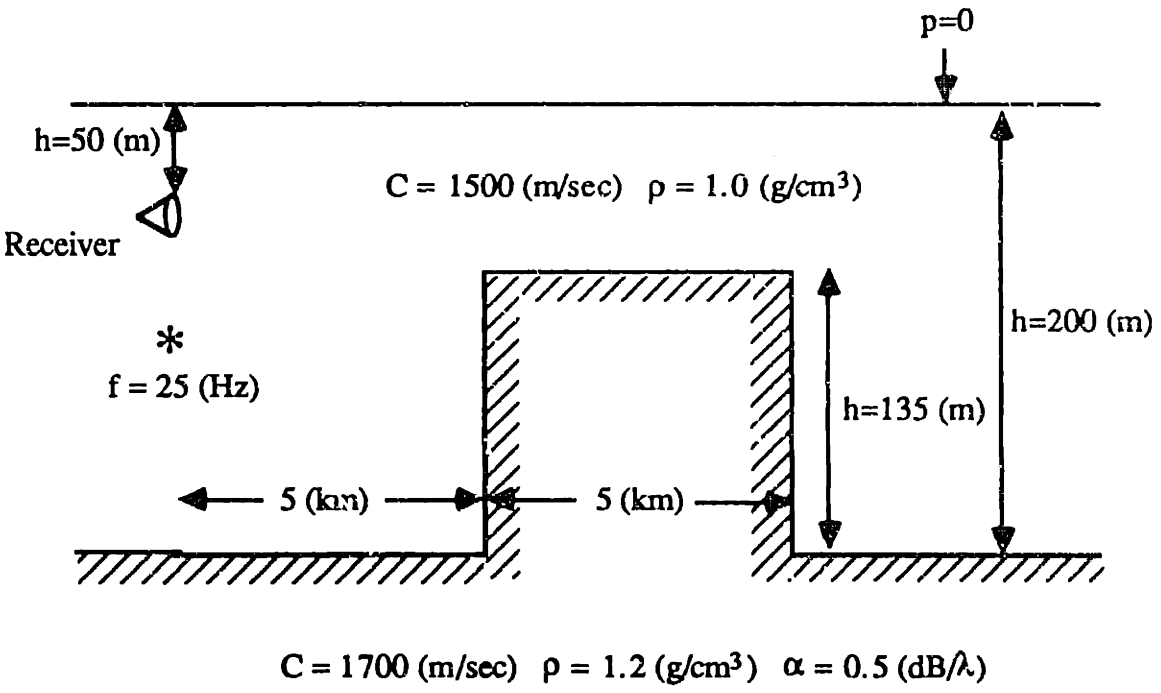

Figure 5.5: Wave propagation in cylindrical ocean environment with bottom seamount of rectangular cross sectional shape. Media parameters are shown and 25 Hz source is at 100 m depth with receivers placed at all ranges at 50 m depth.

function model by Gilbert and Evans [23]. Their method was first in generalizing Green's function method to range dependent problems, but it was based on a *marching* solution technique where the source function is the field at the end of the previous range step. Thus, only a one-way wave equation solution could be found which makes their method just like the parabolic equation method. For an even comparison, this problem is solved by the hybrid BIE+WI method with the back-scattering ignored at the end of the field calculation. This is achieved simply by dropping the back-scattered field term, either of G_L or G_R depending on the location of the source, in the Green's function of Eq. 3.39. Fig. 5.6 shows the transmission loss *vs.* range for receiver at the depth of 50 m calculated by various methods. Thick solid line is from RDFFP of Gilbert and Evans [23] and dashed line is calculated in two different ways (these are indistinguishable on the plot): first, the coupled mode model CUPYL [16] was used with back-scatter turned off to solve the one-way wave equation; second, the wide-angle version of parabolic

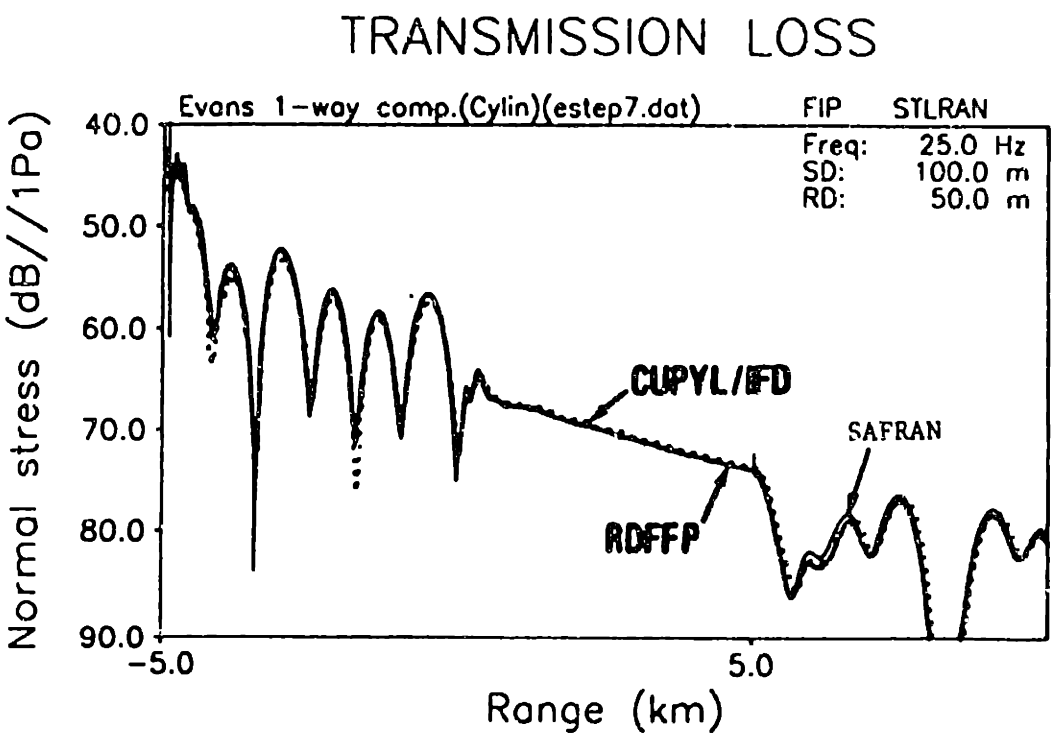

Figure 5.6: One-way wave propagation transmission loss for the ocean with bottom seamount.

equation model IFD [37] was used. The thin solid line is from the hybrid BIE+WI numerical code SAFRAN, and excellent agreement can be observed between these methods. The little difference in troughs are due to different sampling points in range. The small spike belongs to the right half-infinite sector after the seamount vanishes and occurs due to aliasing when the FFT is performed. The difference in the third sector arises because of the inherent problem with energy conservation using the one-way wave equation solution technique [42] whereas the hybrid BIE+WI method entirely satisfies the energy conservation. Fig. 5.7 shows the hybrid result with the back-scattered component switched-on, and a small interference pattern can be observed at all ranges except for the right half-space sector.

As pointed out by Gilbert and Evans [23], using the Green's function method to solve range dependent problems is advantageous since we deal directly with its spectral components and valuable information on mode conversion phenomena can be obtained by looking at its kernels. This is demonstrated in the next section.

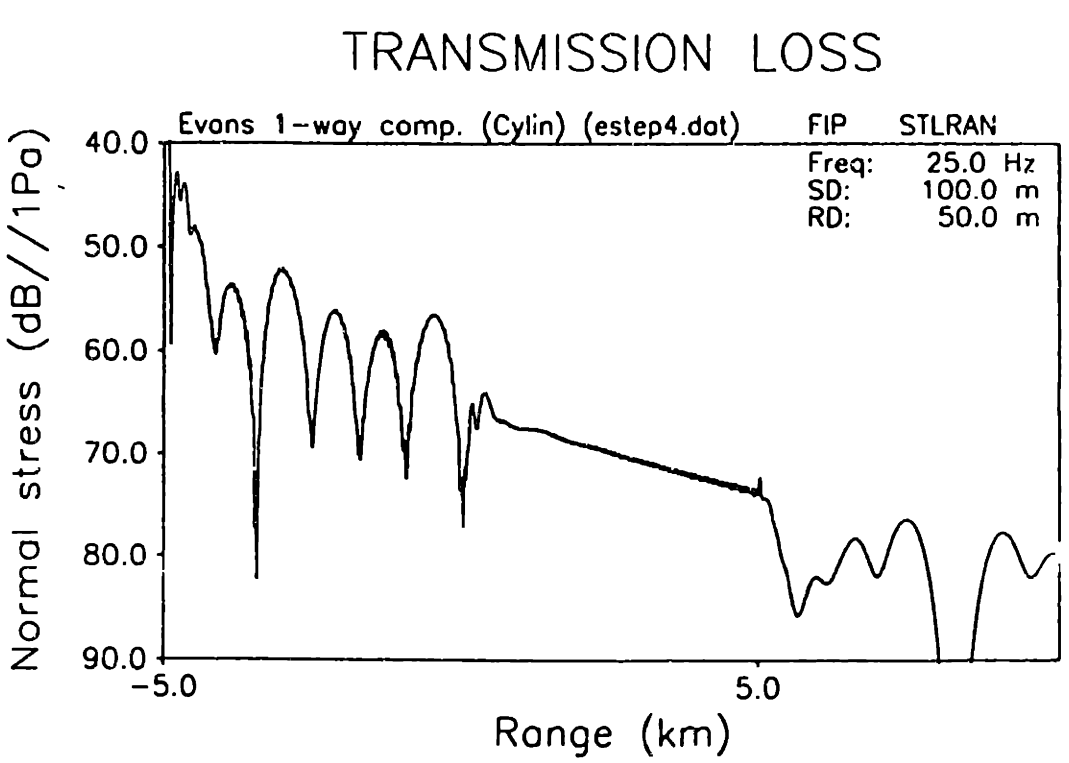

Figure 5.7: Both-way wave propagation transmission loss for the ocean with bottom seamount.

5.1.4 Salt Diapir Problem

We now consider a problem similar to that of the previous section except that the plane geometry plus the seamount is replaced by a buried salt diapir as shown in Fig. 5.8, where three separate vertical strips are termed as sector 1,2 and 3 respectively. Note that media parameters are chosen as approximate representative of a real situation where the sub-bottom salt diapir, which is an upswelling of salt from the deep basement containing an extensive layer of salt, has a lower density than the overlying sea bottom. Real salt diapirs have been detected as sharply defined, almost column–like features, in geoseismic sections, and approximately as shown in the figure.

The source frequency and depth dimensions are chosen such that only two trapped modes will be present, thus simplifying the interpretation of the result. A source of frequency 150 Hz is located near the surface of the ocean at $z_s = 1$ m and 0.5 km in range to the left of the salt diapir which continues for 1 km in range.

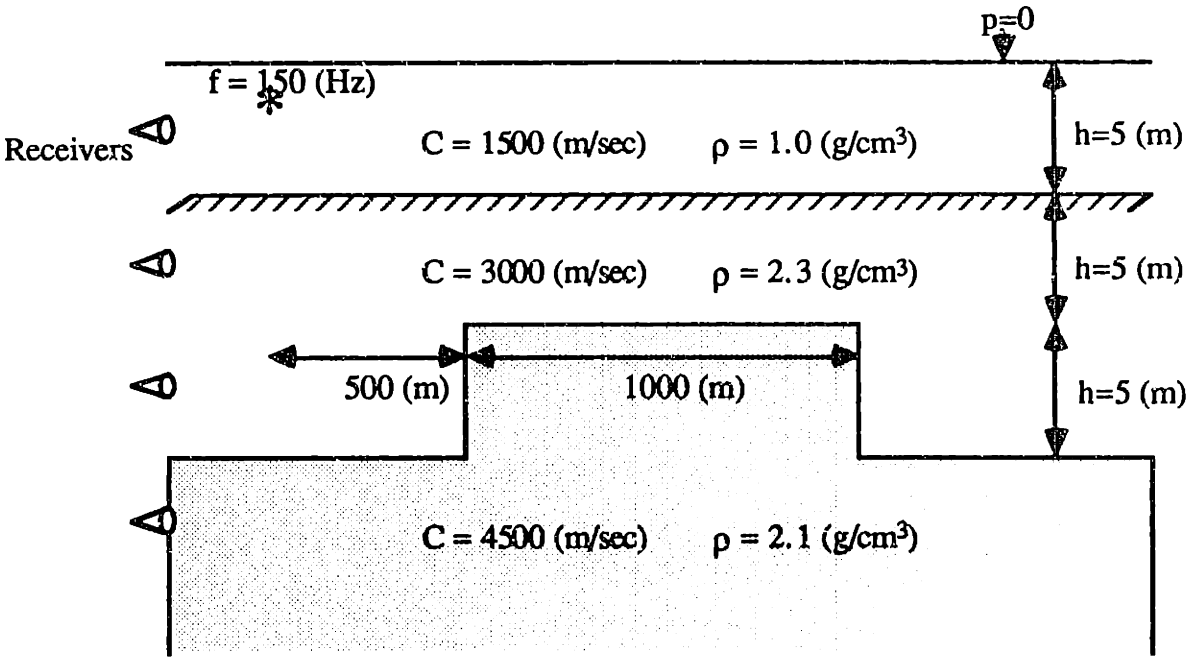

Figure 5.8: Ocean environment with a salt diapir in the sub-bottom. Media parameters are as shown and 150 Hz source is at 1 m depth with 4 receivers located at $z = 2.5, 7.5, 12.5$ and 17.5 m depths.

2^{10} wavenumber sampling points are used to cover a horizontal phase velocity interval from $C_{\min} = -1000$ to $C_{\max} = 1000$ m/sec and a total of 4 polynomials and 10 equivalent point sources are used. The bottom half-space is modeled to a depth of 20 m.

Initially, 4 receivers are placed at depths RD = 2.5, 7.5, 12.5 and 17.5 m. Fig. 5.9 shows the transmission losses at these receiver depths *vs* range. The elevated salt diapir is from range = 0 to 1 km and the source is at range = −0.5 km. Fig. 5.10 shows the horizontal wavenumber spectrum at the start of each of the three environmental regions at all receiver depths. In the open water channel, originally there would be two propagating modes; however, the second mode is cut off in sector 2 due to the bottom salt diapir and consequently, only one mode is dominating in sector 3.

At the bottom receiver, RD = 7.5 m, the layer is still homogeneous in range with a medium wavenumber $h_B = 0.31$. Looking at the integrand of the 1st sector of

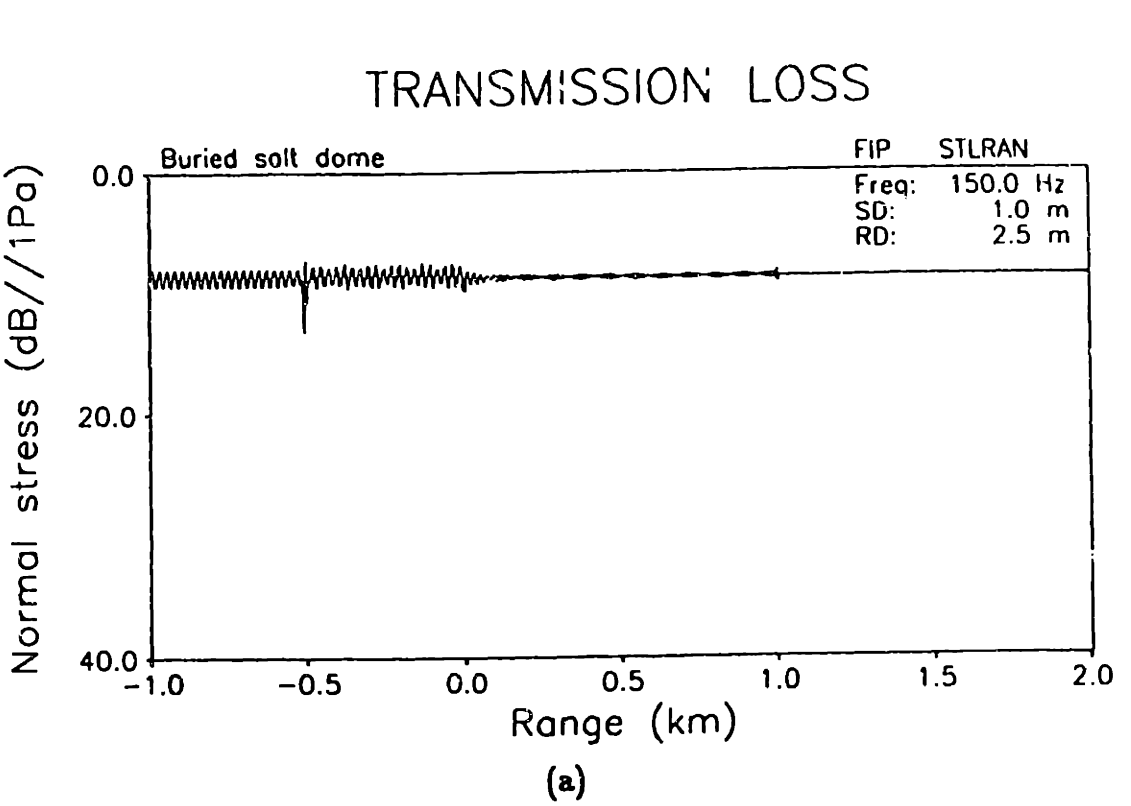

(a)

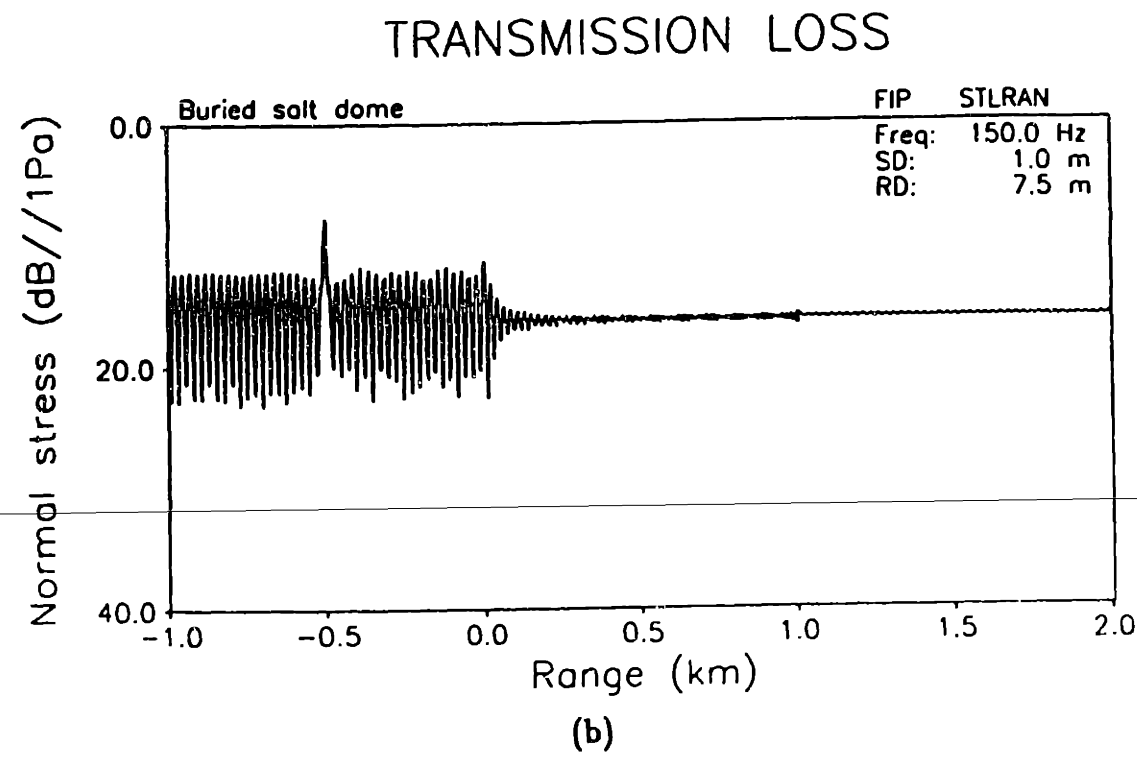

(b)

Figure 5.9: Transmission loss *vs.* range at: (a) $z = 2.5$ m ; (b) $z = 7.5$ m ;(continued)

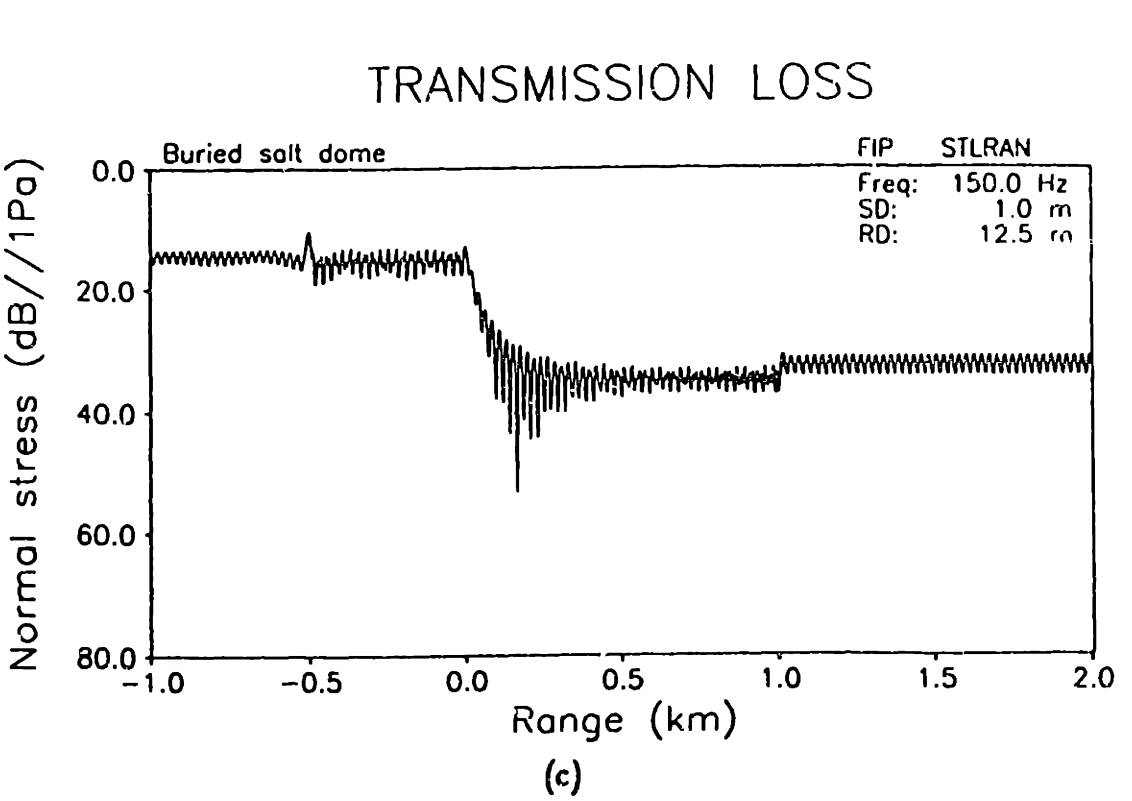

(c)

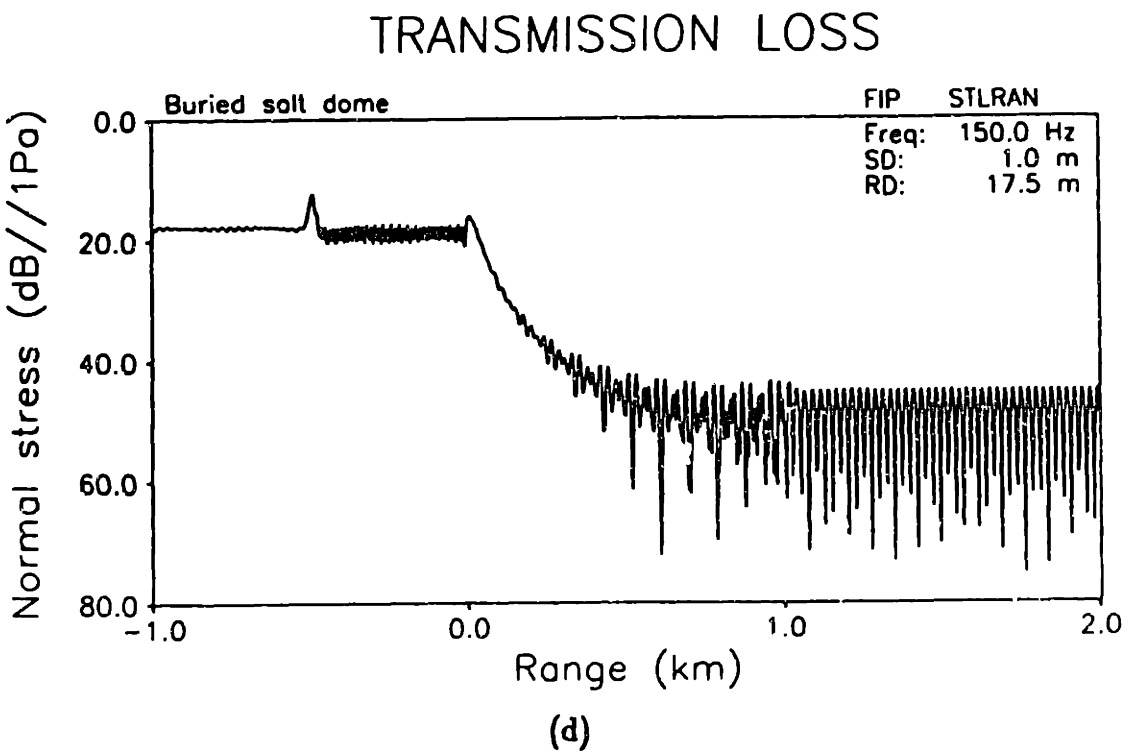

(d)

Figure 5.9: Transmission loss *vs.* range at: (c) $z = 12.5$ m ; (d) $z = 17.5$ m.

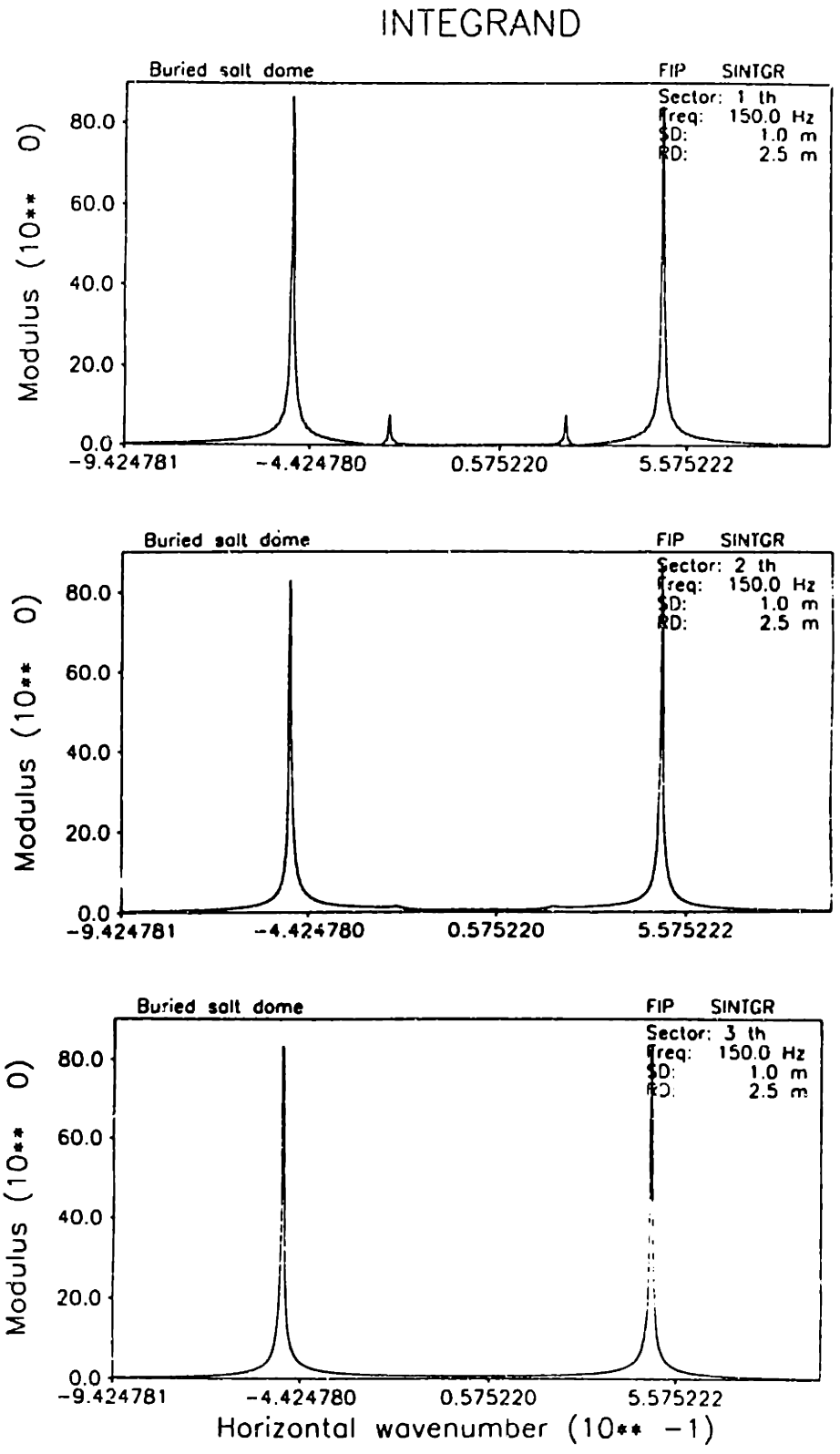

Figure 5.10: Horizontal wavenumber spectrum at the start of each of the three environmental regions for receiver depths: (a) $z = 2.5$ m ;(continued)

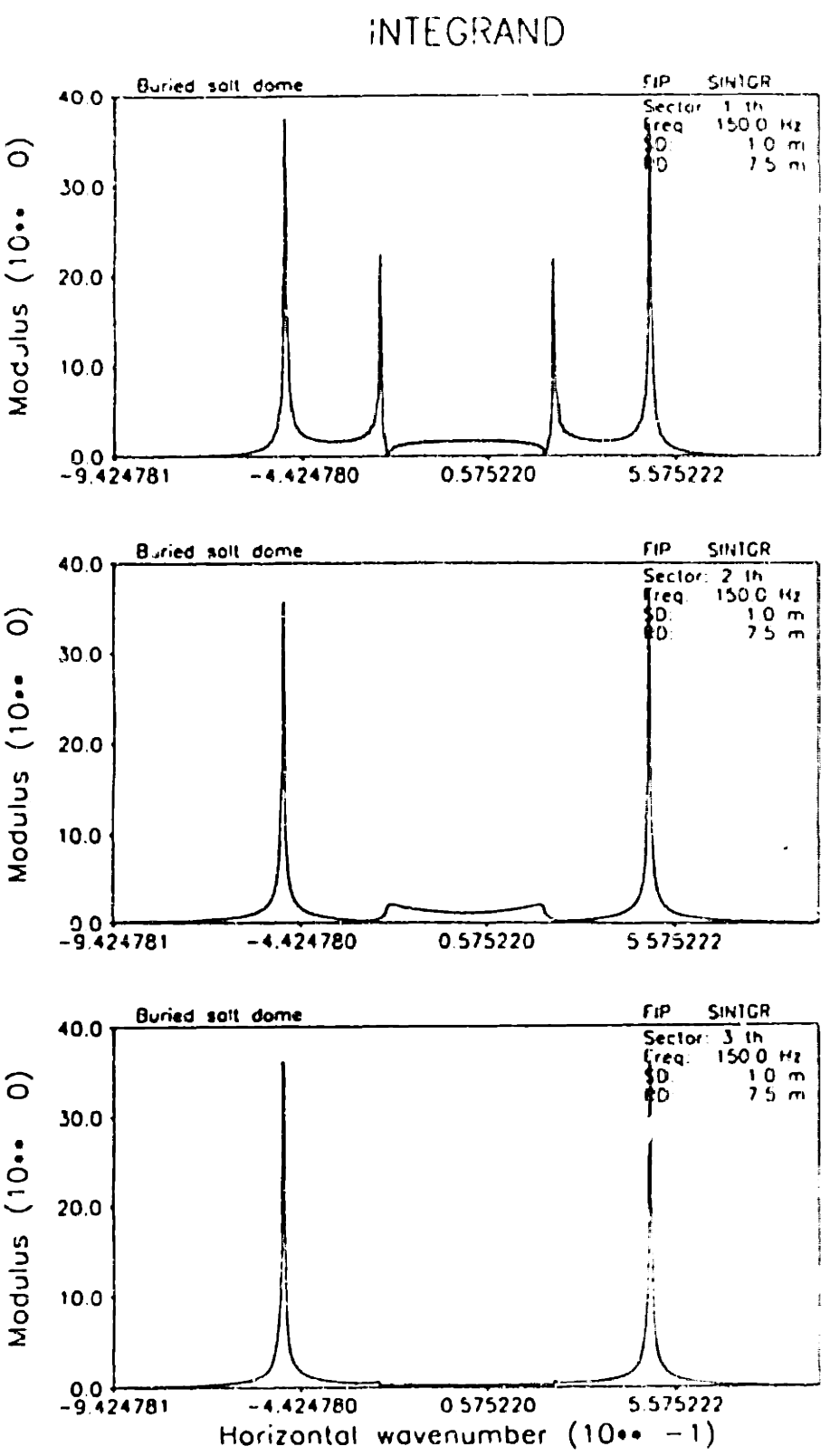

Figure 5.10: (b) $z = 7.5$ m ; (continued)

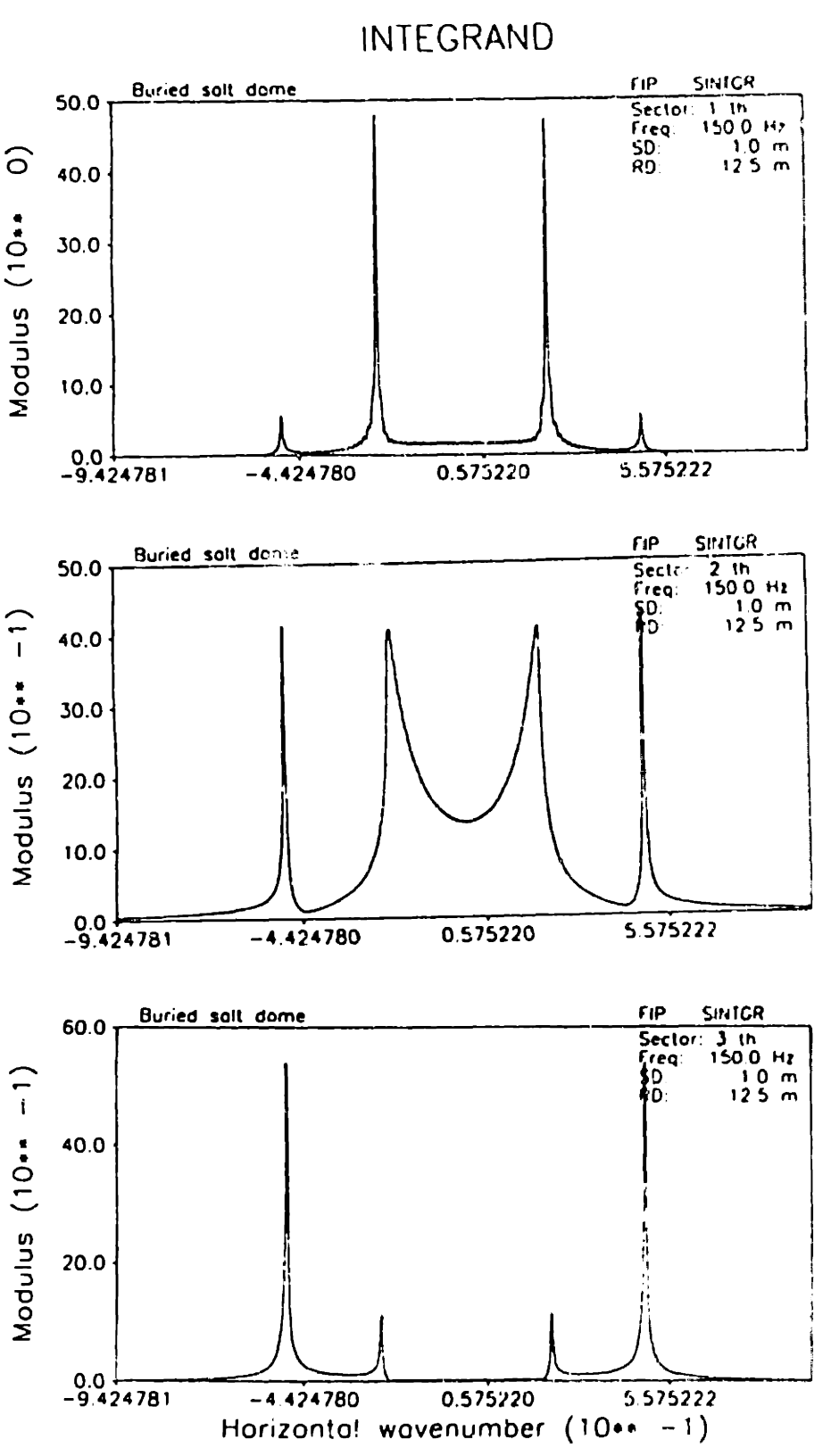

Figure 5.10: (c) $z = 12.5$ m ; (continued)

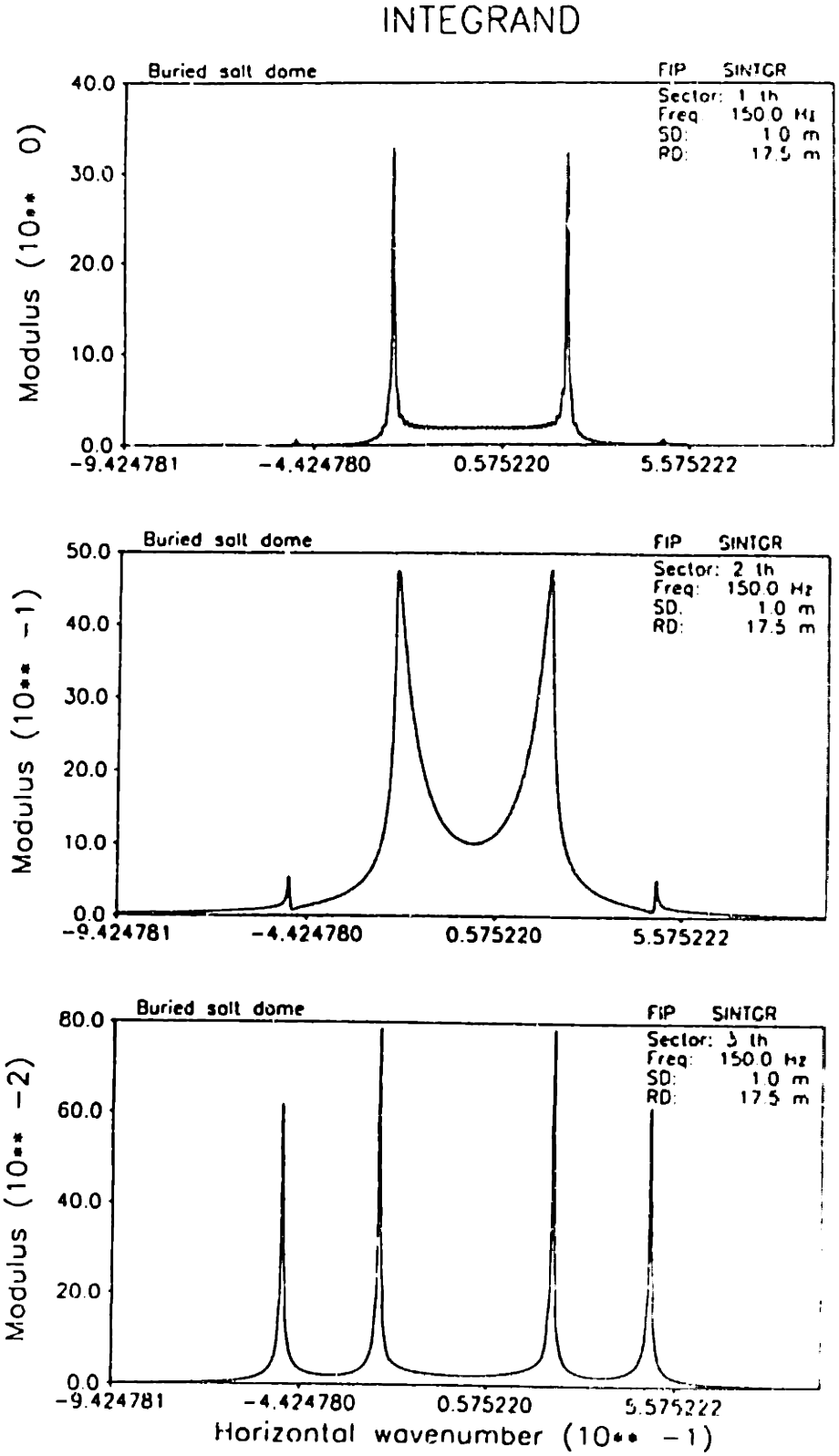

Figure 5.10: (d) $z = 17.5$ m.

Fig. 5.10(b), the magnitude of the propagating second mode increases relative to the evanescent first mode, giving a severe interference pattern in the transmission loss plot. As the signal propagates into sectors 2 and 3, this second mode is cut off. The first mode has most of its energy confined in the water column, and shows a rapidly decaying evanescent tail in the bottom, and thus is not affected by the presence of the salt diapir, which is seen in the unchanging first mode in all sectors. At RD = 12.5 m where the medium changes in range, the second mode dominates in sector 1. Due to the salt diapir in sector 2, there is a slight shift of mode wavenumber which is just below the cut off of $h_3 = 0.21$ and begins to transform to a continuous spectrum. As the signal reaches sector 3, the magnitude of the now-propagating second mode is drastically reduced compared to near constant evanescent first mode. At RD = 17.5 m, the same phenomenon is observed giving rise to a sharp drop in the transmission loss curve as the salt diapir is encountered. This anomaly in the acoustic propagation has been experimentally observed in the Barents sea, where a known salt diapir occurs in the region of basement outcrop (see Hug [27]).

Finally, the contoured transmission loss over depth and range is given in Fig. 5.11 where an attenuation of 0.1 dB/λ is introduced in every media. The propagating first modal shape can be observed throughout the water channel with the additional second mode in sector 1. Slight interference arising from the back-scattered field due to the sub-bottom salt diapir can also be seen. Over an elevated column such as the salt diapir region, the transmission loss is relatively high. This indicates the presence of an inhomogeneous feature (relative to the surrounding region) in the sub-bottom structure.

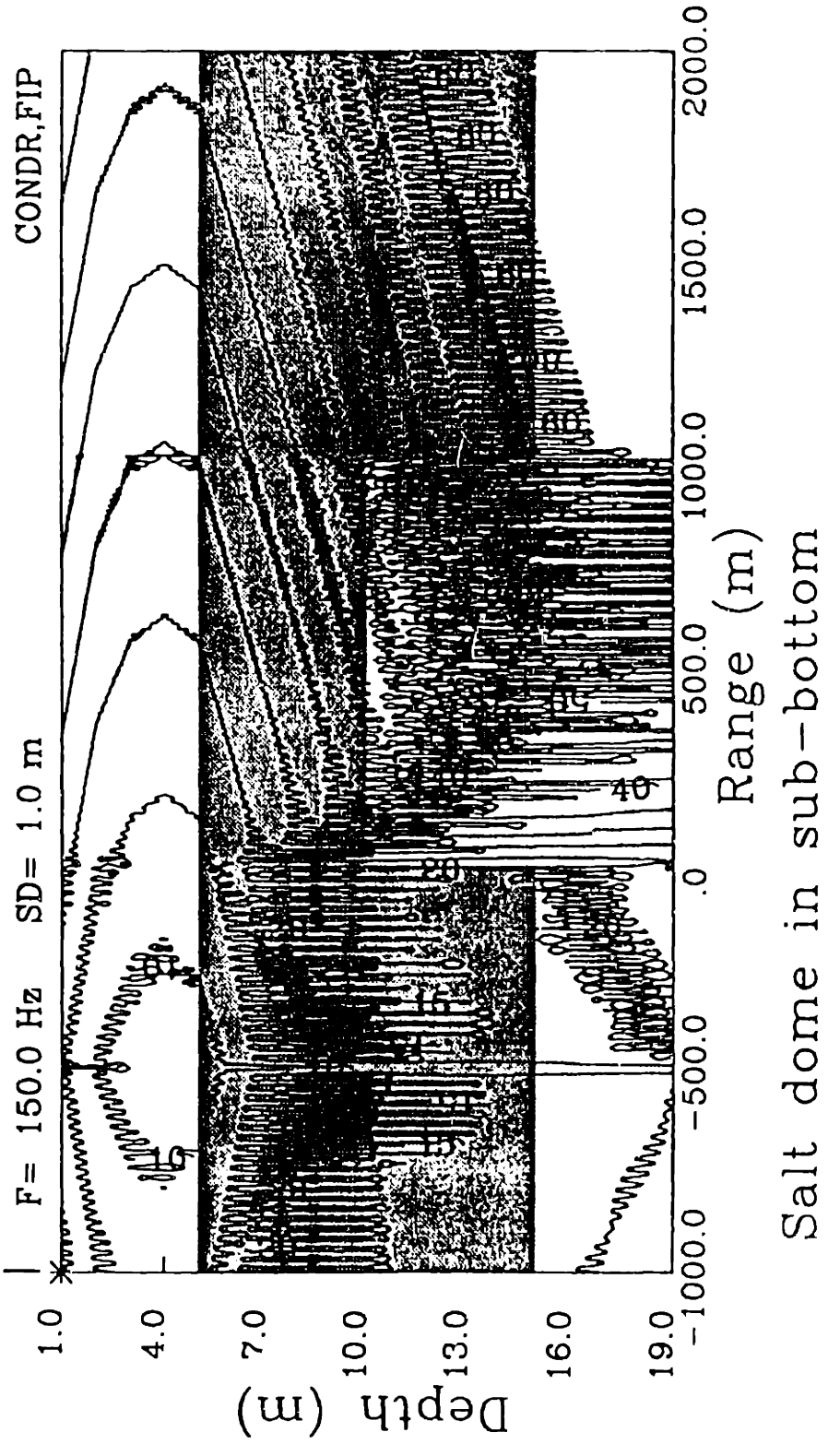

Figure 5.11: Contoured transmission loss for buried salt diapir of Fig.5.8. Dark shaded area is the bottom and the light shaded area represents the salt diapir.

5.2 Generation of Reverberated Field for Matched Field Processing

Matched field processing is a parameter estimation technique for localizing the range, depth and bearing of a point source from the signal field propagating in an acoustic waveguide. Specifically, matched field localization employs an environmental model to match the acoustic field received by an array of sensors, with calculated replicas of the expected field for all possible source locations. The general approach of matching involves the correlation of the pressure field at the receivers in a hydrophone array with a field calculated at the receivers that is based on assumed model of the environment. The model-based calculation field is used as the replica and is dependent on an assumed source range and depth. A high degree of correlation between the received pressure field and the calculated pressure field at a particular range and depth is an indication of a source at that range and depth.

Most of previous works on matched field processing has been related to passive sonar systems employing hydrophone arrays to localize a point source. An active sonar system for localizing an inhomogeneity of finite extent has, in contrast, been paid little attention. Because of the tools readily available, *i.e.* the present hybrid BIE+WI scheme to generate synthetic data of a reverberated field from an active sonar system and a robust matched field processing algorithm designed by Schmidt *et al.* [44], we may now investigate the performance of localizing anomalies of finite extent in an otherwise homogeneous ocean environment using the matched field processing scheme.

An active sonar matched field processing is performed in three steps.

1. First we select an ocean environment with an inherent inhomogeneity. This ocean environment must be solvable by the hybrid BIE+WI scheme. By placing an active source of known frequency, we may synthesize the reverberated field from the inhomogeneity at an array of receivers placed near the source range.

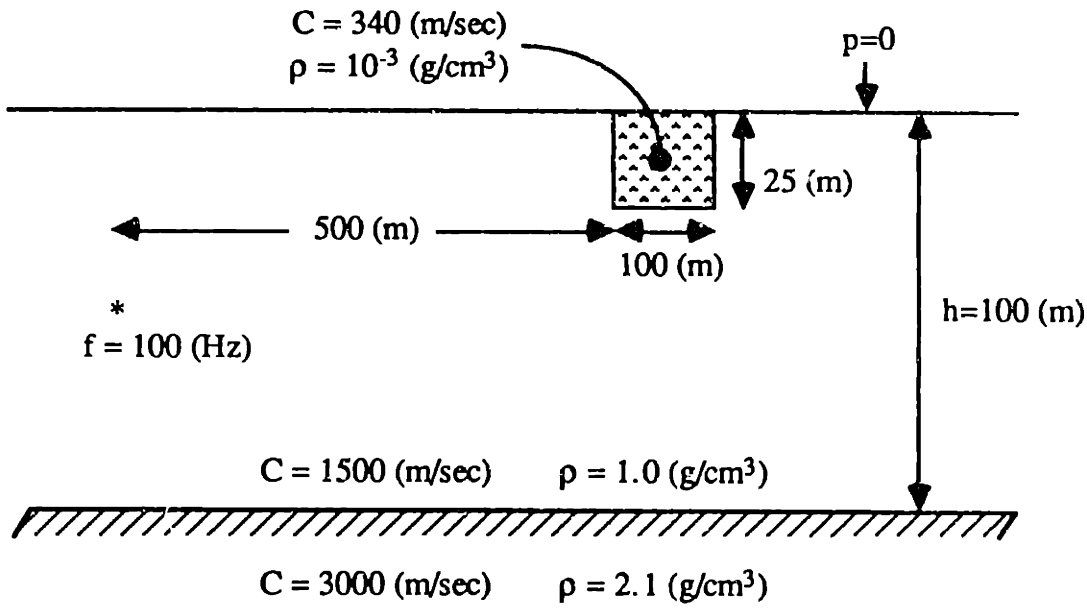

Figure 5.12: Cross sectional diagram of cylindrically symmetric ocean environment with an air plume of finite dimension near the surface of the ocean.

2. Using only the information provided by the signals arriving at the array of receivers together with environmental parameters of a homogeneous ocean, apply the point source localizing matched field processing scheme.

3. From the results of the signal processing we then attempt to detect and (if possible) estimate the location and size of the inhomogeneity.

For numerical simulation, consider a cylindrically symmetric ocean environment, as shown in Fig. 5.12. At range = 500 m from the source location, an inhomogeneity consisting of air bubbles trapped near the ocean surface, which we call a *plume*, exists. The plume is modeled as continuum having parameters close to those of air. A 100 Hz source is located at the mid-depth of the water channel, and a receiving vertical hydrophone array is at the same range location. Using the hybrid BIE+WI technique, only the back-reverberated signals are measured. Fig. 5.13 shows the depth dependent Green's function of the back-scattered field for 2 receivers, one in the water column and the other placed in the seabed. The reason for both

the negative and the positive spectrum being plotted for a cylindrical geometry was explained at the end of Chapter 3. For the matched field processing to yield reliable results, the vertical array hydrophone spacing must be less than half the vertical wavelength of the highest mode that contributes significantly to the sound field [61]. Since the vertical wavelength of the significant highest mode present (11th mode) is seen to be 17.6 m (from the figure), 16 hydrophones are placed from 10 to 122.5 m at 7.5 m spacing. This gives a slight spatial oversampling and so we avoid wavenumber aliases when we sample the field. In generating the synthetic reverberated field, 2^{10} wavenumber sampling points are used to cover the horizontal phase velocity interval from $C_{\min} = 1000$ to $C_{\max} = 1.0 \times 10^8$ m/sec and a total of 4 polynomials(P_0, P_1, P_2, P_3) and 10 equivalent point sources are used. The bottom half-space is modeled to a depth of 200 m which is found to be sufficient.

Given the information provided by the signals arriving at the array of the vertical receivers, in addition to the environmental parameters of the homogeneous ocean, we could develop a new algorithm to localize a volume inhomogeneity, but this task is beyond the scope of this thesis. Instead, two methods of array processing for *point* source localization in correlated noise are employed: first the maximum likelihood method (MLM) described by Baggeroer *et al.* [3], and second, the more robust multiple constraint method (MCM) by Schmidt *et al.* [44]. Since these numerical codes are used and identical terminology adopted, reference is made to above cited papers concerning the detailed derivations and expressions. Referring to Fig. 5.14 adopted from Baggeroer [3], ambiguity surfaces are constructed from replica fields from a *point* source that scan through $\hat{R}, \hat{H}$ space. Since the ambiguity surfaces provide an indication of the similarity between the assumed fields (replicas) and the actual received data, for localization of a point source, a desirable feature of these contour plots is the occurrence of a single prominent peak at the true source location. The point source localizing algorithm applied to the plume problem is shown in Fig. 5.15, where the range and depth are sampled by 25 m and 10 m,

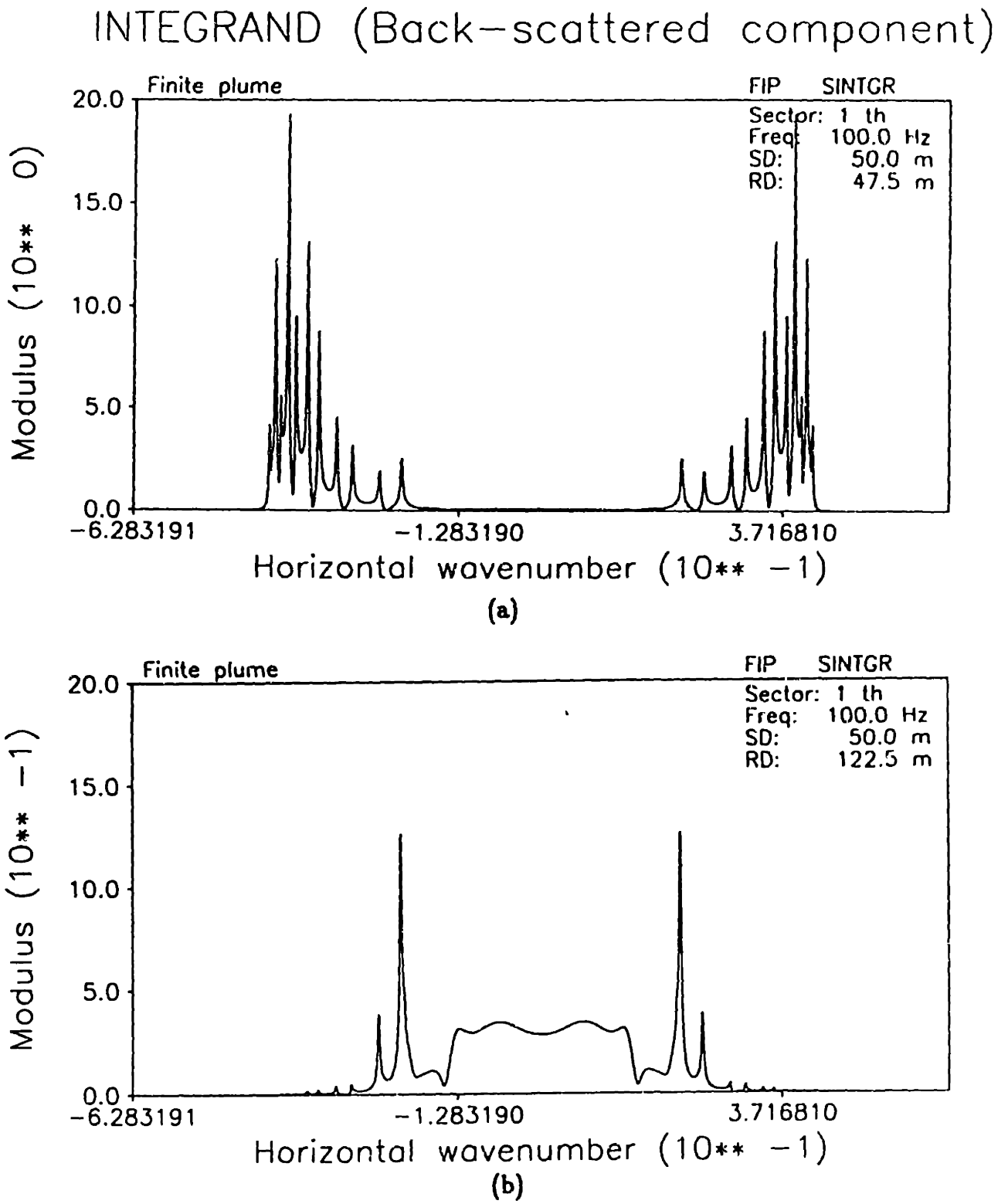

Figure 5.13: Wavenumber kernel for the back-scattered acoustic pressure: (a) in the water column at depth $z = 47.5$ m; (b) in the seabed at depth $z = 122.5$ m.

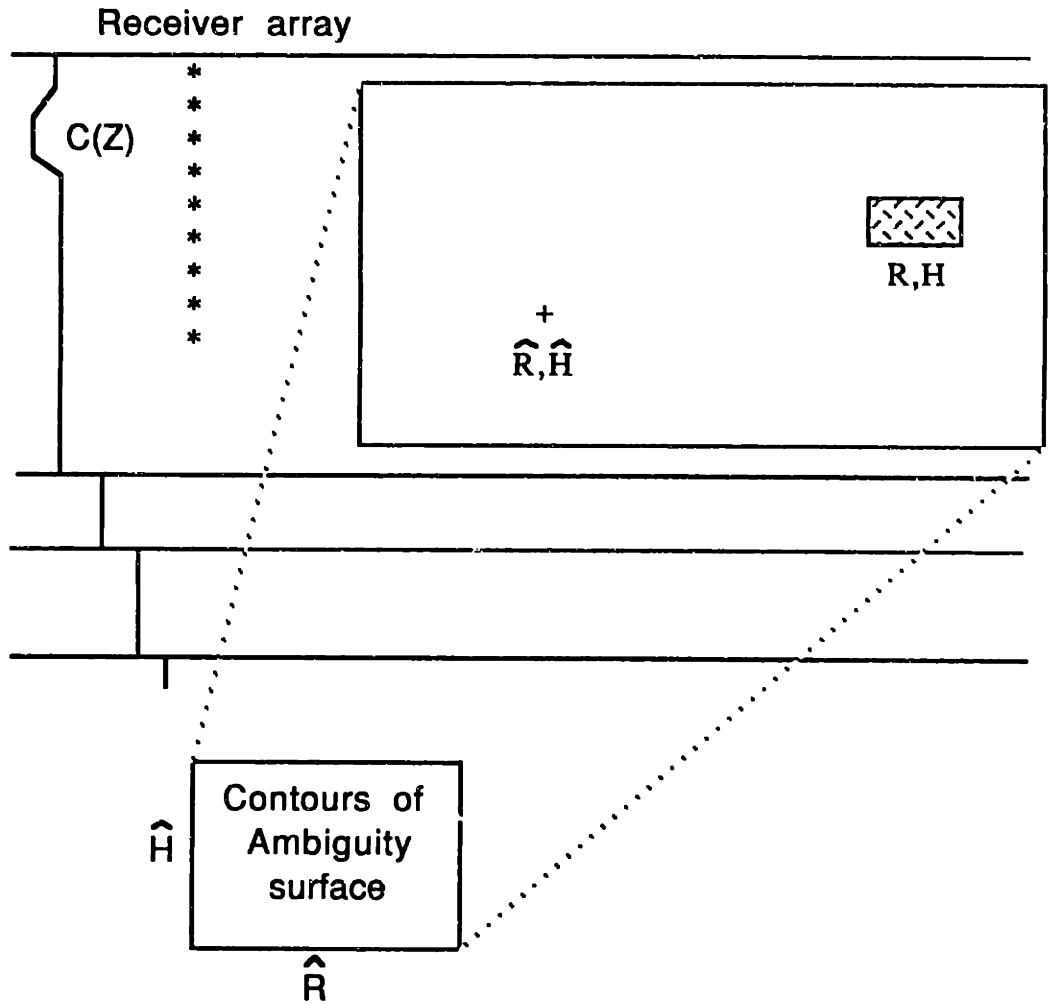

Figure 5.14: Figure formats for ambiguity surfaces versus (R, H), the true volume inhomogeneity and $(\hat{R}, \hat{H})$, the scanning space parameters. The ambiguity surfaces are constructed from replica fields from a *point* source that scan through $\hat{R}, \hat{H}$ space and a peak is expected for the match with received signal structure, back-scattered from the inhomogeneity, which should occur inside the volume enclosing the inhomogeneity.

respectively, with an additive white noise of −20 dB. Each contour in the ambiguity surfaces denotes a 1 dB increase in the estimator output.

MLM and MCM beamformers were both able to detect the plume inhomogeneity, which are indicated by light shading near the ocean surface. High ambiguity surfaces are spread out over a region of space, as compared to an almost single "point" peak behavior for a point source localization in this kind of relatively simple environment using the MFP algorithm which has a high resolution feature. This spread in the estimated poor target location is caused by the volume inhomogeneity which basically is a mismatch of environmental parameters in terms of point source localization, causing the detected source location to spread out over a region. In essence, we are using point source localizing schemes in order to find a distributed target – and so the match can never be perfect. The spread region of high ambiguity surface group is seen to closely relate the true location and size of the inhomogeneity. The central peak of high ambiguity surfaces is shifted towards the receivers, and away from the true geometric center of the plume, which is due to higher scattering from the vertical surface closer to the receiver. MCM shows more ambiguity (sidelobes) than the ML beamformer because of its robustness to mismatch in the environmental parameters to locate a point source. The sea bottom reveals almost no ambiguity, as expected.

When the plume is infinitely extended in the range direction away from the source so that it becomes a half-infinite strip of 25 m depth starting from range = 500 m, the MFP results of ambiguity surfaces for both the MLM and MCM beamforming do not change considerably compared to the finite plume problem. Since only the back-scattered pressure field information is provided, which will not differ much for the finite and half-infinite plumes of small size, this behavior is expected of the point source localizing matched field processing scheme. Matched field processing for localizing a plume of larger dimension, creating high back-scattered field at the receiving array is performed to investigate if the estimation of the volume scatterer

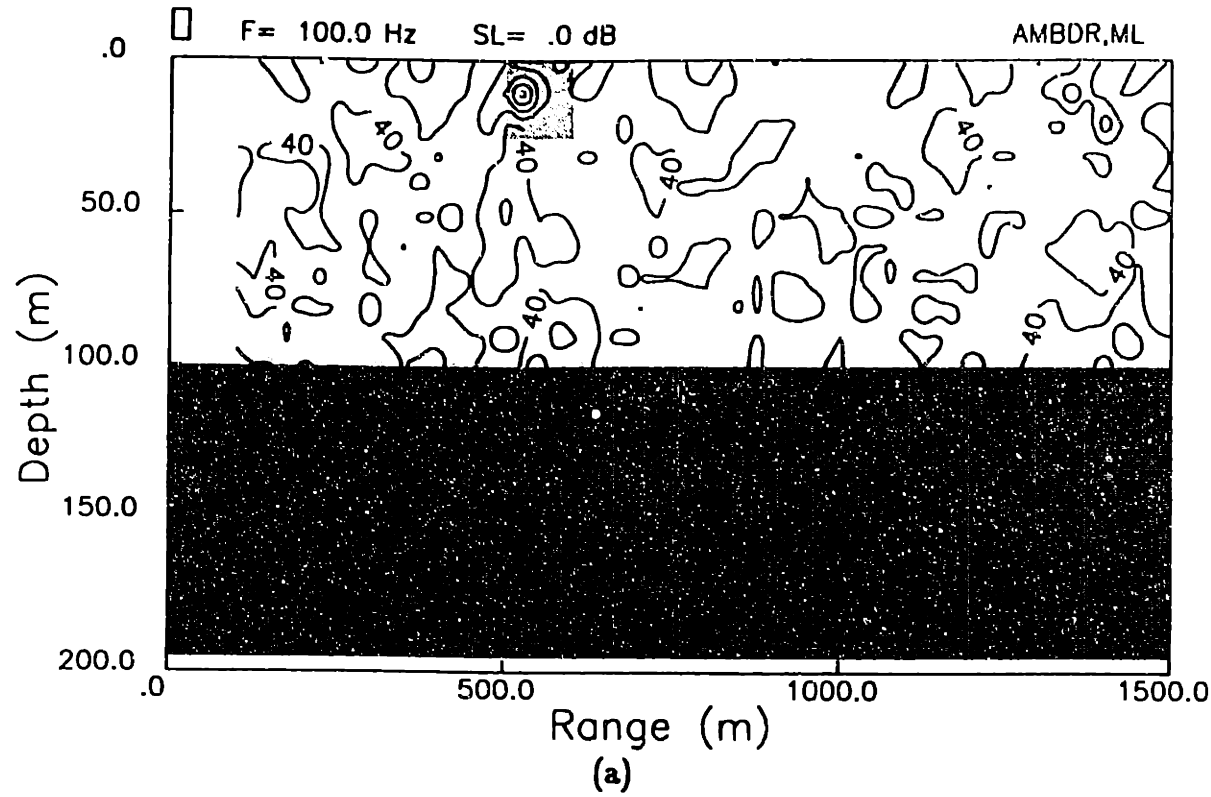

(a)

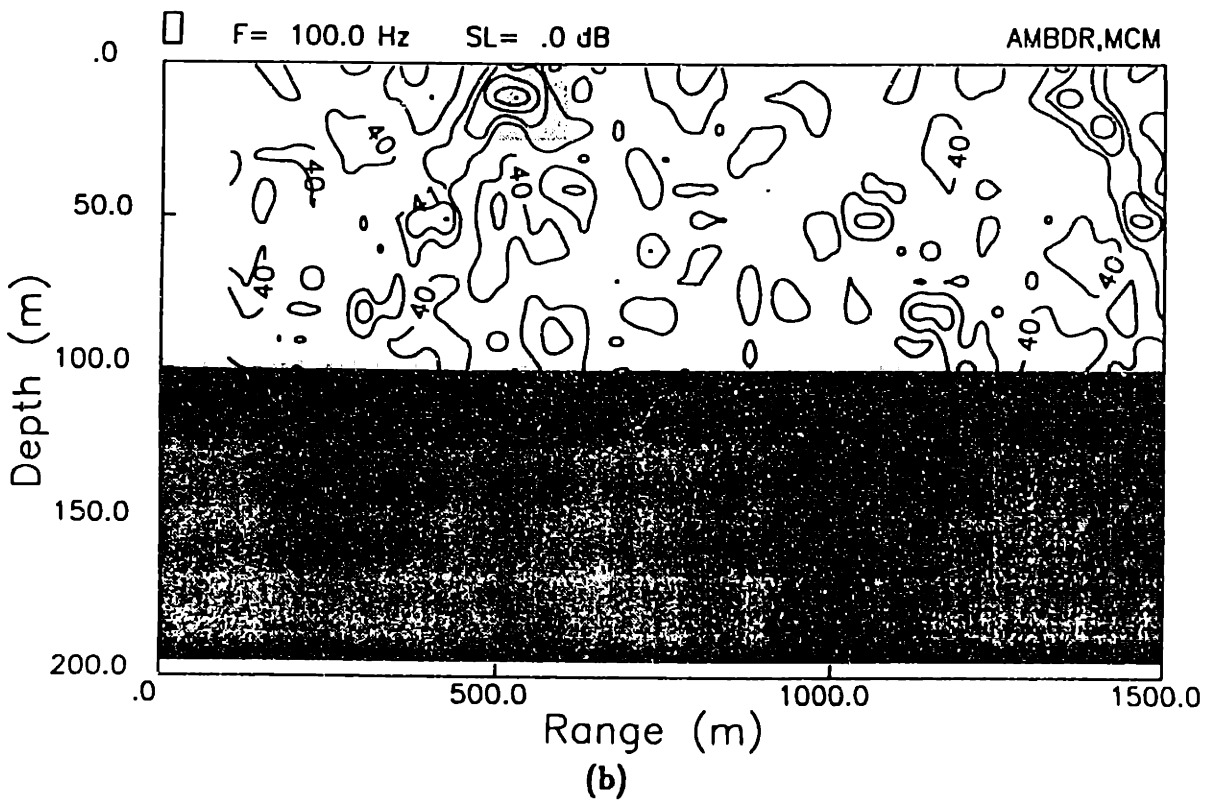

(b)

Figure 5.15: Contours of ambiguity function for the plume problem (Fig.5.12) using: (a) MLM beamformer ; (b) MCM beamformer. Lightly shaded area represents the plume and dark shaded area is the sea bottom

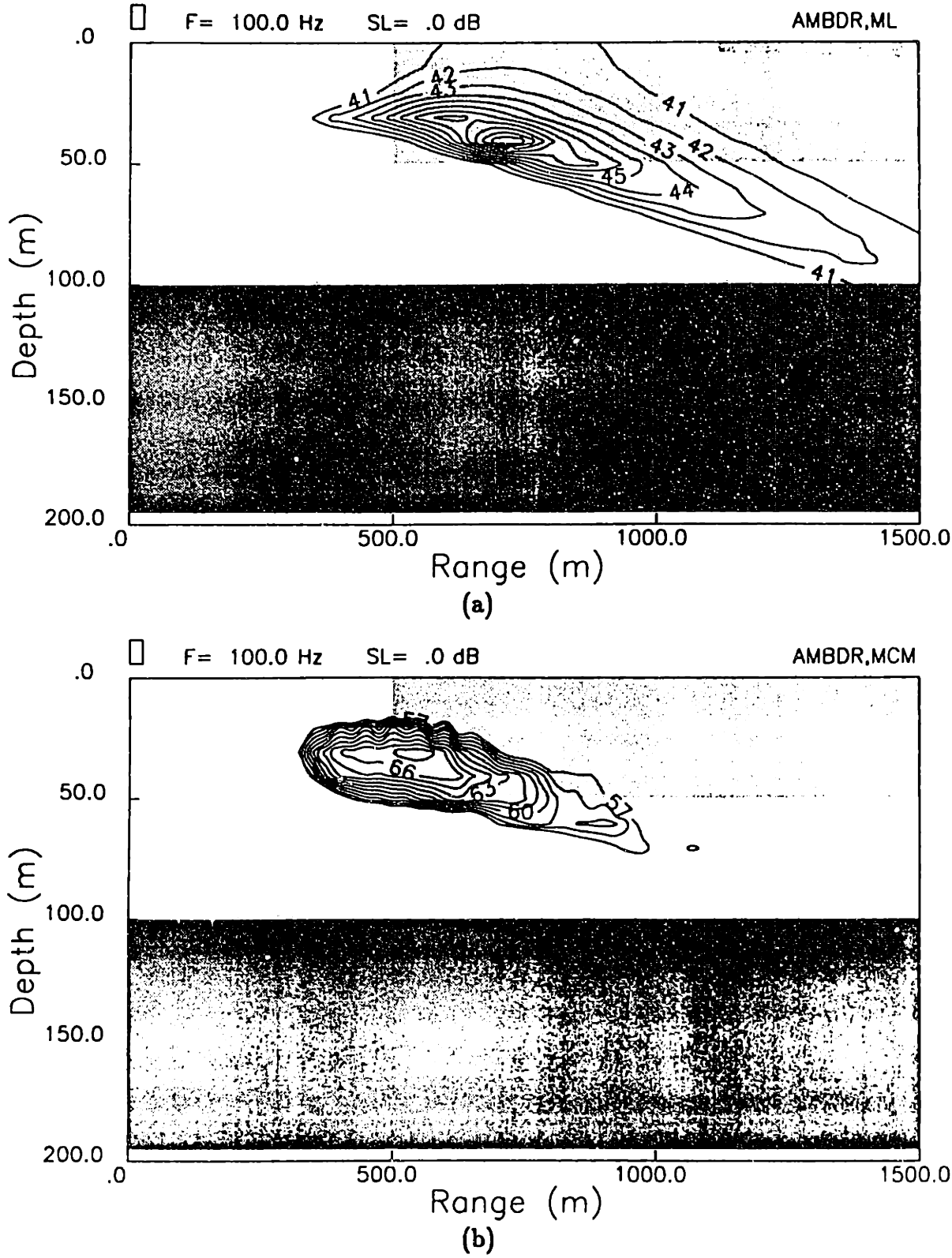

Figure 5.16: Contours of ambiguity function for the half-infinite plume using: (a) MLM beamformer ; (b) MCM beamformer. Lightly shaded area represents the plume and dark shaded area is the sea bottom

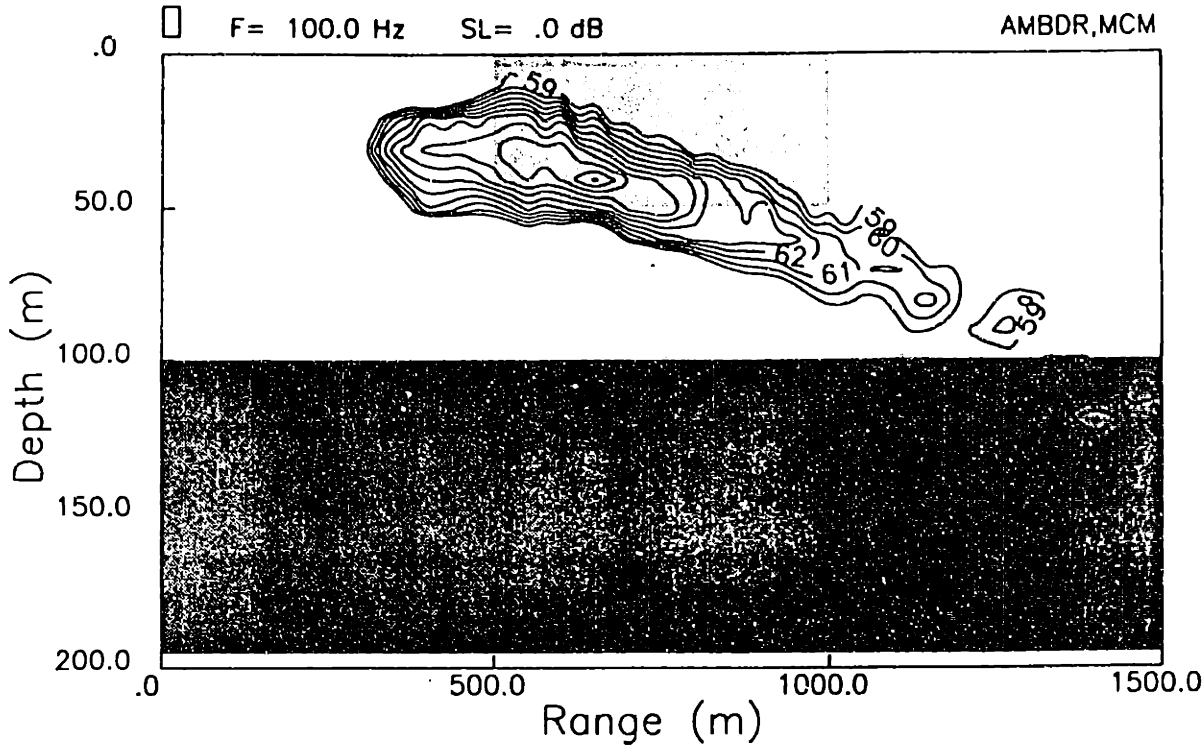

(a)

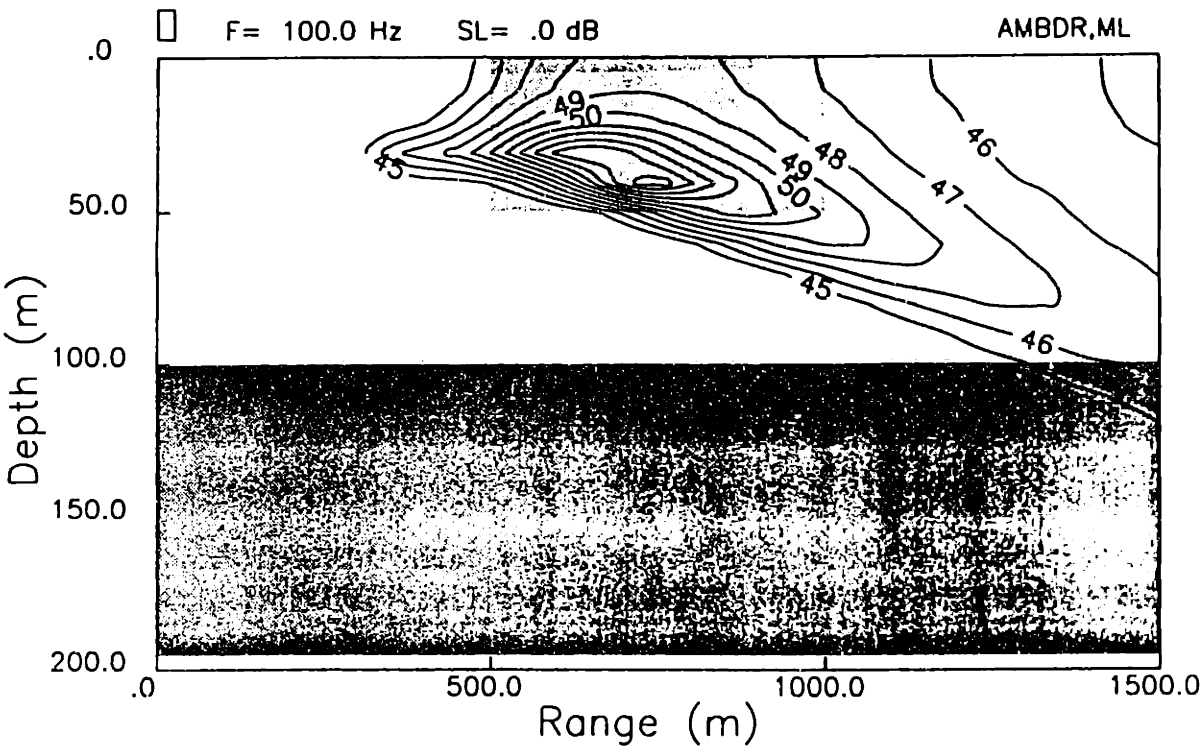

(b)

Figure 5.17: Contours of ambiguity function for the finite plume using: (a) MLM beamformer ; (b) MCM beamformer. Lightly shaded area represents the plume and dark shaded area is the sea bottom

is possible. These results are shown in Fig. 5.17 and Fig. 5.16 for both the finite and half-infinite plume, with light shaded areas representing the plume locations. Because of the strong back-reverberated field, both the MLM and MCM reveal no other ambiguous surfaces except at the true plume location. The maximum level of the ambiguity function for the MCM is seen to be 15 dB higher than the MLM beamformer for both cases of the plume configuration. Thus in the case of a low signal to noise ratio, the performance of the MCM to localize these kinds of inhomogeneities will be better than the MLM beamformer.

In the half-infinite plume MCM beamforming case, the central peak point of the ambiguity surfaces occur at a depth slightly below the center of the vertical surface that is facing the receivers and at range close to this surface. The half-infinite inhomogeneity is localized as a finite inhomogeneity since the infinite tail of the plume does not contribute significantly to the back-scattering. MCM beamforming for the finite plume of Fig. 5.17 shows more clearly the overall location and dimension of the volume. The center of the clustered ambiguity surface has now receded closer to its true geometric center with 2 dB higher estimation for the peak value compared to the infinite case. This results from the sharp edge at the far vertical surface which identifies itself more to the receiver that there is an inhomogeneity at that location.

Without detailed further studies, we applied two point source localizing matched field processing schemes to identify volume inhomogeneities within a waveguide from the synthetic back-reverberated pressure fields generated by the hybrid BIE+WI method. It is found that inhomogeneities are at least detectable and in some cases it is even possible to estimate their location and dimension.

Chapter 6

Conclusions and Suggestions for Future Studies

6.1 Conclusions

A hybrid super element method for discretely varying range dependent ocean waveguide propagation has been developed based on a hybrid Galerkin boundary integral and wavenumber integration approach. The wavenumber integration approach is used to generate solutions within range homogeneous segments, providing the kernel of the integral equation. The Galerkin boundary integral approach is used for the matching of the boundary conditions at the range discontinuities. The overall performance of the BIE+WI method is excellent compared with the analytic, coupled mode and parabolic equation solutions.

There are several advantages of the present method compared to alternative global range dependent solution techniques.

- The full wave solution is obtained, including both forward propagating and back-reverberated waves. These waves can be treated separately enabling analysis of reverberation from individual features in the environment.

- Short as well as long range propagation and reverberation can be treated

efficiently.

- As in the case of traditional wavenumber integration methods, the field within each sector is directly represented as a wavenumber integral, the kernel of which is important for physical interpretation purposes.
- This basic idea is applicable to an elastic medium range dependent environment simply by introducing additional variables which represents shear waves.

Compared to other methods employing boundary integral formulation, the present method has more applicability to global range dependent problems in ocean acoustic due to the following features.

- The wavenumber integration within each sector enables elimination of the range discretization within each sector from the degrees of freedom. The length of each sector can therefore be chosen arbitrarily large without affecting the number of degrees of freedom in the BIE solution.
- The Galerkin boundary integral formulation reduces the degrees of freedom to the amplitudes of the distribution functions in the vertical direction. Additionally, this method is robust in the choice of degrees of freedom.
- Efficient computation of the Green's function for layered media is achieved by means of a modified SAFARI code.
- Finally, a marching solution can be obtained if multiple back-scattering is ignored, which significantly reduces the computational requirements.

Without detailed further studies, we applied two matched field processing schemes for localizing a point source to actively identify any volume inhomogeneity within a waveguide from the synthetic back-reverberated pressure fields generated by the present method. By using the replicas of the homogeneous waveguide, it has been found that inhomogeneities are at least detectable and in some cases it is even possible to estimate their location and dimension.

6.2 Contributions

This thesis provides a number of new contributions to the field of underwater acoustics and signal processing. These contributions may be classified into three areas.

- A new range dependent solution technique has been developed for solving the wave propagation problem in two-dimensional seismo-acoustic media. It incorporates the Galerkin boundary integral and the wavenumber integration method. Furthermore, a numerical code has been developed for an acoustic medium case.

- Extensive convergence analysis of the basis function expansion has been performed. This analysis enables the future underwater acoustician to employ the Galerkin boundary integral method since it is shown to converge rapidly.

- We have demonstrated the possibility of an active sonar system for the detection and the localization of a bulk inhomogeneity. Specifically, this possibility was shown by applying a point source matched field processing scheme to localize a bulk inhomogeneity in an otherwise homogeneous ocean environment.

6.3 Suggestions for Future Studies

It has been demonstrated that when the boundary integral equation and wavenumber integration methods are combined we have a much larger possibility of efficiently solving a complex inhomogeneous wave propagation problem. Some of these possibilities are mentioned which should be the future studies to be carried out. Direct extensions of the proposed method can be described as follows.

- Extension to treat elastic media simply by including the shear wave components into all field components. The only additional work involved is to set up the influence matrix for shear waves. (The wavenumber integral method

already exists which can produce homogeneous solutions for the elastic media.)

- Time domain solution of the signals by Fourier synthesis can be accomplished with relative ease without resorting to the Kirchoff integral equation.

- Various seismic sources of higher order other than the current point monopole, which has already been studied and exists in the range independent version of the global matrix method, can be introduced to examine physical phenomena arising especially in seismology and structural acoustics.

- If a velocity profile other than isovelocity within a layer is incorporated, which has known eigenfunction in depth such as n^2 linear profile, then a more realistic modeling of the ocean would be possible with less number of layers.

Aside from these, the modeling of the half-infinite space should be studied with the goal of finding a more convenient, more efficient alternative to the dummy interface. The conventional method using the basis function has been shown to fail due to the poor representation of the basis function expansion in terms of a horizontal wave number integral.

Following the basic theme of the present BIE+WI method, another area in which it may be useful is in rough surface scattering in layered inhomogeneous media problems. This has been done for the layered homogeneous media using a perturbation method but has not been applied in the range dependent case.

Further studies for inclusion of the irregular inhomogeneities other than a rectangular shape, such as the finite ice sheets with keels protruding into the water, in a range dependent environment combining the proposed solution technique with the regular boundary element method in layered media should be pursued for dealing with more complex real ocean environments.

To enable a consistent treatment of the various effects influencing the sound propagation and reverberation in a realistic ocean environment, a seismo-acoustic

propagation model for simulation of three-dimensional reverberation from facets in an otherwise horizontally stratified ocean should be developed using the present basic idea, allowing for simulation of out-of-plane scattering and reverberation, which are important in the active bistatic or passive sonar scenarios.

Appendix A

Field Representation in Laterally Inhomogeneous Elastic Medium

In this appendix, a concise derivation along with full final expressions, needed to implement the proposed hybrid method to treat elastic medium case, are given. Since it follows the same context of the acoustic medium derivation outlined in Chapter 3, explanations are given for newly introduced concepts only. First the elastic equivalent of displacement solution in terms of the basis function expansion is given followed by the horizontal wavenumber integral representation. Then the accompanying homogeneous solutions arising from matched horizontal interface boundary conditions are sought both in terms of the horizontal wavenumber integral representation and the orthogonal basis function expansion. Next, the contribution from the compressional sources and its homogeneous solutions are given, both in terms of wavenumber integral representations and basis function expansions. The notations are consistent with Chapter 3.

The introduction of shear wave terms, makes the expressions more complicated, and makes it necessary to express the field equations in a matrix form. For the basis function expansion, which is used to match vertical interface boundary conditions, the first vector form of the following equation is used. For the horizontal wavenumber integral representation, used for matching of horizontal interface

boundary conditions, the second vector form is used for the field variables.

$$\mathbf{v}(x,z) = \left\{ \begin{array}{c} u(x,z) \\ w(x,z) \\ \sigma_{xx}(x,z)/\mu \\ \sigma_{xz}(x,z)/\mu \end{array} \right\} \quad \text{or} \quad \mathbf{v}(x,z) = \left\{ \begin{array}{c} u(x,z) \\ w(x,z) \\ \sigma_{zz}(x,z)/\mu \\ \sigma_{xz}(x,z)/\mu \end{array} \right\} \tag{A.1}$$

where u and w are displacements in the horizontal and vertical direction respectively followed by normal and shear stress terms normalized by the shear Lamè constant μ.

The basis function expansion is written, using orthogonal polynomials identical to those of Chapter 3, as

$$\mathbf{v}(x,z) = \sum_{m=1}^{\infty} \mathbf{V}_m(x) P_{m-1}\left(\frac{z - \frac{l}{2}}{\frac{l}{2}}\right) \tag{A.2}$$

where the expansion coefficient functions are

$$\mathbf{V}_m(x) = \left\{ \begin{array}{c} U_m(x) \\ W_m(x) \\ T_m(x) \\ S_m(x) \end{array} \right\} . \tag{A.3}$$

In the following, only these expansion functions are given except for the displacement source solution which is written out in-full for clarity.

A.1 Displacement Source Solution

Extension of the present hybrid technique to treat an elastic medium is straightforward by including the shear wave displacement potential similar to Eq. 3.10 as

$$\hat{\varphi}(x,z) = i \int_{-\infty}^{\infty} B(\eta)\, e^{-x\delta} e^{-i\eta(z-\frac{l}{2})}\, d\eta \tag{A.4}$$

where η is the vertical wavenumber, $i\delta$ is the horizontal wavenumber, $i\delta = i\sqrt{\eta^2 - k^2}$, and k is medium shear wavenumber.

In addition to the normal displacement type source distribution of Eq. 3.8, another arbitrary source must be added at the vertical cut to represent the shear wave terms. We can either choose between the vertical displacement or the shear stress or the normal stress type sources. Here, they are chosen to be the "shear stress" type, which renders the field expressions in a more compact form than the other types of sources. Thus it is more appropriate to name this section as "Normal displacement–shear stress source solution". To be consistent with the main context, we will simply call them displacement solution.

Basis Function Expansion

Following the same derivation of acoustic medium case with additional shear wave terms gives us the following expressions:

$$\begin{aligned}
\hat{u}_n(x,z) &= \frac{2\pi}{l}\sum_{m=1}^{\infty}\hat{U}_{nm}(x)P_{m-1}\left(\frac{z-\frac{l}{2}}{\frac{l}{2}}\right)\\
\hat{w}_n(x,z) &= \frac{2\pi}{l}\sum_{m=1}^{\infty}\hat{W}_{nm}(x)P_{m-1}\left(\frac{z-\frac{l}{2}}{\frac{l}{2}}\right)\\
\hat{\sigma}_{xx_n}(x,z)/\mu &= \frac{2\pi}{l}\sum_{m=1}^{\infty}\hat{T}_{nm}(x)P_{m-1}\left(\frac{z-\frac{l}{2}}{\frac{l}{2}}\right)\\
\hat{\sigma}_{zz_n}(x,z)/\mu &= \frac{2\pi}{l}\sum_{m=1}^{\infty}\hat{S}_{nm}(x)P_{m-1}\left(\frac{z-\frac{l}{2}}{\frac{l}{2}}\right)\ . \qquad \text{(A.5)}
\end{aligned}$$

As with the acoustic medium case, a factor of $2\pi/l$ is necessary in the displacement source solution. Expansion coefficient functions are given by Eq. A.6 through Eq. A.9. Note in particular that the depth integration has been performed analytically producing spherical Bessel function, implying that the Galerkin method is used in matching boundary conditions at the vertical cuts.

$$\begin{aligned}
\hat{\mathbf{V}}_m(x) &= \frac{l}{2\pi}(2m-1)(-1)^{m-1}\sum_{k=1}^{\infty}i^{k+m-2}\\
&\int_{-\infty}^{\infty}(\hat{U}_k(0)\hat{\mathbf{K}}_u+\hat{S}_k(0)\hat{\mathbf{K}}_s)\ \hat{\mathbf{E}}\ j_{m-1}\left(\frac{l\eta}{2}\right)j_{k-1}\left(\frac{l\eta}{2}\right)d\eta \qquad \text{(A.6)}
\end{aligned}$$

$$\hat{\mathbf{E}} = \mathrm{diag}\left[e^{-z\gamma}, e^{-z\delta}\right] \qquad \text{(A.7)}$$

$$\hat{\mathbf{K}}_u = \frac{1}{k^2}\begin{bmatrix} -(2\eta^2 - k^2) & 2\eta^2 \\ -i\eta(2\eta^2 - k^2)/\gamma & 2i\eta\delta \\ (2\eta^2 k^4/h^2 + (2\eta^2 - k^2)^2)/\gamma & -4\eta^2\delta \\ i\eta(\eta^2 - 2k^2) & -i\eta(\eta^2 - 2k^2) \end{bmatrix} \tag{A.8}$$

$$\hat{\mathbf{K}}_s = \frac{1}{k^2}\begin{bmatrix} i\eta & -i\eta \\ -\eta^2/\gamma & \delta \\ -i\eta(\eta^2 - k^2)/\gamma & 2\eta\delta \\ 2\eta^2 & -(2\eta^2 - k^2) \end{bmatrix} \tag{A.9}$$

where $\hat{U}_{nm}(0)$: Strength of normal displacement source of order m at layer n

$\hat{S}_{nm}(0)$: Strength of shear stress source of order m at layer n

μ : Lamè constant

l : Layer thickness

P_m : Legendre polynomial of order m

j_m : Spherical Bessel function of order m

η : vertical wavenumber

$i\gamma$: Compressional horizontal wavenumber $i\sqrt{\eta^2 - h^2}$

$i\delta$: Shear horizontal wavenumber $i\sqrt{\eta^2 - k^2}$

h : Medium compressional wavenumber

k : Medium shear wavenumber.

Horizontal Wavenumber Integral Representation

From the contour deformation of the vertical wavenumber integral, the following horizontal wavenumber integral representations are obtained which are valid outside the layer of interest but still applicable on the interfaces:

$$\hat{\mathbf{v}}(x,z) = \sum_{m=1}^{\infty}\int_{-\infty}^{\infty}(\hat{U}_m(0)\hat{\mathbf{K}}_u + \hat{S}_m(0)\hat{\mathbf{K}}_s)\ \hat{\mathbf{E}}\ \hat{\mathbf{J}}_m\ e^{-isx}\,ds \tag{A.10}$$

where each of the matrices are given by Eq. A.11 through Eq. A.14. Although duplicate notations with basis function expansions are used for these matrices because

of similarity in nature, the individual elements are different.

$$\hat{\mathbf{E}} = \text{diag}\left[e^{-|s-\frac{l}{2}|\alpha},\, e^{-|s-\frac{l}{2}|\beta}\right] \tag{A.11}$$

$$\hat{\mathbf{J}}_m = \left\{ \begin{array}{c} i^{m-1} j_{m-1}\left(-\text{sign}(z-\frac{l}{2})\frac{il\alpha_n}{2}\right) \\ i^{m-1} j_{m-1}\left(-\text{sign}(z-\frac{l}{2})\frac{il\beta_n}{2}\right) \end{array} \right\} \tag{A.12}$$

$$\hat{\mathbf{K}}_u = \frac{1}{k^2}\begin{bmatrix} is(2\alpha^2+k^2)/\alpha & -2is\alpha \\ \text{sign}(z-\frac{l}{2})(2\alpha^2+k^2) & -\text{sign}(z-\frac{l}{2})2s^2 \\ -(2s^2-k^2)(2\alpha^2+k^2)/\alpha & 4s^2\alpha \\ -\text{sign}(z-\frac{l}{2})2is(2\alpha^2+k^2) & \text{sign}(z-\frac{l}{2})2is(2s^2-k^2) \end{bmatrix} \tag{A.13}$$

$$\hat{\mathbf{K}}_s = \frac{1}{k^2}\begin{bmatrix} \text{sign}(z-\frac{l}{2})is & -\text{sign}(z-\frac{l}{2})is \\ \beta & -s^2/\beta \\ -\text{sign}(z-\frac{l}{2})(2s^2-k^2) & \text{sign}(z-\frac{l}{2})2s^2 \\ -2is\beta & -2is(2s^2-k^2)/\beta \end{bmatrix} \tag{A.14}$$

where s : Horizontal wavenumber

$i\alpha$: Compressional vertical wavenumber $i\sqrt{s^2-h^2}$

$i\beta$: Shear vertical wavenumber $i\sqrt{s^2-k^2}$.

A.2 Displacement Homogeneous Solution

Homogeneous solutions accompanying the displacement sources are comprised of each contribution from the normal displacement sources and the shear stress sources.

Horizontal Wavenumber Integral Representation

Field equations can be written as a superposition of homogeneous solutions for normal displacement sources ($\hat{U}_{lk}(0)$) and shear stress sources ($\hat{S}_{lk}(0)$) located at each finite layer ($l = 2, \ldots, N-1$) for each order ($k = 1, 2, \ldots$).

$$\mathbf{v}_n(x,z) = \sum_{l=2}^{N-1}\sum_{k=1}^{\infty}\int_{-\infty}^{\infty} \mathbf{K}\,\hat{\mathbf{E}}\,[\hat{U}_{lk}(0)\bar{\mathbf{A}} + \hat{S}_{lk}(0)\bar{\mathbf{C}}]\; e^{-isx}\,ds \tag{A.15}$$

where the matrices are given by

$$\bar{\mathbf{K}} = \begin{bmatrix} -is & -is & i\beta & -i\beta \\ -\alpha & \alpha & s & s \\ (2s^2-k^2) & (2s^2-k^2) & -2s\beta & 2s\beta \\ 2is\alpha & -2is\alpha & -i(2s^2-k^2) & -i(2s^2-k^2) \end{bmatrix} \quad \text{(A.16)}$$

$$\bar{\mathbf{E}} = \text{diag}\left[e^{-s\alpha}, e^{(s-l)\alpha}, e^{-s\beta}, e^{(s-l)\beta}\right] \quad \text{(A.17)}$$

$$\bar{\mathbf{A}} = \left\{ A^-_{n,lk} \;\; A^+_{n,lk} \;\; B^-_{n,lk} \;\; B^+_{n,lk} \right\}^T \quad \text{(A.18)}$$

$$\bar{\mathbf{C}} = \left\{ C^-_{n,lk} \;\; C^+_{n,lk} \;\; D^-_{n,lk} \;\; D^+_{n,lk} \right\}^T . \quad \text{(A.19)}$$

The unknown vectors $\bar{\mathbf{A}}$ and $\bar{\mathbf{C}}$ are the down- and up-going (superscript $\mp$) compressional (A and C) and shear (B and C) waves due to displacement and shear stress sources. Thus each combination of indices l and k represents a single SAFARI run.

Basis Function Expansion

Using the orthogonality relation of Legendre polynomials, expansion functions can be extracted as

$$\bar{\mathbf{V}}_m(x) = (2m-1)i^{m-1} \sum_{l=2}^{N-1} \sum_{k=1}^{\infty} \int_{-\infty}^{\infty} \bar{\mathbf{K}}\, \bar{\mathbf{E}}\, \bar{\mathbf{J}}\, [\hat{U}_{lk}(0)\bar{\mathbf{A}} + \hat{S}_{lk}(0)\bar{\mathbf{C}}]\, e^{-ixs}\, ds \quad \text{(A.20)}$$

where the matrices are given by

$$\bar{\mathbf{K}} = \begin{bmatrix} -is & -is & i\beta & -i\beta \\ -\alpha & \alpha & s & s \\ -(2\alpha^2+k^2) & -(2\alpha^2+k^2) & 2s\beta & -2s\beta \\ 2is\alpha & -2is\alpha & -i(2s^2-k^2) & -i(2s^2-k^2) \end{bmatrix} \quad \text{(A.21)}$$

$$\bar{\mathbf{E}} = \text{diag}\left[e^{-\frac{l\alpha}{2}}, e^{-\frac{l\alpha}{2}}, e^{-\frac{l\beta}{2}}, e^{-\frac{l\beta}{2}}\right] \quad \text{(A.22)}$$

$$\bar{\mathbf{J}} = \text{diag}\left[j_{m-1}(\frac{il\alpha}{2}), \varsigma_m j_{m-1}(\frac{il\alpha}{2}), j_{m-1}(\frac{il\beta}{2}), \varsigma_m j_{m-1}(\frac{il\beta}{2})\right] \quad \text{(A.23)}$$

$$\bar{\mathbf{A}} = \left\{ A^-_{n,lk} \;\; A^+_{n,lk} \;\; B^-_{n,lk} \;\; B^+_{n,lk} \right\}^T \quad \text{(A.24)}$$

$$\bar{\mathbf{C}} = \left\{ C^-_{n,lk} \;\; C^+_{n,lk} \;\; D^-_{n,lk} \;\; D^+_{n,lk} \right\}^T \quad \text{(A.25)}$$

where $\varsigma_m = (-1)^{m-1}$.

A.3 Source Solution

Analogous to the conventional SAFARI code, this method has no limitation on the implementation of various seismic sources [33]. Although this is true, compressional real point sources are derived in this Appendix, which demands that only point sources are allowed in the acoustic medium layer.

Horizontal Wavenumber Integral Representation

Field equations for an acoustic point source are given by

$$\mathring{\mathbf{v}}_n(x,z) = \int_{-\infty}^{\infty} \mathring{\mathbf{K}} e^{-|s-s_s|\alpha_n} e^{-i(x-x_s)s} ds \tag{A.26}$$

with

$$\mathring{\mathbf{K}} = \begin{Bmatrix} -is/\alpha \\ -1 \\ (2s^2 - k^2)/\alpha \\ 2is \end{Bmatrix} \tag{A.27}$$

where z_s : Source depth

x_s : Source range

Basis Function Expansion

Again, extracting an expansion coefficient function using the orthogonality gives us

$$\mathring{\mathbf{V}}_m(x) = (2m-1)i^{m-1} \int_{-\infty}^{\infty} \mathring{\mathbf{K}} e^{-\frac{|s|}{2}} j_{m-1}(\frac{il\alpha}{2}) e^{-i(x-x_s)s} ds \tag{A.28}$$

where

$$\mathring{\mathbf{K}} = \begin{Bmatrix} -is/\alpha \\ -1 \\ (2\alpha^2 + k^2)/\alpha \\ i2s \end{Bmatrix} \tag{A.29}$$

A.4 Source Homogeneous Solution

The homogeneous solution accompanying a real point source in a layered media is straightforward.

Horizontal Wavenumber Integral Representation

Similar to the displacement homogeneous solutions, the horizontal wavenumber integral is given by the following equation:

$$\tilde{\mathbf{v}}_n(x,z) = \int_{-\infty}^{\infty} \tilde{\mathbf{K}}\ \tilde{\mathbf{E}}\ \tilde{\mathbf{A}}\ e^{-i(x-x_o)s}\, ds \tag{A.30}$$

where each matrix is identical to displacement homogeneous solution

$$\tilde{\mathbf{K}} = \begin{bmatrix} -is & -is & i\beta & -i\beta \\ -\alpha & \alpha & s & s \\ (2s^2-k^2) & (2s^2-k^2) & -2s\beta & 2s\beta \\ 2is\alpha & -2is\alpha & -i(2s^2-k^2) & -i(2s^2-k^2) \end{bmatrix} \tag{A.31}$$

$$\tilde{\mathbf{E}} = \mathrm{diag}\left[e^{-sz}, e^{(z-l)\alpha}, e^{-s\beta}, e^{(z-l)\beta}\right] \tag{A.32}$$

$$\tilde{\mathbf{A}} = \left\{ A_n^- \quad A_n^+ \quad B_n^- \quad B_n^+ \right\}^T . \tag{A.33}$$

Note how the depth separated portion is written such that waves generated at each horizontal interface decays as they propagate away, rendering the scheme unconditionally stable.

Basis Function Expansion

$$\tilde{\mathbf{V}}_m(x) = (2m-1)i^{m-1} \int_{-\infty}^{\infty} \tilde{\mathbf{K}}\ \tilde{\mathbf{E}}\ \tilde{\mathbf{J}}\ \tilde{\mathbf{A}}\ e^{-i(x-x_o)s}\, ds \tag{A.34}$$

where each matrices, given in the following equations, are also identical to that of displacement homogeneous solutions except for the unknown vector $\tilde{\mathbf{A}}$.

$$\tilde{\mathbf{K}} = \begin{bmatrix} -is & -is & i\beta & -i\beta \\ -\alpha & \alpha & s & s \\ -(2\alpha^2 + k^2) & -(2\alpha^2 + k^2) & 2s\beta & -2s\beta \\ 2is\alpha & -2is\alpha & -i(2s^2 - k^2) & -i(2s^2 - k^2) \end{bmatrix} \tag{A.35}$$

$$\tilde{\mathbf{E}} = \text{diag}\left[e^{-\frac{il\alpha}{2}}, e^{-\frac{il\alpha}{2}}, e^{-\frac{il\beta}{2}}, e^{-\frac{il\beta}{2}}\right] \tag{A.36}$$

$$\tilde{\mathbf{J}} = \text{diag}\left[j_{m-1}(\frac{il\alpha}{2}), \varsigma_m j_{m-1}(\frac{il\alpha}{2}), j_{m-1}(\frac{il\beta}{2}), \varsigma_m j_{m-1}(\frac{il\beta}{2})\right] \tag{A.37}$$

$$\tilde{\mathbf{A}} = \left\{ A_n^- \quad A_n^+ \quad B_n^- \quad B_n^+ \right\}^T \tag{A.38}$$

where $\varsigma_m = (-1)^{m-1}$.

Appendix B

Horizontal Wavenumber Integral for Displacement Sources

The displacement sources which are originally written in terms of a vertical wavenumber integral must be deformed into an integral in terms of a horizontal wavenumber so that we can utilize the conventional numerical code of the direct global matrix method for layered media (SAFARI) to arrive at the corresponding homogeneous solutions. In order to convert the integral (Eq. 3.10)

$$\phi(x,z) = \int_{-\infty}^{\infty} A(\eta)\, e^{-z\sqrt{\eta^2-k^2}}\, e^{-\imath(s-\frac{1}{2})\eta}\, d\eta \qquad \text{(B.1)}$$

which is an integration over the vertical wavenumber η, we make use of the contour integration scheme as follows.

CASE I ($z < l/2$)

Consider a closed contour integration in the complex ξ plane of the following (Fig. B.1)

$$I = \oint A(\imath\sqrt{\xi^2-h^2})\, e^{-\imath s\xi}\, e^{(s-\frac{1}{2})\sqrt{\xi^2-k^2}}\, \frac{\imath\xi}{\sqrt{\xi^2-h^2}}\, d\xi \qquad \text{(B.2)}$$

where the analytic function A is same as that of Eq. B.1 and h is the acoustic medium wavenumber with a small negative imaginary part accounting for the vol-

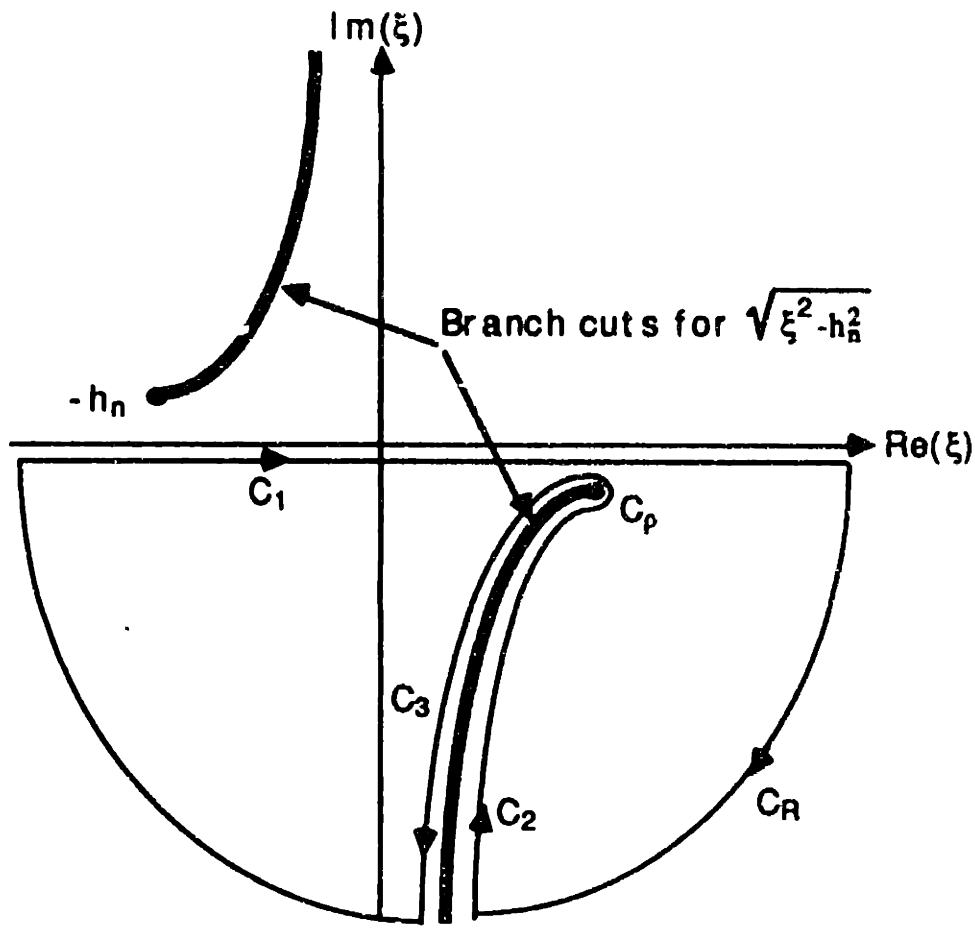

Figure B.1: Closed integration contour for wavenumber conversion.

ume attenuation which can be either specified or taken from an empirical formula[43].

The branch cuts originating from the square root singularities $\pm h$ and extending to infinity are chosen such that $\sqrt{\xi^2 - h^2}$ becomes purely imaginary along the branch cut. Denoting each contribution of the closed contour as depicted in Fig. B.1 and realizing that there are no singularities inside the closed contour, Cauchy's theorem gives us

$$I = I_{C_1} + I_{C_2} + I_{C_3} + I_{C_\rho} + I_{C_R} = 0. \tag{B.3}$$

Since C_1 is running along the real axis of the complex ξ plane,

$$I_{C_1} = \int_{-\infty}^{\infty} A(i\sqrt{s^2 - h^2})\, e^{-ixs}\, e^{(s-\frac{1}{2})\sqrt{s^2-h^2}}\, \frac{is}{\sqrt{s^2 - h^2}}\, ds \tag{B.4}$$

and this is the required horizontal wavenumber integral representation. Along C_2 and C_3, the arguments of $\sqrt{\xi^2 - h^2}$ are $-\frac{\pi}{2}$ and $\frac{\pi}{2}$ respectively so that the following change of variables are valid:

$$\sqrt{\xi^2 - h^2} = -i\eta \quad \text{along } C_2 \tag{B.5}$$

$$\sqrt{\xi^2 - h^2} = +i\eta \quad \text{along } C_3\,. \tag{B.6}$$

With the above change of variables,

$$\begin{aligned} I_{C_2} + I_{C_3} &= \int_{\infty}^{0} A(\eta)\, e^{-x\sqrt{\eta^2-h^2}}\, e^{-i(s-\frac{1}{2})\eta}\, d\eta - \int_{0}^{\infty} A(-\eta)\, e^{-x\sqrt{\eta^2-h^2}}\, e^{i(s-\frac{1}{2})\eta}\, d\eta \\ &= -\int_{-\infty}^{\infty} A(\eta)\, e^{-x\sqrt{\eta^2-h^2}}\, e^{-i(s-\frac{1}{2})\eta}\, d\eta \\ &= -\phi(x,z) \end{aligned} \tag{B.7}$$

where the last equality comes directly from Eq. B.1. Denoting the kernel of Eq. B.2 as $f(\xi)$, on the circular arc C_ρ, the value of $(\xi - h)f(\xi) \to 0$ uniformly as $\rho \to 0$. Thus from the theorem on limiting contours,

$$I_{C_\rho} = \lim_{\rho \to 0} \int_{C_\rho} f(\xi)\, d\xi = 0\,. \tag{B.8}$$

Finally, the contribution along the infinite circular arc C_R vanishes if the kernel $f(\xi)$ without the $e^{-ix\xi}$ part, where $x > 0$ for our choice of coordinate system, tends uniformly to zero

$$I_{C_R} = \lim_{R \to \infty} \int_{C_R} f(\xi)\, d\xi = 0 \tag{B.9}$$

according to Jordan's lemma. Now from Eq. 3.13 and using the principal asymptotic expansion for large argument of the Bessel function [1]

$$\begin{aligned}\frac{f(\xi)}{e^{-is\xi}} &\sim \frac{1}{\sqrt{\xi^2-h^2}}\, e^{(s-\frac{l}{2})\sqrt{\xi^2-h^2}}\, j_{m-1}(il\sqrt{\xi^2-h^2}/2) \\ &\sim \frac{1}{(\xi^2-h^2)^{\frac{1}{2}}}\left(e^{(s-l)\sqrt{\xi^2-h^2}} + e^{s\sqrt{\xi^2-h^2}}\right). \qquad \text{(B.10)}\end{aligned}$$

So as long as $z \leq 0$, the kernel tends uniformly to zero along the infinite circular arc and I_{C_R} becomes zero. Collecting Eq. B.3 through Eq. B.10, we arrive at the desired equivalent horizontal wavenumber integral representation as

$$\phi(x,z) = \int_{-\infty}^{\infty} A(i\sqrt{s^2-h^2})\, e^{-isx}\, e^{(s-\frac{l}{2})\sqrt{s^2-h^2}}\, \frac{is}{\sqrt{s^2-h^2}}\, ds \qquad \text{(B.11)}$$

which is valid for $z \leq 0$.

CASE II ($z > l/2$)

Following the same analogy as the previous case, the horizontal wavenumber integral valid for $z \geq l$ becomes

$$\phi(x,z) = \int_{-\infty}^{\infty} A(-i\sqrt{s^2-h^2})\, e^{-isx}\, e^{-(s-\frac{l}{2})\sqrt{s^2-h^2}}\, \frac{is}{\sqrt{s^2-h^2}}\, ds\ . \qquad \text{(B.12)}$$

Collecting Eq. B.11 and Eq. B.12,

$$\phi(x,z) = i\int_{-\infty}^{\infty} A(-\text{sign}(z-\frac{l}{2})i\sqrt{s^2-h^2})\, e^{-|s-\frac{l}{2}|\sqrt{s^2-h^2}}\, \frac{s}{\sqrt{s^2-h^2}}\, e^{-isx}\, ds \qquad \text{(B.13)}$$

which is valid for $z \leq 0$ and $z \geq l$. Although this equation is not valid inside the finite layer where the displacement solution is located, it is still useful to find the accompanying homogeneous solutions for layered medium using the direct global matrix method since the boundary conditions are applied at the interface of the layers where the expression is still valid. This same problem is also reported by

Devaney [14], where horizontal wavenumber spectrum expansion does not converge inside the horizontal strip bounded by planes parallel to the x axis and containing a distribution of continuous sources.

It was stated in Chapter 3 that, until now, the half spaces do not possess a basis function expansion suitable for modification into a horizontal wavenumber integral representation. An example of expansion in terms of Laguerre orthogonal polynomials is illustrative of the difficulty in modeling the half spaces. First, the basis function expansion is written as

$$\begin{aligned} \mathcal{U}_n(x,z) &= \sum_{m=1}^{\infty} \hat{U}_{nm}(x) e^{-\frac{cz}{2}} L_{m-1}(cz) \\ \mathcal{P}_n(x,z) &= \sum_{m=1}^{\infty} \hat{S}_{nm}(x) e^{-\frac{cz}{2}} L_{m-1}(cz) \end{aligned} \tag{B.14}$$

where L_m is the Laguerre polynomial of order m, c is a constant and the exponential serves as the dual purpose of the weighting function and to represent the decaying of the field at infinity. Following the same procedure of Chapter 3, we arrive at the expression given by Eq. B.2 but with a different function $A(i\sqrt{\xi^2 - k^2})$. This function possesses an essential singularity located at the negative imaginary axis of the complex ξ plane. Closed contour integration as in Fig. B.1 produces a residue value, which is independent of the horizontal wavenumber, yielding this expansion incompatible with the wavenumber integration method.

Appendix C

Equivalent Point Source Representation of Displacement Sources

For the purpose of evaluating the field along all ranges for the desired receiver depths, it is preferable to unify all solutions in terms of a horizontal wavenumber integral representation where an FFT technique can be adopted for numerical efficiency. In the previous appendix it has been shown that this is not feasible for the displacement solutions where the horizontal wavenumber spectrum representation is not valid in that particular layer where the displacement sources are located. To overcome this cumbersome problem we shall derive a discretized equivalent point source horizontal wavenumber representation of the continuous line displacement sources.

We start from Eq. B.13 combined with Eq. 3.13 for the displacement source horizontal wavenumber spectrum representation valid outside the layer

$$\phi(x,z) = -\int_{-\infty}^{\infty} \left[\sum_m i^{m-1} \hat{U}_{nm}(0) j_{m-1}(-\text{sign}(z-\tfrac{l}{2})\tfrac{il\alpha}{2}) \right] \frac{e^{-|z-\frac{l}{2}|\alpha}}{\alpha} e^{-isx}\, ds \quad \text{(C.1)}$$

where $i\alpha = i\sqrt{s^2 - k^2}$ is the vertical wavenumber. Although this equation is not valid inside the layer because of a non-convergence problem, it may be transformed

into an expression containing an integral over the source distribution which is valid inside the strip containing the sources. Remembering that the spherical Bessel function was produced by the line sources, substitution of the integral representation [1]

$$j_{m-1}(\frac{ls}{2}) = (-i)^{m-1}\frac{1}{l}\int_0^l e^{is(z_s-\frac{l}{2})}\, P_{m-1}\left(\frac{z_s-\frac{l}{2}}{\frac{l}{2}}\right) dz_s \qquad \text{(C.2)}$$

into Eq. C.1 gives us

$$\phi(x,z) = -\int_{-\infty}^{\infty}\left\{\frac{1}{l}\int_0^l e^{-|s-z_s|\alpha}\left[\sum_m \hat{U}_{nm}(0)P_{m-1}\left(\frac{z_s-\frac{l}{2}}{\frac{l}{2}}\right)\right]dz_s\right\}\frac{e^{-izs}}{\alpha}ds\,. \qquad \text{(C.3)}$$

The above equation converges for every field point z and is in the form of a continuous distribution of simple acoustic point sources. The term inside the square bracket is the amplitude of the source strength, composed of all orders of the Legendre polynomials (which are the basis function which we employed for the solution of the boundary integral equation using Galerkin's method).

Numerical evaluation of the integral inside the curly bracket of Eq. C.3 is time consuming. Instead we will efficiently discretize the integration by a summation of point sources with adequate strength. Discretization into equally spaced point sources is numerically proved to be inefficient, and requires a fine discretization for the total energy to be matched. Since we have chosen the Legendre polynomial as the basis function, intuitively, we will benefit by locating these equivalent point sources at Gauss-Legendre quadrature points with matching weights to yield better results. Using a quadrature scheme [54], the total energy of the equivalent point sources better matches that of the line sources. Replacing the integration in Eq. C.3 with summation,

$$\phi(x,z) = -\sum_{j=1}^{N}\int_{-\infty}^{\infty}\left[\sum_m \hat{U}_{nm}(0)P_{m-1}\left(\frac{z_j-\frac{l}{2}}{\frac{l}{2}}\right)W_j\right]\frac{e^{-|s-z_j|\alpha}}{\alpha}e^{-izs}ds \qquad \text{(C.4)}$$

where Gauss-Legendre quadrature points and its weight z_j and W_j respectively are

$$\begin{aligned} z_j &= j\text{th} \quad \text{zero of} \quad P_N(\frac{z-l/2}{l/2}) \\ W_j &= \frac{2}{1-z_j^2}\left[P_N'(\frac{z_j-l/2}{l/2})\right]^2 \end{aligned} \qquad \text{(C.5)}$$

and N is the total number of equivalent point sources. Using this scheme it is numerically verified that N can be relatively small, approximately equal to twice the number of Legendre polynomial expansion used, and represents the actual field without any appreciable error.

Appendix D

Influence Function Integrations

For the computation of influence coefficients, following integral types need to be evaluated:

$$\begin{aligned} I_1 &= \int_{-\infty}^{\infty} e^{-s\alpha} j_h(s) j_m(s)\, ds \\ I_2 &= \int_{-\infty}^{\infty} \frac{e^{-s\alpha}}{\alpha} j_h(s) j_m(s)\, ds \\ I_3 &= \int_{-\infty}^{\infty} \frac{s}{\alpha}\, e^{-\alpha} j_m(i\alpha)\, e^{-ixs}\, ds \\ I_4 &= \int_{-\infty}^{\infty} \frac{1}{\alpha}\, e^{-\alpha} j_m(i\alpha)\, e^{-ixs}\, ds \end{aligned} \tag{D.1}$$

where j represents spherical Bessel function and $\alpha = \sqrt{s^2 - h^2}$, with h being the complex medium wavenumber with a small negative imaginary part and its real value denoted as h_0. The integration limits may be changed to $(0, \infty)$ since the kernels can be separated into a sum of odd and even functions. The Gauss-Tchebycheff quadrature formula will be used whenever possible, given by [1]

$$\int_0^1 \frac{f(y)}{\sqrt{y(1-y)}} dy = \sum_{i=1}^{n} w_i f(y_i) + R_n \tag{D.2}$$

where Gauss-Tchebycheff quadrature points y_i, its weight w_i and remainder R_n respectively are

$$y_i = \frac{1}{2}\left(1 + \cos\frac{(2i-1)\pi}{2n}\right)$$

$$w_i = \frac{\pi}{n}$$
$$R_n = \frac{\pi}{(2n)!\,2^{2n-1}} f^{(2n)}(\xi) \quad -1 < \xi < 1\,. \tag{D.3}$$

TYPE I_1

This integral poses no problem when evaluated numerically since for $x = 0$, analytic results are given in a closed form [24] and when $x \neq 0$, the kernel decays very fast once the integration variable s exceeds h_0.

TYPE I_2

This integral type exhibits an almost singular behavior when s is around h_0. Thus we separate the integration limits from $(0, h_0)$ and (h_0, ∞). With the change of variables $t = s/h_0$ and $t = (s - h_0)/s$ respectively for the separated integration limits, it becomes

$$\begin{aligned} I_2 &= \int_0^1 e^{-s\sqrt{h_0^2t^2 - h^2}} \sqrt{\frac{t(1-t)}{h_0^2t^2 - h^2}}\; j_k(h_0t) j_m(h_0t)\; \frac{h_0 dt}{\sqrt{t(1-t)}} \\ &+ \int_0^1 e^{-s\sqrt{h_0^2/(1-t)^2 - h^2}} \sqrt{\frac{t}{(1-t)(h_0^2 - h^2(1-t)^2)}} \\ &\quad j_k(h_0/(1-t)) j_m(h_0/(1-t))\; \frac{h_0 dt}{\sqrt{t(1-t)}}\,. \end{aligned} \tag{D.4}$$

If the kernels are regular inside the integration interval, the numerical quadrature scheme, with square-root weight functions included explicitly, succeeds with a fast convergence rate. Thus its behavior at an almost singular point $s = h_0$ and $s \to \infty$ is examined, which corresponds to $t = 0$, and $t = 1$ with the above change of variables.

The integrand behaves well for $t \to 0$. When $t \to 1$ it is well behaved when $x \neq 0$ because of the exponential decay. Even if $x = 0$, since the decaying rate of the envelope of the spherical Bessel function for all orders is at least

$$\lim_{t \to 1} j_k\left(\frac{1}{1-t}\right) \sim (1-t) \tag{D.5}$$

the amplitude of the kernel goes to 0 as $\sqrt{\frac{(1-t)^3}{h_0^2-h^2(1-t)^2}}$.

TYPE I_3

In addition to the square root singular behavior, the integrand is seen to vanish slowly as $s \to \infty$. Envelope of the kernel for large complex argument has the asymptotic expansion [1]

$$\lim_{\alpha\to\infty} e^{-\alpha} j_m(i\alpha) \sim \frac{1}{\alpha}(1 + e^{-2\alpha}) . \tag{D.6}$$

Although the decay is slow for large s, its contribution to the integral value is negligible due to highly oscillating integrand with no stationary values which means that the integrand cancels out. Numerically this is taken care of by applying a Hanning window over the interval $s \in (s_0, s_0 + T_c)$

$$W_H(s) = \begin{cases} 1 & 0 < s < s_0 \\ \frac{1}{2}(1 + \cos(\frac{\pi(s-s_0)}{T_c})) & s_0 < s < s_0 + T_c \\ 0 & s_0 + T_c < s \end{cases} \tag{D.7}$$

where s_0 is normally taken to be $5h_0$ and window interval T_c to be $10h_0$.

Following the same partitioning of integration interval and the change of variables for I_2, the integral can be written as

$$\begin{aligned} I_3 &= \int_0^1 e^{-\sqrt{h_0^2t^2-h^2}} j_m(i\sqrt{h_0^2t^2-h^2}) \sqrt{\frac{t^3(1-t)}{h_0^2t^2-h^2}} \sin(h_0xt) \frac{h_0^2dt}{\sqrt{t(1-t)}} \\ &+ \int_0^1 e^{-\sqrt{h_0^2/(1-t)^2-h^2}} j_m(i\sqrt{h_0^2/(1-t)^2-h^2}) \\ &\quad \sqrt{\frac{t}{(1-t)^3(h_0^2-h^2(1-t)^2)}} \sin(\frac{h_0x}{1-t}) \frac{h_0^2dt}{\sqrt{t(1-t)}} . \end{aligned} \tag{D.8}$$

The kernel is seen to be regular for $t \to 0$. When $t \to 1$, because of the windowing of the kernel, it is also well behaved with a fast convergence when numerical quadrature scheme is used.

TYPE I_4

Compared to I_3 this integral type converges to zero as $1/s^2$ instead of $1/s$, for $s \to \infty$. Following the same division of integration limits and the change of variables as that of I_2, it becomes

$$
\begin{aligned}
I_4 &= \int_0^1 e^{-\sqrt{h_0^2t^2-h^2}} j_m(i\sqrt{h_0^2t^2-h^2}) \sqrt{\frac{t(1-t)}{h_0^2t^2-h^2}} \cos(h_0xt) \frac{h_0dt}{\sqrt{t(1-t)}} \\
&+ \int_0^1 e^{-\sqrt{h_0^2/(1-t)^2-h^2}} j_m(i\sqrt{h_0^2/(1-t)^2-h^2}) \\
&\quad \sqrt{\frac{t}{(1-t)(h_0^2-h^2(1-t)^2)}} \cos(\frac{h_0x}{1-t}) \frac{h_0dt}{\sqrt{t(1-t)}} .
\end{aligned}
\tag{D.9}
$$

The behavior of the kernel inside the integration interval (including end points) are regular for the first and the second part where the envelope of second part tends to zero as $\sqrt{\frac{t(1-t)}{(h_0^2-h^2(1-t)^2)^3}}$ for $t \to 1$. The numerical quadrature scheme is shown to be fastly converging for all types of integration mentioned above.

Bibliography

[1] Milton Abramowitz and I.A. Stegun. *Handbook of Mathematical Functions.* Dover Publications, 1972.

[2] K. Aki and P.G. Richards. *Quantitative Seismology: Theory and Methods. Vol.2.* W.H. Freeman and Company, San Francisco, 1980.

[3] A.B. Baggeroer, W.A. Kuperman, and H. Schmidt. Matched field processing: Source localization in correlated noise as an optimum parameter estimation problem. *J. Acoust. Soc. Am.*, 83:571–587, 1988.

[4] M. Bouchon. Discrete wavenumber representation of elastic fields in three-space dimensions. *Journ. Geophys. Res.*, 84:3609–3614, 1979.

[5] M. Bouchon and K. Aki. Discrete wavenumber representation of seismic source wave fields. *Bull. Seismol. Soc. Am.*, 67:259–277, 1977.

[6] M. Bouchon, M. Campillo, and S. Gaffet. A boundary integral equation-discrete wavenumber representation method to study wave propagation in multilayered media having irregular interfaces. *Geophysics*, 54:1134–1140, 1989.

[7] L. Brekhovskikh and Yu. Lysanov. *Fundamentals of Ocean Acoustics.* Springer-Verlag, New York, 1982.

[8] M. Campillo and M. Bouchon. Synthetic SH seismograms in a laterally varying medium by the discrete wavenumber method. *Geophys. J. R. Astr. Soc.*, 83:307–317, 1985.

[9] C.H. Chapman and R. Drummond. Body-wave seismograms in inhomogeneous media using Maslov asymptotic theory. *Bull. Seis. Soc. of Amer.*, 72:S277–S317, 1982.

[10] M.D. Collins. Benchmark calculations for higher order-parabolic equation. *J. Acoust. Soc. Am.*, 87:1535–1538, 1990.

[11] D. Colton and R. Kress. *Integral Equations Methods in Scattering Theory.* John Wiley & Sons, 1983.

[12] G. Dahlquist and A. Bjorck. *Numerical Methods.* Prentice-Hall, 1974.

[13] T.W. Dawson and J.A. Fawcett. A boundary integral equation method for acoustic scattering in a waveguide with nonplanar surfaces. *J. Acoust. Soc. Am.*, 87:1110–1125, 1990.

[14] A.J. Devaney and E. Wolf. Multipole expansions and plane wave representations of the electromagnetic field. *J. Math. Phys.*, 15:234–244, 1974.

[15] F.R. DiNapoli and R.L. Deavenport. Theoretical and numerical Green's function field solution in plane multilayered medium. *J. Acoust. Soc. Am.*, 67:92–105, 1980.

[16] R.B. Evans. A coupled mode solution for acoustic propagation in a waveguide with stepwise depth variations of a penetrable bottom. *J. Acoust. Soc. Am.*, 74:188–195, 1983.

[17] W.M. Ewing, W.S. Jardetzky, and F. Press. *Elastic Waves in Layered Media.* McGraw-Hill, New York, 1957.

[18] L.B. Felsen. Benchmarks: An option for quality assessment. *J. Acoust. Soc. Am.*, 87:1497–1498, 1990.

[19] C.A.J. Fletcher. *Computational Galerkin Methods.* Springer-Verlag, New York, 1984.

[20] S. Gaffet and M. Bouchon. Effects of two-dimensional topographies using the discrete wavenumber - boundary integral method in P-SV cases. *J. Acoust. Soc. Am.*, 85:2277–2283, 1989.

[21] P. Gerstoft and H. Schmidt. A boundary element approach to ocean seismo-acoustic facet reverberation. *Submitted to J. Acoust. Soc. Am.*, 1990.

[22] P. Gerstoft, O. Vilmann, and S. Krenk. Computational aspects of synthetic seismograms for layered media. *J. Acoust. Soc. Am. Suppl. 1*, 86:S65, 1989.

[23] K.E. Gilbert and R.B. Evans. A green's function method for one-way wave propagation in a range dependent ocean environment. In T. Akal and J.M. Berkson, editors, *Ocean Seismo-Acoustics*, pages 21–28, Plenum Press, New York, 1986.

[24] I.S. Gradshteyn and I.M. Ryzhik. *Table of Integrals, Series and Products.* Academic Press, 1980.

[25] N.A. Haskell. The dispersion of surface waves on multi-layered media. *Bull. Seismol. Soc. Am.*, 43:17–34, 1953.

[26] P.A. Heelan. Radiation from a cylindrical source of finite length. *Geophysics*, 18:685–696, 1953.

[27] E.H. Hug. A propagation anomaly observed in the Barents sea. In T. Akal and J.M. Berkson, editors, *Ocean Seismo-Acoustics*, pages 217–222, Plenum Press, New York, 1986.

[28] F.B. Jensen and C.M. Ferla. Numerical solution of range-dependent benchmark problems in ocean acoustics. *J. Acoust. Soc. Am.*, 87:1499–1510, 1990.

[29] F.B. Jensen, W.A. Kuperman, M.B. Porter, and H. Schmidt. Computational Ocean Acoustics. 1990. Book under preparation for publication.

[30] H. Kawase. Time-domain response of a semi-circular canyon for incident SV, P and Rayleigh waves calculated by the discrete wavenumber boundary element method. *Bull. Seismol. Soc. Am.*, 78:1415–1437, 1988.

[31] B.L.N. Kennett. Guided wave propagation in laterally varying media –I. theoretical development. *Geophys. J. R. Astr. Soc.*, 79:235–255, 1984.

[32] B.L.N. Kennett. Reflections, rays and reverberations. *Bull. Seismol. Soc. Am.*, 64:1685, 1974.

[33] J.S. Kim. *Radiation from Directional Seismic Sources in Laterally Stratified Media with Application to Arctic Ice Cracking Noise.* PhD thesis, Massachusetts Institute of Technology, May 1989.

[34] S. Krenk and H. Schmidt. Elastic wave scattering by a circular crack. *Phil. Trans. R. Soc. Lond.*, A308:167–198, 1982.

[35] S. Krenk and H. Schmidt. Vibration of an elastic circular plate on an elastic half space - A direct approach. *Journ. Appl. Mech.*, 48:161–168, 1981.

[36] W.A. Kuperman and H. Schmidt. Rough surface elastic wave scattering in a horizontally stratified ocean. *J. Acoust. Soc. Am.*, 79:1767–1777, 1986.

[37] D. Lee and K.E. Gilbert. Recent progress in modeling bottom-interacting sound propagation with parabolic equations. In *OCEANS 82 Conference Record*, pages 172–177, Washington D.C., 1982.

[38] I.T. Lu. Analysis of acoustic wave scattering by scatterers in layered media using the hybrid ray-mode(boundary integral equation) method. *J. Acoust. Soc. Am.*, 86:1136–1142, 1989.

[39] S.T. McDaniel. Parabolic approximations for underwater sound propagation. *J. Acoust. Soc. Am.*, 58:1178–1185, 1975.

[40] C.L. Pekeris. Theory of propagation of explosive sound in shallow water. *Geo. Soc. Am. Mem.*, 27, 1948.

[41] A.D. Pierce. Extension of the method of normal modes to sound propagation in an almost-stratified medium. *J. Acoust. Soc. Am.*, 37:19–27, 1965.

[42] M.B. Porter, C.M. Ferla, and F.B. Jensen. The problem of energy conservation in one-way wave equations. *J. Acoust. Soc. Am. Suppl. 1*, 86:S54, 1989.

[43] H. Schmidt. *SAFARI: Seismo-Acoustic Fast Field Algorithm for Range Independent Environments. User's Guide.* SR 113, SACLANT ASW Research Centre, La Spezia, Italy, 1987.

[44] H. Schmidt, A.B. Baggeroer, W.A. Kuperman, and E.K. Scheer. Environmentally tolerant beamforming for high resolution matched field processing: Deterministic mismatch. *J. Acoust. Soc. Am.*, 88:1851–1862, 1990.

[45] H. Schmidt and J. Glattetre. A fast field model for three-dimensional wave propagation in stratified environments based on the global matrix method. *J. Acoust. Soc. Am.*, 78:2105–2114, 1985.

[46] H. Schmidt and F.B. Jensen. A full wave solution for propagation in multilayered viscoelastic media with application to Gaussian beam reflection at fluid-solid interfaces. *J. Acoust. Soc. Am.*, 77:813–825, 1985.

[47] H. Schmidt and S. Krenk. Asymmetric vibration of a circular elastic plate on an elastic half space. *Int. Journal of Solids and Structures*, 18:91–105, 1982.

[48] H. Schmidt and G. Tango. Efficient global matrix approach to the computation of synthetic seismograms. *Geophys. J. R. Astr. Soc.*, 84:331–359, 1986.

[49] G.T. Schuster. A hybrid BIE + Born series modeling scheme: Generalized Born series. *J. Acoust. Soc. Am.*, 77:865–879, 1985.

[50] G.T. Schuster and L.C. Smith. A comparison among four direct boundary integral methods. *J. Acoust. Soc. Am.*, 77:850–864, 1985.

[51] G.T. Schuster and L.C. Smith. Modeling scatterers embedded in plane-layered media by a hybrid Haskell-Thomson and boundary integral equation method. *J. Acoust. Soc. Am.*, 78:1387–1394, 1985.

[52] R.P. Shaw. Acoustics. In D.E. Beskos, editor, *Computational Methods in Mechanics., Vol.3 Boundary Element Methods in Mechanics*, North-Holland, New York, 1987.

[53] R.A. Stephen. Solutions to range-dependent benchmark problems by the finite-difference method. *J. Acoust. Soc. Am.*, 87:1527–1534, 1990.

[54] A.H. Stroud and D. Secrest. *Gaussian Quadrature Formulas.* Prentice-Hall, 1966.

[55] F.D. Tappert. The parabolic approximation method. In J.B. Keller and J.S. Papadakis, editors, *Wave Propagation in Underwater Acoustics*, Springer-Verlag, New York, 1977.

[56] D.J. Thomson. Wide-angle parabolic equation solutions to two range-dependent benchmark problems. *J. Acoust. Soc. Am.*, 87:1514–1520, 1990.

[57] D.J. Thomson, G.H. Brooke, and J.A. DeSanto. Numerical implementation of a modal solution to a range-dependent benchmark problem. *J. Acoust. Soc. Am.*, 87:1521–1526, 1990.

[58] C.T. Tindle, A.P. Stamp, and K.M. Guthrie. Virtual modes and the surface boundary condition in underwater acoustics. *J. Sound Vib.*, 49:231–240, 1976.

[59] I. Tolstoy and C.S. Clay. *Ocean Acoustics: Theory and Experiment in Underwater Sound.* McGraw-Hill, New York, 1966.

[60] E.K. Westwood. Ray model solutions to the benchmark wedge problems. *J. Acoust. Soc. Am.*, 87:1539–1545, 1990.

[61] G.R. Wilson, R.A. Koch, and P.J. Vidmar. Matched mode localization. *J. Acoust. Soc. Am.*, 84:310–320, 1988.